7 2014

U.PORTO
FEUP FACULDADE DE ENGENHARIA
UNIVERSIDADE DO PORTO

MODELING AND SIMULATION OF FLOW AND HEAT TRANSFER IN SHELL-TYPE POWER TRANSFORMERS

RÓMULO TIAGO LOUREIRO DA SILVA OLIVEIRA

DISSERTAÇÃO DE MESTRADO APRESENTADA
À FACULDADE DE ENGENHARIA DA UNIVERSIDADE DO PORTO EM
ENGENHARIA QUÍMICA

Mestrado Integrado em Engenharia Química

Modeling and Simulation of Flow and Heat Transfer in Shell-Type Power Transformers

Tese de Mestrado

de

Rómulo Tiago Loureiro da Silva Oliveira

Desenvolvida no âmbito da unidade curricular de Dissertação

Realizado em

EFACEC Energia

Orientador na FEUP: Prof. José Carlos Lopes
Orientador na EFACEC Energia: Eng. Hugo Campelo

Departamento de Engenharia Química

Julho 2014

Acknowledgements

I would like to acknowledge support and dedication of Prof. José Carlos Lopes and Eng. Hugo Campelo, who oriented me during this dissertation. With whom I learned new things, perfected my skills and expanded my ideas. I would also like to acknowledge EFACEC Energia for the possibility to realize my dissertation in the company, where all the conditions were provided.

A special acknowledgement to Prof. Madalena Dias for all the time and help provided which proved invaluable for me.

I would like to acknowledge my family and friends, who always supported me on every occasion as without them it would not be possible for me to be here writing the final words of this dissertation. Although on this category, a special acknowledgment to my girlfriend who was an essential support for me (this may be a short reference but feeling are not measured in words).

A special mention must be made to those who closely journeyed with me during these years of college. As during those days the majority of the time was spent in college, it is only fair to make a special acknowledgment to that people - although I am grateful for everyone that crossed my path, I feel I must make a special mention to Ruby, Catarina, Eva and Alexandra who more closely and actively coexisted with me. Starting together, some wandered away as others joined in. The road was never straight nor easy, as we picked our friends from the ground we quickly found ourselves being in need of a hand to get up. I'm sure they will turn out to be fantastic engineers no matter the circumstances. I just want to close this eulogy with one of the phrases that stuck with me: "Clear skies never made good pilots".

I would also like to acknowledge all the unsung heroes that in any way, shape or form contributed to my success. And also those who defied and opposed me.

Abstract

Power transformers are a keystone in electrical grids, representing the largest portion of capital investment. These machines are designed to operate for extended periods of time and their outage have a considerable economic impact. Proper cooling plays a vital role in the transformers lifetime.

This work focus of understanding the hydro and thermal dynamics of the flow inside shell power transformers. For this purpose, state of the art computational simulations were used. From the knowledge gathered, mathematical expressions were developed to integrate a previously developed network model, specific to shell power transformers.

While a lot of conclusions and new knowledge was achieved on this work, the highlight is the mathematical expressions developed. These expressions lead to a considerable improvement in accuracy on the previously developed network model.

Keywords: CFD; Network Models; Power Transformers; Shell-Type; Hydrodynamics; Heat Transfer.

Resumo

Os transformadores de potência são peças fundamentais nas redes elétricas, representando a maior porção do investimento de capital. Estas máquinas são desenhadas para operar por extensos períodos de tempo e a sua interrupção tem consideráveis impactos económicos. O arrefecimento adequado tem um papel vital no tempo de vida dos transformadores.

Este trabalho foca-se na compreensão das dinâmicas do escoamento e térmicas no interior de transformadores shell. Para este efeito foram usadas simulações computacionais com recurso às melhores técnicas disponíveis. Da informação resultante, expressões matemáticas foram desenvolvidas para integrar um modelo de redes (previamente desenvolvido e específico para transformadores shell.)

Embora foram alcançadas diversas conclusões e gerado novo conhecimento, o foco vai para as expressões matemáticas desenvolvidas. Estas expressões levaram a um aumento considerável da precisão do modelo de redes previamente desenvolvido.

Palavras-Chave: CFD; Modelos de Rede; Transformadores de Potência; Shell-Type; Hidrodinâmica; Transferência de Calor.

Declaração

Declara, sob compromisso de honra, que este trabalho é original e que todas as contribuições não originais foram devidamente referenciadas com identificação da fonte.

Table of Contents

Page

Table of Figures

Table of Tables

Page

Notation

A	fitting parameter	
A	area	[m^2]
$\vec{A}$	facet area	[m^2]
A_f	flow area	[m^2]
A_{hx}	heat exchange area	[m^2]
A_p	*hot plate* surface area	[m^2]
a	channel height	[mm]
b	channel width	[mm]
C	fitting parameter	
C_p	specific heat capacity	[J/(kg·K)]
d_h	hydraulic diameter	[m]
f	Darcy friction factor	
h	heat transfer coefficient	[W/(m^2·K)]
L	channel length	[m]
$\dot{m}$	mass flow rate	[kg/s]
Nu	Nusselt Number	
$\mathrm{Nu}_{\mathrm{lim}}$	Limiting Nusselt Number	
n	fitting parameter	
P	average pressure	[Pa]
Q	volumetric flow rate	[m^3/s]
Re	Reynolds number	
RF	Recirculation factor	
T	average temperature	[K]
T_h	hot plate surface temperature	[K]
V_c	coil volume	[m^3]
v	average velocity in channel	[m/s]
$\vec{v}$	velocity vector magnitude	[m/s]
$\overline{v}_{1.33\mathrm{H}}$	average G velocity for 1.33H	[cm/s]
$\overline{v}_{\mathrm{G}}$	average G velocity	[cm/s]
W	dissipated heat	[W]

Greek Letters

α	aspect ratio	
Δ	difference operator	
κ	fluid thermal conductivity	[W/(m·K)]
λ	heat dissipated in the coil	[W/m^3]
μ	fluid viscosity	[Pa·s]
ρ	fluid density	[kg/m^3]
τ	shear stress	[Pa/m^2]
Φ_q	heat flux	[W/m^2]
φ	Scale factor	

Indexes

$\uparrow$	full scale geometry
$\downarrow$	scaled down geometry
in	evaluated in the channel inlet
out	evaluated in the channel outlet
w	evaluated in the channel walls

Abbreviations

AC	Alternating Current
BC	Boundary Condition
CFD	Computational Fluid Dynamics
CTC	Continuously Transposed Cable
DC	Direct Current
EHV	Extra-High Voltage
LV	Low Voltage

Glossary

Cell Center Values: Values in the center of the mesh cells.

Core Transformer: Transformer construction configuration where the windings surround the magnetic core.

CTC: Continuously Transposed Cable is a technique of transposing cable strands in order to minimize voltage differences and circulating currents.

Dielectric Losses: Losses attributed to the material inherent dissipation of electromagnetic energy into heat.

Discretization Scheme: Numerical method for approximating a continuous model with a discrete counterpart.

Eddy Current: Electrical current induced by a variation in the conductor magnetic field. These current generate resistive losses.

Facet Area: Area of a mesh cell face.

Hot-Plate: Model abstraction in which the washer is considered to contact with a surface of constant heat flux.

Magnetic Core: Structure that enable the electromagnetic coupling of the transformer.

Node Values: Values in the vertices of the mesh cells.

Power Transformer: Device that (amongst other uses) allows for current and voltage conversion between its terminals.

Preprocessed Surface: Surface created prior to simulating the model.

Primary Winding: Winding that receives the transformer electrical input.

Secondary Winding: Winding that receives the transformer electrical output.

Shell Transformer: Transformer construction configuration where the magnetic core surrounds the windings.

Short-Circuit Strength: Ability of the transformer to endure the mechanical and thermal deformations caused by short-circuits.

Spacer: Pressboard pieces between coils that contribute to electrical isolation and structural stability.

VA: Volt-Ampere is a unit of apparent power, useful only when working with alternating current

Washer: Space between coils where coolant fluid flows.

1 Introduction

1.1 Project Presentation and Framing

In the early days of electricity distribution was direct current (DC). DC operates at relative low voltage and high current. Joule's law states that energy losses are directly proportional to the square of the current. This implies that even a small reduction in current (or rise in voltage for the same total power) results in a substantial lowering of the energy losses. This pursuit for transmitting electricity at high voltage and low current led to the invention of power transformers.

A transformer is a device for stepping up, isolating or stepping down the voltage of an alternating electric signal, and it is widely used for transferring energy from an alternating current in the primary winding to that in one or more secondary windings (Lopéz-Fernández et al., 2013). Regarded as one of the most influential electrical innovations of all time, power transformers are key assets of electrical grids by enabling a feasible transmission and distribution of the electric current from the generation locations to the end-consumers. A transformer is composed of two or more electrical circuits compromising primary and secondary windings, each made of multi-turn coils, with one or more magnetic cores coupling the coils by transferring magnetic flux between them. In its simplest form a transformer consists of a laminated iron core around which are wound two or more sets of windings.

The importance of transformers is due to the vital role that they play in the electrical grid, which has made possible the power generated at low voltages (LVs) to be stepped up to extra-high voltages (EHVs) for transmission over long distances and then transformed back to LVs for utilization at proper load centers. Power transformers represent the largest portion of capital investment in transmission and distributions substations. In addition, power transformer outages have a considerable economic impact on the operation of an electrical grid. As a result these machines are designed and manufactured in order to guarantee the operation within strict safety limits and to achieve the required performance for an extended period of time.

The total energy involved in a large power transformer is in the order of hundreds of MW. Despite operating with high thermo dynamical efficiencies, the energy loss parcel is in the

order of hundreds of kW. This energy loss is transformed into heat by the Joule effect. The heat generated in this process must be removed from the system – by means of immersing the transformer in a circulating cooling fluid - otherwise the transformer lifetime would be affected. The higher the temperature the transformer operates, the less time it will last (Hochart 1988).

There are two main different types of power transformers: core-type and shell-type. The core-type transformer is adaptable to a wide range of design parameters and economical to manufacture. The shell-type has high kVA-to-weight ratio, find favor on EHVs and high MVA applications, have better short-circuit strength characteristics and are more immune to transit damage; this comes at the price of a more laborious intensive manufacturing process.

The scope of this work is to study the hydrodynamics and heat transfer of the cooling channels in shell-type power transformers resorting to Computational Fluid Dynamics (CFD) Simulations. Subsequently this knowledge will be used to develop mathematical expressions for the prediction of important flow parameters. These parameters will then be applied to a simulator developed in a partnership between FEUP and EFACEC (FluSHELL simulator). FluSHELL is specific to shell-type power transformers and is capable of predicting the flow field and temperature distribution inside the transformer. This work was produced during a period of 5 months at the R&D department of EFACEC.

1.2 Thesis Objectives

This project has 3 main objectives:

1. study and description of the flow in the cooling channels of a shell-type transformer;
2. development of mathematical expressions to integrate the FluSHELL simulator;
3. compare the performance of the FluSHELL simulator with the developed mathematical expressions.

1.3 Thesis Organization

This thesis is divided in four chapters.

Chapter 1 presents an introduction to the project and power transformers in general.

In chapter 2 a more detailed look of the project is presented, namely a description of the physical characteristics of the transformer and the best techniques for modelling and simulating a power transformer.

Chapter 3 presents the technical description of the work done and main results.

In chapter 4 the main conclusions and final appreciation of the project are presented.

2 Context and State of the Art

2.1 Description of a Shell-Type Power Transformer

2.1.1 Basic Power Transformer Description

A transformer is an electrical device that transfers energy between two circuits through electromagnetic induction. A transformer may be used as a safe and efficient voltage converter to change the AC voltage at its input to a higher or lower voltage at its output without changing the frequency. Other uses include current conversion, isolation with or without changing voltage and impedance conversion.

The basic design of a transformer consists of two or more electrical circuits compromising primary and secondary windings: the coil that receives the electrical input energy referred to as the primary winding; and the output coil referred as the secondary winding. Each of these windings is made of multi-turn coils of conductors with one or more magnetic cores coupling the coils by transferring magnetic flux between them. In its simplest form, a transformer consists of a laminated iron core around which are wound two or more sets of windings; voltage is applied to one set of windings of the primary, and the load is connected to the secondary.

The operation of a transformer is based on two principles of the laws of electromagnetic induction: an alternating electric current flowing through the primary winding of a transformer generates a varying electromagnetic field in its surroundings which induces a varying magnetic flux in the core of the transformer. The varying electromagnetic field in the vicinity of the secondary winding induces an electromotive force in the secondary winding, which appears as a voltage across the output terminals.

2.1.2 Shell-Type Power Transformer Characteristics

The basic difference between a core-type and a shell-type transformer consists on the arrangement of the steel core with reference to the windings (Figure 2.1). In the core-type transformer, the winding surrounds the laminated steel core. In the shell-type transformer the steel core surrounds the windings. Each of these types of construction has its own advantages and disadvantages. Core-type transformers were the subject of study in a

previous master dissertation from FEUP (Assembleia 2008), as well as other previous studies with FEUP (Campelo 2009).

In the shell-type design the core is wrapped or stacked around the coil. This leads to flat oval-shaped coils called *pancake* coils, with HV and LV windings stacked on top of each other, generally in more than one layer in an alternating way. In this type of interleaved arrangement, individual coils are stacked separated by insulating barriers and cooling channels. The center of the coil is hollow and square shaped, core limbs with square cross section then pass through the hollow center of the coils laid horizontally so the coils are stacked horizontally on edge. The return paths for the core go around the coils forming a *shell* around the windings, hence this this type of transformers being called shell.

Shell-type transformers tends to be preferred for extra high voltage and higher MVA applications because, though more labor-intensive to manufacture, shell-type transformers are characterized as having inherently better kVA-to-weight ratio, better short-circuit strength characteristics and higher immunity to transit damage.

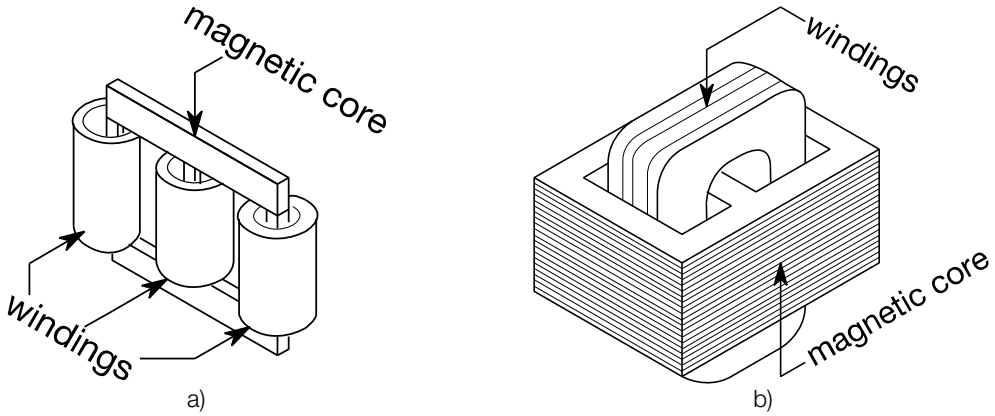

Figure 2.1 Schematic representation: a) core transformer; b) shell transformer.

2.1.3 The Magnetic Core

The power transformer core, which provides the path to channel the magnetic flux, consists of thin sheets of high-grade steel called laminations, which are electrically separated by a thin coating of insulating material. The sheet can be stacked, with the windings built separately and assembled around the core section.

Transformers for use at power or audio frequencies typically have cores made of silicon steel – steel specially tailored to produce certain magnetic properties such as small hysteresis area and high permeability. Present designs construct the core by stacking layers

of thin laminations. Laminating the steel contributes to confine eddy currents to highly elliptical paths that enclose little flux, and so reduce their magnitude.

2.1.4 Windings

The power transformer windings are typically stranded with a rectangular cross section. Multiple strands can be wound in parallel and joined together at the ends of the winding. Individual strands may be subjected to differences in the alternating flux field due to their relative positions within the winding, which create differences in voltages between the strands and drive circulating currents through the conductor loops. It is then necessary to transpose the strands at various points throughout the windings to cancel out these voltage differences and eliminate or greatly reduce the circulating currents that are sources of stray losses. A variation of this technique, involving many rectangular conductor strands combined into a cable, is called continuously transposed cable (CTC).

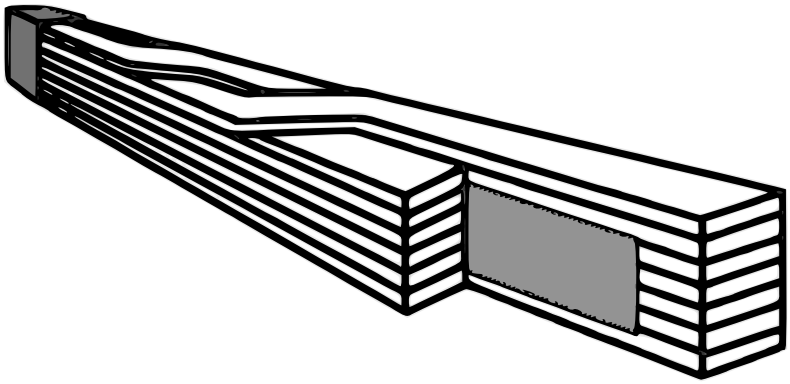

Figure 2.2 CTC cable representation.

The coils are placed in alternating groups of HV and LV windings, referred to as an interleaved arrangement, around the core. This arrangement offers various advantages:

- reduces the reactance between the coils around the core, improving the operation of the transformer particularly in large size transformers where heavy currents are experienced;
- allows the short circuit forces of the HV and LV windings to act in opposite directions, thus, partially cancelling each other out and further increasing the short circuit withstand capability of the transformer;
- for a shell-type transformer, as the transformer capacity increases, the size of each coil is kept similar, but more HV and LV groups are added. This reduces the ampere-turns per winding group, keeping the short circuit force inside the transformer relatively constant for very large capacity units.

2.1.5 Cooling

To place the cooling problem in perspective, the accepted rule of thumb is that the life expectancy of insulation in all electric machines including all transformers is halved for every 7 ºC to 10 ºC increase in operating temperature. This life expectancy halving rule narrows down to about 7 ºC to 8 ºC in the case of transformer winding cellulose insulation (Grigsby 2001).

There are many forms of losses in a transformer, and although they have different sources, the ensuing result of these losses is heat buildup. Transformer losses can be divided into two general categories: load losses and no-load losses. No-load losses are independent of the applied load and include:

- hysteresis losses in the core laminations;
- eddy current losses in the core laminations, tank core clamps, bolts and other metallic components;
- losses by Joule effect due to no load exciting current:
- dielectric losses.

Load losses consist of the Joule copper losses across the winding electrical resistances that are produced by the applied current and of the stray currents in the windings that appear when the load is applied.

Cooling is performed by circulating a coolant fluid – based solely on natural or forced convection - through the windings. This flow can be somehow controlled through the use of strategically placed spacers – made of celluloid paper - within the winding. Spacers provide desired dielectric distance between conductors and tank wall, and adequate flow of coolant fluid around the windings; the use of mineral oil as a coolant fluid allows for optimization of both dielectric and cooling efficiency of the transformers. These spacers are typically glued to a sheet of insulating material, called a washer, to form comb shaped configurations (Figure 2.3). Windings are entirely covered by the oil/paper insulation and the core tightly surrounds the winding insulation.

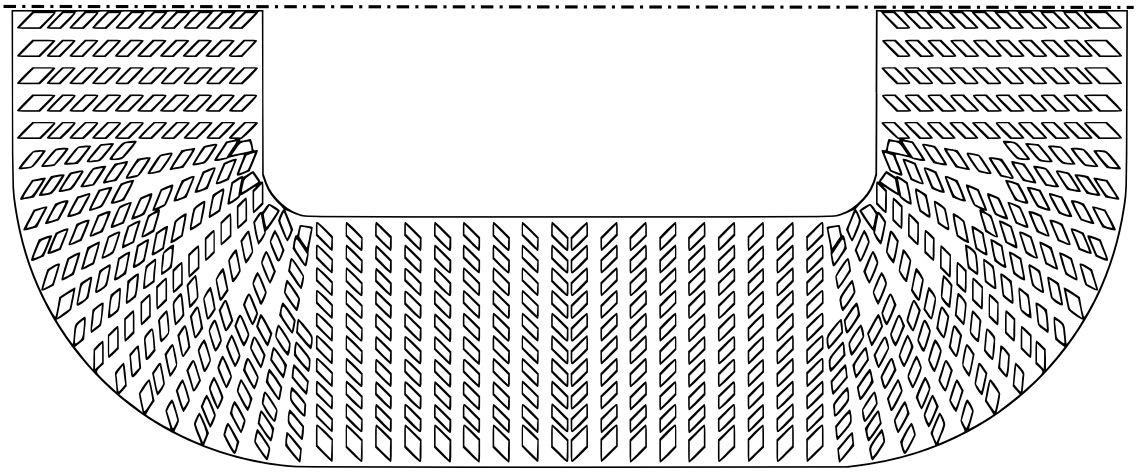

Figure 2.3 Representation of spacers in washer.

2.2 Simulation and Modeling Methodologies

2.2.1 Computational Fluid Dynamics

Computational fluid dynamics is the application of numerical methods and algorithms to solve fluid flow problems. It is a well-established technology that gained popularity around 1960s and continued to grow as the computers grew in computational power. The bases of CFD are the Navier-Stokes equations for single phase flow. These equations – solved in a finite elements or volumes domain - are simplified and complemented by other models describing various physical phenomena, from vorticity to chemical reaction.

Although CFD contains broad physical modeling capabilities needed to model fluid flow, it comes at the expense of high computational power and technical know-how, which makes it unviable for the daily industry needs. In this work the commercial software ANSYS Fluent was used.

2.2.2 Network Modeling

Network modeling is a solid and tried method of modeling phenomena common in system dynamics. These models – although primarily developed for electrical systems – can be applied to hydraulic systems. This methodology as already been successfully applied to prediction velocity and temperature fields on power transformers (Assembleia 2008; Campelo 2012). Electrical systems are modelled with this technique by constructing a mesh of nodes and branches that represent the system. Resistances and voltage sources are then determined with the application of Kirchoff laws to the mesh.

On its hydraulic counterpart, each channel corresponds to a branch and each junction of two or more channels correspond to a node. Electrical properties are converted to hydraulic ones based on an analogy, i.e., voltage corresponds to pressure and current corresponds to mass flow rate. The flow on the system is then solved by applying mass and transport conservation equations in the mesh.

On the thermal side of the problem, each coil bundle is also composed of branches alongside its length, where heat conduction equations are applied. Where the coil contacts the fluid in the washer an energy balance is established between the respective network branches, leading to changes that will have an impact in the flow solution.

The final solution is obtained by iterating the flow and thermal solver until the required accuracy criteria are achieved.

3 Technical Description

3.1 Model Considerations

Modelling a complete shell-type power transformer with CFD is out of reach from the available computational and time resources; therefore it was imperative to restrain the geometry to be modeled, to a representative portion. This representative portion was determined to be a coil and the adjacent washers, as this is the smallest representative geometry of the transformer windings (Figure 3.1). Moreover, this representative geometry can be further simplified – from a computational point of view – by modelling one fourth of it. Applying a symmetry at mid height on the coil and a longitudinal symmetry on the washer (Figure 3.2).

Both coils and washers can have several construction configurations. The configuration used for modelling corresponds to the one used on the construction of the scaled down pilot installation. The reason behind this decision lies on the idea that having a CFD model equal to a pilot installation can be strategically advantageous for further research and development.

The experimental pilot was built at a scale of one third of the original transformer geometry. This means that careful approach must be taken – especially on what relates to momentum and heat transfer - for the model to represent the phenomena at the original scale. The following subsections detail the considerations applied on all CFD simulations performed, unless specifically stated otherwise. Moreover the experimental pilot geometry presents some differences from the original transformer geometry (e.g. the flat insulating pieces). While these differences may prove influential their analysis is out of the scope of this work.

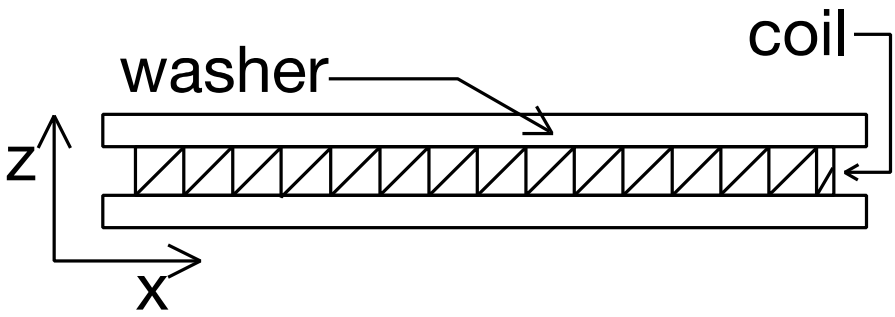

Figure 3.1 Coil and adjacent washers.

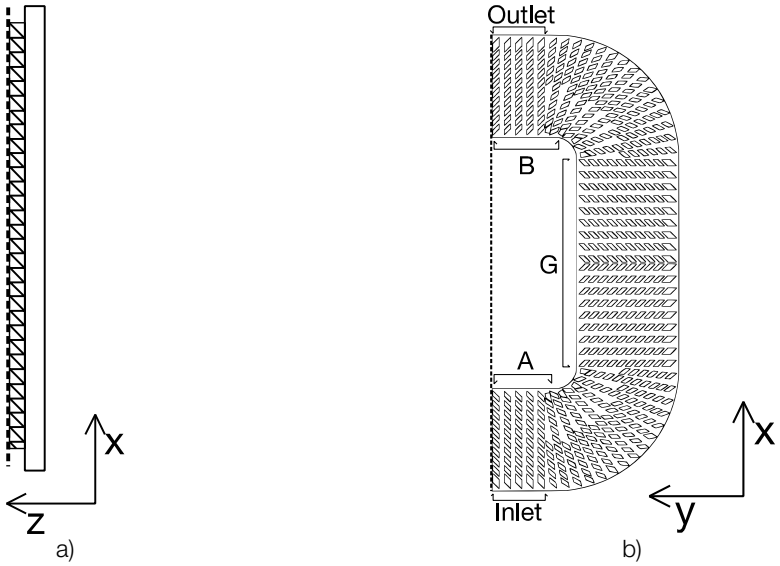

Figure 3.2 Symmetries applied to geometry: a) coil mid height symmetry; b) symmetry along the washer.

3.1.1 Types of Channels

Channels were separated in two categories based on their geometry: transverse and radial channels (Figure 3.3). These two types of channels are separated by a difference in the channel geometries. These geometric differences arise from the way these channels are constructed: transverse channels correspond to the gap between two spacers on the same row of spacers, while radial channels correspond to the gap between rows of spacers. The most distinguishable aspect of both types of channels is the aspect ratio. Since radial channels are constructed based on larger gaps they tend to present higher aspect ratios as defined by

$$\alpha = \frac{b}{a} \tag{3.1}$$

where α is the channel aspect ratio, a is the channel height and b is the channel width.

Another reason to work with this division of the channel types resides on FluSHELL working with this definition. In this sense, the mathematical expressions developed on this work should respect this implementation of the FluSHELL simulator.

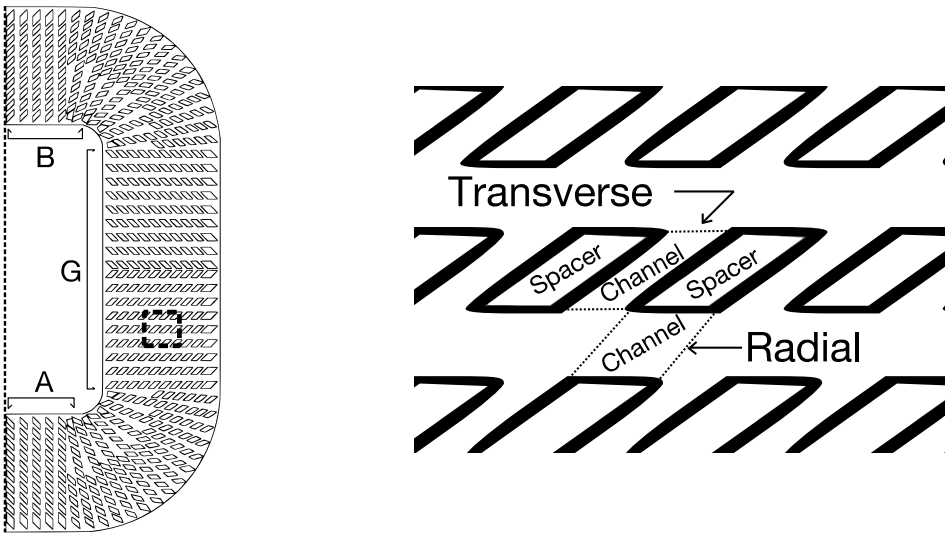

Figure 3.3 Channels in the washer: a) washer overview and zoomed region location; b) detail with the representation of both types of channels.

3.1.2 Flow Field Considerations

In order to keep the similarity of the flow field on the washer, the same average velocity magnitude both for the full scale washer channels and the scaled down washer channels was defined.

$$v^{\uparrow} = v^{\downarrow} \tag{3.2}$$

where $v^{\uparrow}$ is the average velocity in a full scale channel, and $v^{\downarrow}$ is the average velocity in a scaled down channel. In order for this to be verified, the relationship between the Reynolds number of the full scale geometry and the Reynolds number of the scaled down geometry is given by

$$\mathrm{Re}^{\downarrow} = \frac{d_h^{\downarrow}}{d_h^{\uparrow}} \mathrm{Re}^{\uparrow} = \varphi \, \mathrm{Re}^{\uparrow} \tag{3.3}$$

where φ is the scale factor between the scaled down geometry and the full scale geometry, $d_h^{\uparrow}$ is the hydraulic diameter of a full scale channel, $d_h^{\downarrow}$ is the hydraulic diameter of a scaled down channel, $\mathrm{Re}^{\uparrow}$ is the Reynolds number for a full scale channel and $\mathrm{Re}^{\downarrow}$ is the Reynolds number for a scaled down channel. The Reynolds number is defined as

$$\mathrm{Re} = \frac{\rho v d_h}{\mu} \tag{3.4}$$

where ρ is the density of the fluid and μ is the viscosity of the fluid. With a scale factor of $\varphi = 1/3$, the Reynolds number in the scaled down geometry will be three times lower.

$$\mathrm{Re}^{\downarrow} = \frac{1}{3}\mathrm{Re}^{\uparrow} \tag{3.5}$$

Thus the relationship between flow rates for the two geometries is given by

$$Q^{\downarrow} = \frac{A_f^{\downarrow}}{A_f^{\uparrow}} Q^{\uparrow} = \varphi^2 Q^{\uparrow} \tag{3.6}$$

where $A_f^{\uparrow}$ is the flow area of the full scale channel, $A_f^{\downarrow}$ is the flow area of a scaled down channel, $Q^{\uparrow}$ is the flow rate for the full scale geometry and $Q^{\downarrow}$ is the flow rate for the scaled down geometry. This equation then leads to

$$Q^{\downarrow} = \frac{1}{9} Q^{\uparrow} \tag{3.7}$$

As a consequence of this, the scaled down geometry presents a narrower and lower distribution of Reynolds numbers than the full scale geometry.

3.1.3 Heat Transfer Considerations

In order to simplify the modelling and simulation of the geometry, an equivalence was implemented for the coil. In this equivalence the coil bundles were represented by a surface contacting the fluid with a uniform heat flux boundary condition. This approach – referred as *hot plate* - eliminates the problem of contact areas between the coil and the washer.

Since the *hot plate* is an abstraction of a surface of zero thickness, an equivalence had to be established for it to represent the behavior of the coil. In this equivalence the total heat dissipated in the coil was converted in a heat flux condition

$$\lambda V_c = \Phi_q A_p \tag{3.8}$$

where λ is the heat dissipated in the coil, V_c the coil volume, Φ_q the hot plate heat flux and A_p the *hot plate* surface area. This yields a boundary condition of constant heat flux for the hot wall that contacts the fluid. A schematic representation of this can be found in section A.2.

3.1.4 Physical Properties

Simulations were performed using temperature dependent physical properties for the fluid. The fluid used was Nynas Nytro Taurus naphthenic oil, using the physical property functions

- for density, specific heat capacity and thermal conductivity - given by the supplier. Viscosity dependence with temperature was given by (Gomes 2007a). Detailed information of the temperature dependence of these properties can be found in annex B.

3.1.5 Convergence Criteria

All simulations were performed complying with *de facto* standards for CFD simulations, i.e., solver second order discretization schemes and iteration until residuals were at least lower than 10^{-6}. Nonetheless that was not the only criteria applied. Other necessary conditions include the stabilization of oil mass flow rate at the simulations domain boundaries and stabilization of average and maximum temperatures on monitoring surfaces.

3.1.6 Best Practices for Data Extraction

Data extraction should follow best practices guidelines, some of which may affect the accuracy of the extracted values. Of all these guidelines it is worth highlighting the following: the difference of area weighted average and mass weighted average when computing fluid properties; wall values are very sensitive to the extraction method, whenever possible preprocessed surfaces should be used; when extracting cell data (e.g. profiles) the points where the equations are solved should be used (e.g. Fluent solves equations for the cell centers, in this case cell center values should be used instead of node values which are obtained via interpolations).

3.1.7 Parameters to Study

While FluSHELL is able to predict the flow and temperature fields in the washer and coil, the mathematical expressions it uses were developed for a specific set of operating conditions. In order to improve the applicability of FluSHELL it is imperative to widen the correlations range of validity. In this work the goal is to extend the correlations to common transformer design parameters.

The first design parameter to take into account is the washer height. Different washer heights lead to different channel aspect ratios, which in turn develop different hydrodynamic conditions. For this study three different washer heights were simulated, of those it is important to highlight: 1.33 mm is the height from scale down of a real power transformer; 1.95 mm is the height of the experimental pilot available. Table 3.1 shows a summary of the washer heights simulated.

Table 3.1 Summary of heights simulated.

Nominal Height	Height [mm]	Channel Aspect Ratio (Width/Height)
1.33H	1.33	6.21 – 11.0
1.46H	1.46	5.66 – 10.0
1.95H	1.95	4.24 – 7.52

The flow rate is arguably the most important parameter for the correlations. Having a large spectrum of flow conditions is paramount for obtaining correlations that capture the flow features as well as having sufficient data to correctly model it. For this parameter a reference flow rate was chosen and multiples – within common operating conditions - of that flow rate were simulated. Of these multiples it is worth highlighting the multiple 1.38Q as this is a standard operating flow rate of the experimental pilot. Table 3.2 shows a summary of the flow rates simulated. In this table is also shown the parameter $\overline{v}_{1.33\mathrm{H}}$ which is the average velocity in the G zone of the washer for a washer with 1.33 mm of height – which can be directly extrapolated to a full size washer and is an often used design parameter.

Table 3.2 Summary of flow rate simulated conditions.

Nominal Flow Rate	Mass Flow Rate [kg/h]	$\overline{v}_{1.33\mathrm{H}}$ [cm/s]
2Q	146.9	27.4
1.38Q	101.5	19.0
Q	73.4	13.7
0.5Q	36.7	6.8
0.25Q	18.4	3.4

The coil dissipated heat was also a parameter to extend. There were two simulated conditions: 450 W is the standard coil power used on the development of FluSHELL and 1014 W is a common used coil power. Table 3.3 shows a summary of these conditions as well as the parameter heat flux, which is a common design parameter and also a boundary condition used in CFD.

Table 3.3 Summary of coil power simulated conditions.

Nominal Coil Power	Coil Power [W]	Heat Flux [W/dm^2]
450W	450	15.2
1000W	1014	34.3

Simulations were prepared with combinations of these parameters in order to study their influence in the correlations. Some of this combinations were deemed not realistic due to presenting a theoretical fluid temperature rise higher than a pre-established threshold. Table 3.4 shows the realistic combinations for each height.

Table 3.4 Summary of realistic simulation conditions.

	2Q	1.38Q	Q	0.5Q	0.25Q
450W	Realistic				
1000W	Realistic			Not Realistic	

Results were processed in order to observe the effect of changing the washer height and changing the coil power. For this effect the 5 different flow rates of 450W simulations were compared across the 3 different heights to observe the influence of height on the correlations. The 3 feasible flow rates for 1000W simulations were compared with the correspondent flow rates for the 450W simulations for one height to observe the effect of coil power on the correlations.

3.1.8 Recirculation Factor

CFD analysis shows that some degree of recirculation may occur on specific channels on the washer. The FluSHELL simulator assumes that each channel has an inlet and outlet without these recirculations. Thus it is not desirable to include data points were these recirculations appear. For this a parameter called recirculation factor was defined to quantify these recirculations and act as a criterium to exclude data points.

Recirculation factor was defined as

$$RF = \frac{\left| \int \rho \vec{v}_{in} \cdot d\vec{A}_{in} - \int \rho \vec{v}_{out} \cdot d\vec{A}_{out} \right|}{\int \rho \vec{v} \cdot d\vec{A}} \tag{3.9}$$

where RF is the recirculation factor, ρ the fluid density, $\vec{v}_{in}$ the velocity magnitude vectors in the channel inlet, $\vec{A}_{in}$ the facet areas in the channel inlet, $\vec{v}_{out}$ the velocity magnitude vectors in the channel outlet, $\vec{A}_{out}$ the facet areas in the channel outlet, $\vec{v}$ the average velocity magnitude vectors in the channel and $\vec{A}$ the average facet areas in the channel. In this work, the criterion established for the recirculation factor was that it could not be above 2% for a data point to be accepted. RF could be expressed as

$$RF = \frac{\left| \dot{m}_{in} - \dot{m}_{out} \right|}{\dot{m}} \tag{3.10}$$

where $\dot{m}_{in}$ is the mass flow in the channel inlet, $\dot{m}_{out}$ is the mass flow in the channel outlet and $\dot{m}$ the average mass flow in the channel.

Nonetheless, it is erroneous to express the recirculation factor in this form as it may lead to the conclusion that there is a local mass imbalance in the channel – this hypothesis is discarded as CFD residual values for the continuity equation are orders of magnitude below the established criterion for data points exclusion.

The recirculation factor physical meaning resided in its vector form. It arises as a product of sufficiently different velocity profiles in the channel inlet and outlet and their subsequent integration on the inlet and outlet surfaces. Moreover some degree of recirculation factor may also arise from the integration of high magnitude vectors on relative large areas – product of a mesh discretization constraint – that may occur of the flow curvatures near the sharp edges of the spacers.

3.2 Mesh Study

Mesh sensitivity analysis is a standard procedure in CFD. In order to quantify the sensitivity of the results obtained from the simulations, the influence of mesh discretization and solver discretization scheme was analyzed. The mesh analysis focused on two parameters to study: mesh number of elements discretization and solver discretization schemes.

The mesh number of elements discretization study resided on the axial coordinate discretization. This direction was chosen because it has the lower number of elements, the discretization increase on this direction has the most impact of the total number of mesh elements and this direction is directly implied with heat transfer on the washer. For this purpose different meshes with different axial number of elements were prepared with the considered discretizations of 6, 9 and 12 elements in the axial coordinate. The nominal references Mesh6, Mesh9 and Mesh12 were adopted respectively for these meshes. A schematic representation can be found in section A.2.

For the solver discretization scheme study each of the previously prepared meshes was simulated with second order and first order solver discretization schemes. These are the only simulations on this work converged with first order discretization schemes, and were performed in order to evaluate the impact of converging a solution with first or second order discretization schemes.

The analysis was conducted in a sampling of channels. The sampled channels were picked in order to get a broad representation of the various zones of the washer. A descriptive representation of the sampled channels can be found in section A.1.

On these channels the analyzed parameters were:

- average wall temperature (of the channel wall representing the *hot plate*);
- maximum wall temperature;
- average oil temperature rise (difference on the oil temperature between the channel inlet and outlet);
- recirculation factor;
- total shear stress (exerted on the four channel walls);
- average wall-oil temperature (difference between the average wall temperature and the average oil temperature).

3.2.1 Model Boundary Conditions

The boundary conditions used for these simulations are summarized in Table 3.5. It is worth noting that these simulations used a pressure inlet boundary condition which was only used on these mesh study simulations.

Table 3.5 Mesh studies boundary conditions.

Boundary Conditions	
Pressure Inlet [Pa]	800
Heat Flux [W/dm^2]	15.2
Inlet Temperature [°C]	60

3.2.2 Number of Elements

For these simulations the effect of the mesh number of elements, along the axial coordinate, was analyzed. Although the analysis focus on sampled channels, the global results can be found in annex C.

For the results on the sampled channels Mesh12 was taken as a reference, since it has the highest discretization it should yield the results with best accuracy. This comparison was done by calculating the difference between the analyzed mesh and the reference (i.e., in case of Mesh6 the results presented are the difference between Mesh6 and Mesh12 values).

Figure 3.4 shows the difference in the average wall temperature. Figure 3.5 shows the difference in the maximum wall temperature.

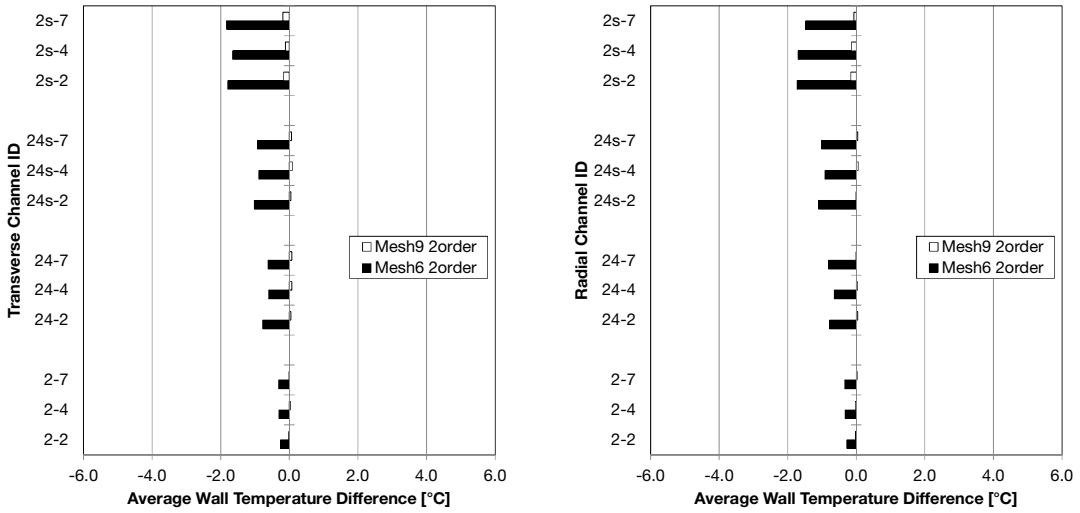

a) b)

Figure 3.4 Number of elements influence on average wall temperature: a) transverse channels; b) radial channels.

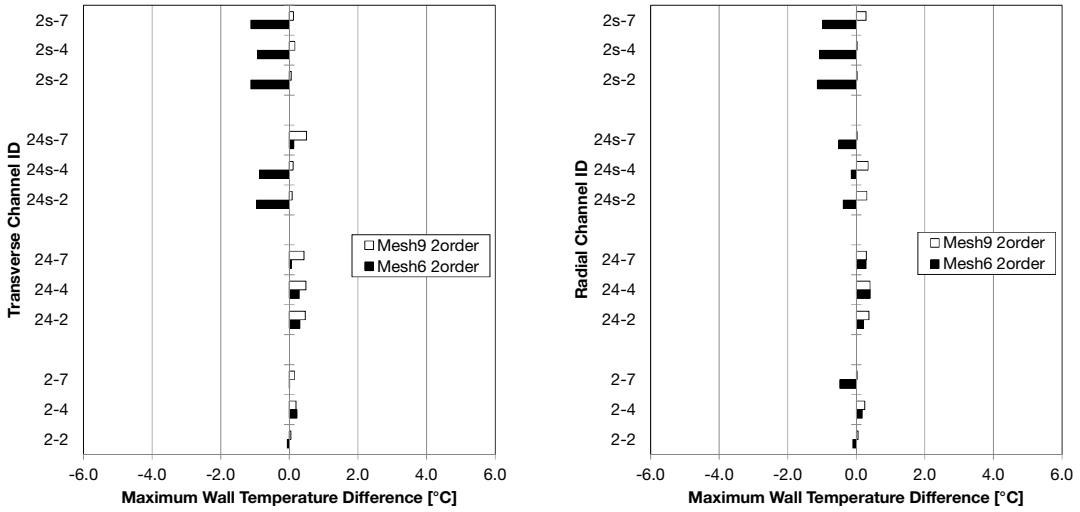

a) b)

Figure 3.5 Number of elements influence on maximum wall temperature: a) transverse channels; b) radial channels.

Figure 3.6 shows the difference in the average oil temperature rise. Figure 3.7 shows the difference in the recirculation factor.

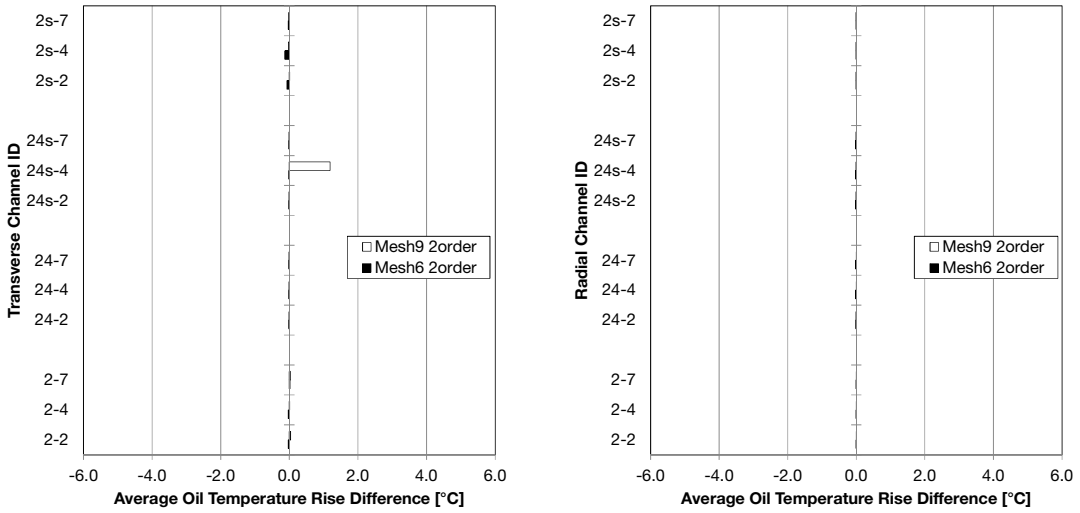

a) b)

Figure 3.6 Number of elements influence on average oil temperature rise: a) transverse channels; b) radial channels.

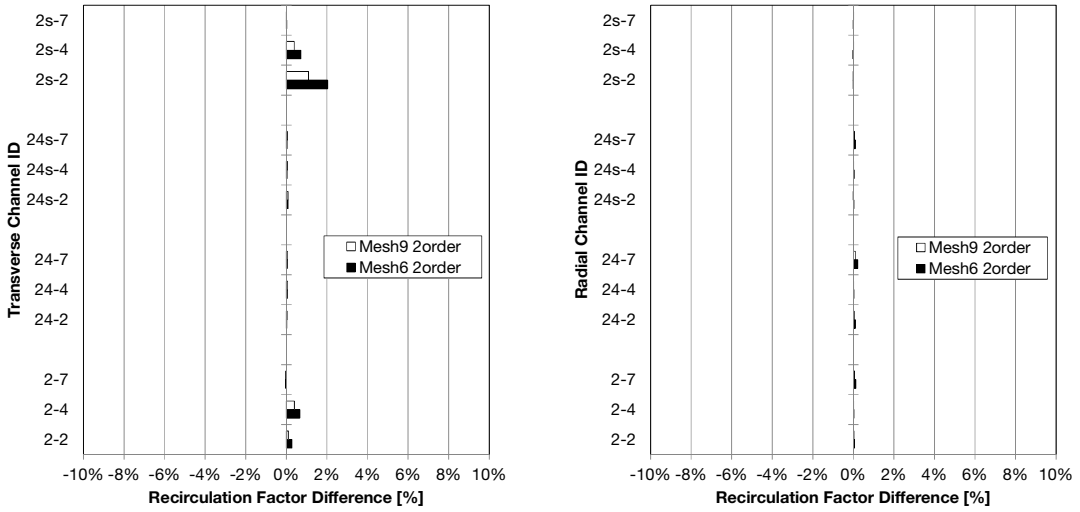

a) b)

Figure 3.7 Number of elements influence on recirculation factor: a) transverse channels; b) radial channels.

Figure 3.8 shows the difference in the total channel shear stress. Figure 3.9 shows the difference in the average wall-oil temperature.

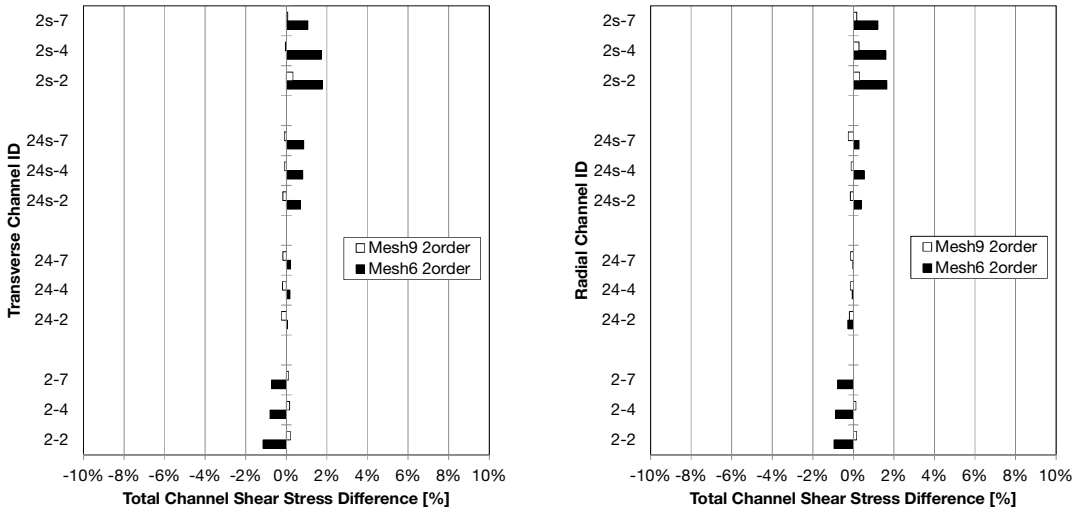

a) b)

Figure 3.8 Number of elements influence on total channel shear stress: a) transverse channels; b) radial channels.

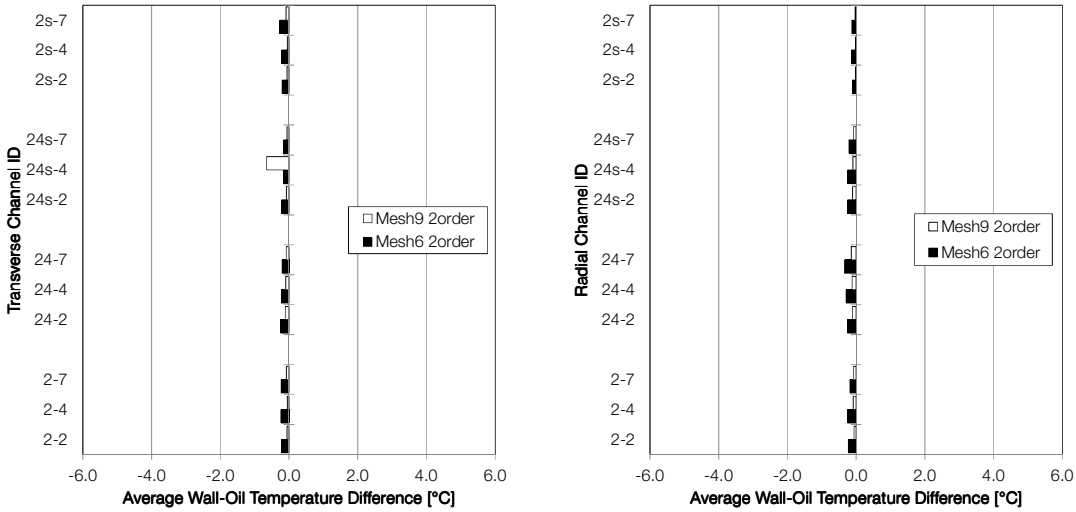

a) b)

Figure 3.9 Number of elements influence on average wall-oil temperature: a) transverse channels; b) radial channels.

Table 3.6 shows the percent difference of the average wall-oil temperature. It is a support table for the interpretation of Figure 3.9 as it shows the relative significance of the observed temperature differences.

Table 3.6 Percent differences of average wall-oil temperature values

	Percent Differences [%]			
	Transverse channels		Radial channels	
Channel	Mesh6	Mesh9	Mesh6	Mesh9
2s-7	-3.5	-1.1	-1.7	-0.4
2s-4	-2.7	-0.6	-1.7	-0.3
2s-2	-2.3	-0.7	-1.4	-0.2
24s-7	-2.0	-0.7	-2.7	-1.0
24s-4	-2.0	-8.2	-3.1	-1.2
24s-2	-2.7	-1.0	-3.1	-1.3
24-7	-2.5	-1.0	-4.4	-1.9
24-4	-2.8	-1.2	-3.6	-1.5
24-2	-3.1	-1.4	-3.2	-1.4
2-7	-2.8	-1.0	-2.3	-1.0
2-4	-2.5	-0.5	-3.3	-1.2
2-2	-3.1	-0.8	-3.3	-0.9

3.2.3 Solver Discretization Scheme

For these simulations the effect of the solver discretization scheme was analyzed. Although the analysis focus on sampled channels, the global results can be found in annex C.

For the results on the sampled channels the respective second order simulation was taken as a reference, since second order methods should yield the results with best accuracy. This comparison was done by calculating the difference between the analyzed mesh and the reference (i.e., in case of Mesh6 the results presented are the difference between values of Mesh6 with first order methods and Mesh6 with second order methods).

Figure 3.10 shows the difference in the average wall temperature. Figure 3.11 shows the difference in the maximum wall temperature.

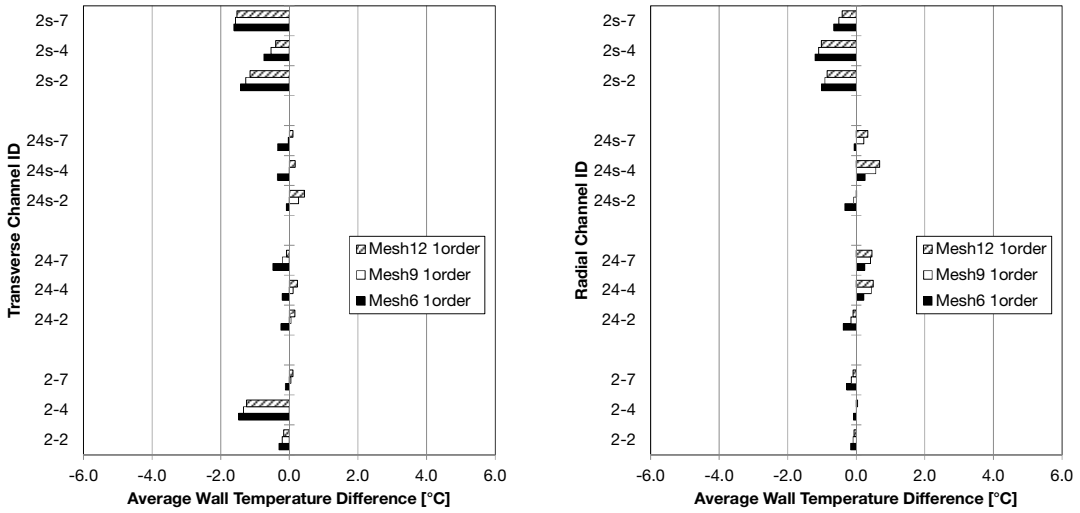

a) b)

Figure 3.10 Discretization scheme influence on average wall temperature: a) transverse channels; b) radial channels.

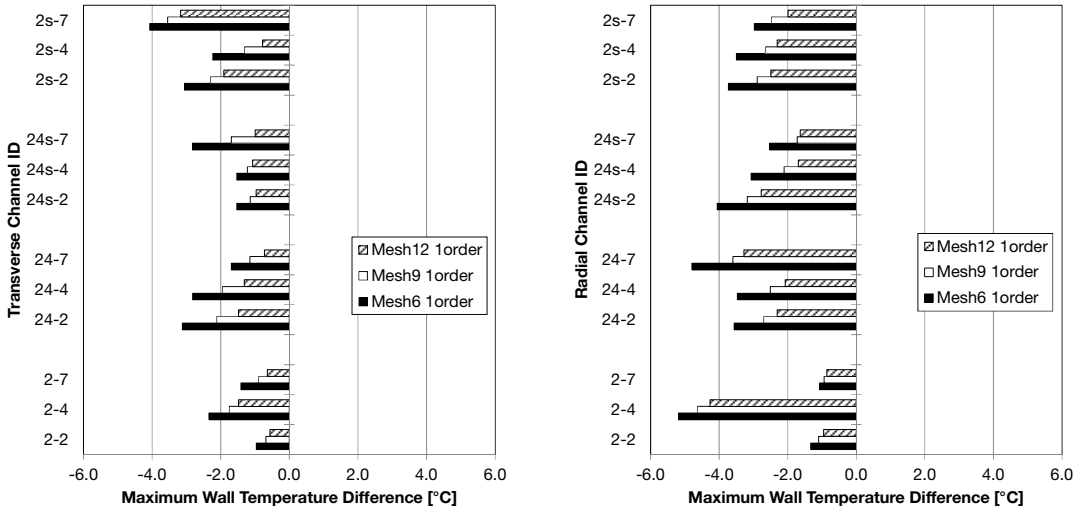

a) b)

Figure 3.11 Discretization scheme influence on maximum wall temperature: a) transverse channels; b) radial channels.

Figure 3.12 shows the difference in the average oil temperature rise. Figure 3.13 shows the difference in the recirculation factor.

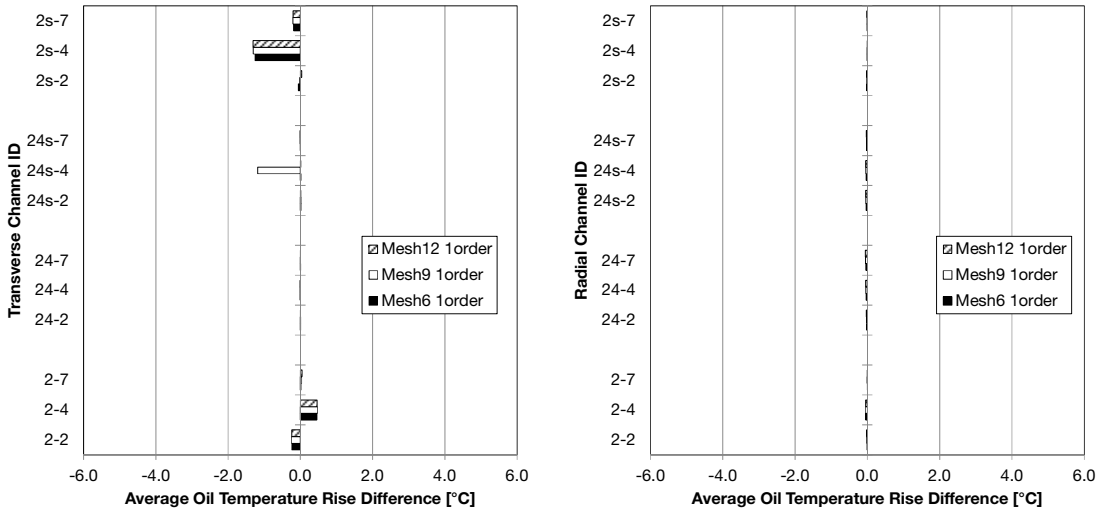

a) b)

Figure 3.12 Discretization scheme influence on average oil temperature rise: a) transverse channels; b) radial channels.

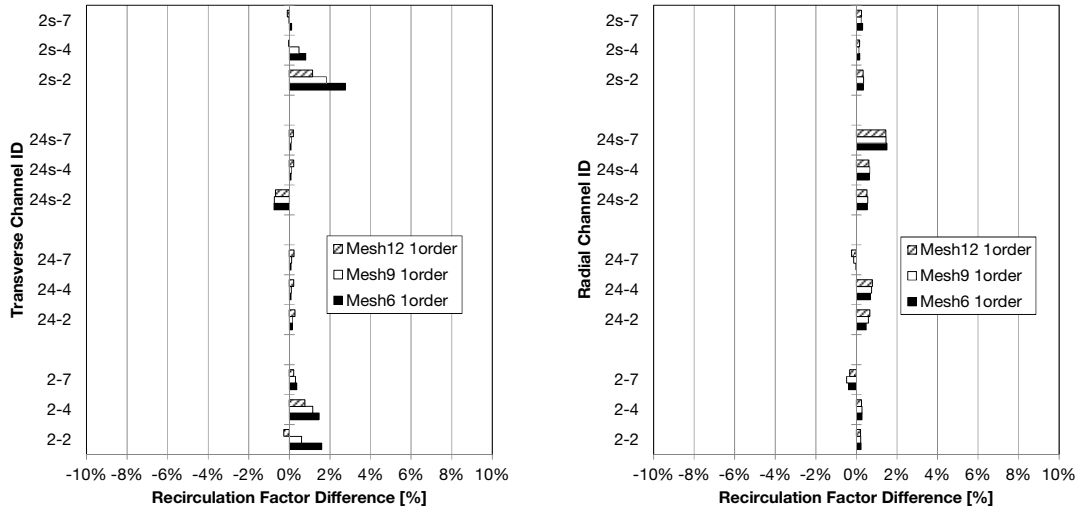

a) b)

Figure 3.13 Discretization scheme influence on recirculation factor: a) transverse channels; b) radial channels.

Figure 3.14 shows the difference in the total channel shear stress. Figure 3.15 shows the difference in the average wall-oil temperature.

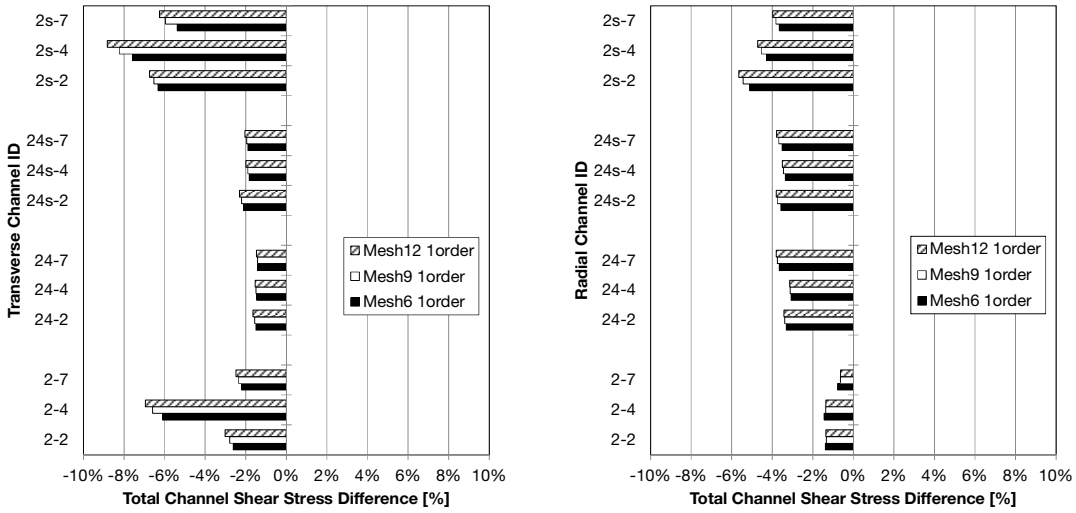

a) b)

Figure 3.14 Discretization scheme influence on total channel shear stress: a) transverse channels; b) radial channels.

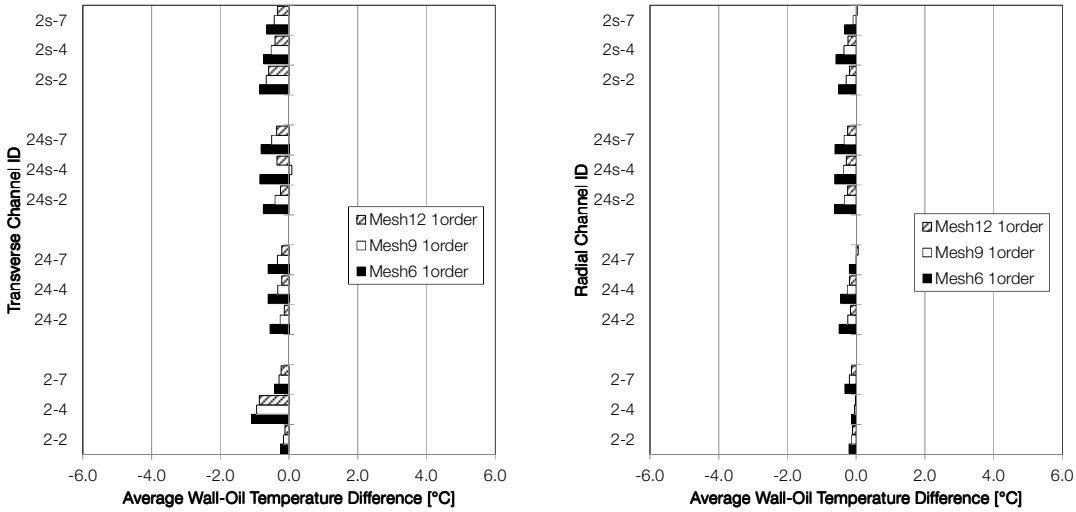

a) b)

Figure 3.15 Discretization scheme influence on average wall-oil temperature difference: a) transverse channels; b) radial channels.

Table 3.7 shows the percent difference of the average wall-oil temperature. It is a support table for the interpretation of Figure 3.15 as it shows the relative significance of the observe temperature differences.

Table 3.7 Percent difference of average wall-oil temperature values.

	Percent Differences [%]					
	Transverse channels			Radial channels		
Channel	Mesh6	Mesh9	Mesh12	Mesh6	Mesh9	Mesh12
2s-7	-8.8	-5.7	-4.3	-4.7	-1.2	0.4
2s-4	-9.4	-6.4	-5.1	-7.7	-4.5	-3.0
2s-2	-10.4	-7.9	-7.0	-6.7	-3.7	-2.4
24s-7	-10.5	-6.4	-4.5	-8.2	-4.6	-3.2
24s-4	-10.9	1.1	-4.5	-8.2	-4.8	-3.6
24s-2	-10.0	-5.4	-3.2	-8.5	-4.5	-3.2
24-7	-8.0	-4.3	-2.6	-2.7	0.1	0.8
24-4	-8.0	-4.3	-2.7	-5.9	-3.3	-2.4
24-2	-7.5	-3.4	-1.8	-6.6	-3.2	-2.1
2-7	-5.5	-3.8	-2.9	-4.4	-2.6	-1.8
2-4	-11.9	-10.1	-9.2	-1.9	-0.7	-0.2
2-2	-3.6	-2.3	-1.7	-3.1	-2.0	-1.5

3.2.4 Mesh Study Conclusions

From the results observed in the mesh studies it is possible to conclude that:

- although there is influence of the number of elements discretization, the differences are for the most part negligible;
- solver discretization scheme shows non negligible influence in the solution results; second order solver discretization schemes should be used to maximize solution accuracy;
- taking into account absolute and relative measures the most sensitive parameter on this work is the wall-oil temperature difference: thus the influence of these differences in the Nusselt number should be the target of further research.

3.3 Flow Hydrodynamic Analysis

The flow in a washer was already studied on a companion paper (Gomes 2007b) where it was concluded from CFD simulations that changing the flow rate lead to essentially the same flow pattern, with lower velocity magnitudes and smaller recirculation zones as the flow rate decreases. These conclusions were also supported by the results form laser experiments.

This study focused on the aspects that influence the development of mathematical expressions for modelling flow and heat transfer within the current scope. The analysis reported in this section is divided in washer-wide results and local results. Washer-wide results are comprised mainly by property maps on the whole domain, while local results focus on a representative location (same locations used in mesh studies, see section A.1). A special focus was also taken to the inlet region of the washer.

While this section focus on details of the various property fields (i.e. velocity, temperature and pressure) the global results for the simulations performed can be found in annex C. Also worth noting that as the mesh studies conducted showed negligible differences for the impact of number of elements, these simulations were conducted on a mesh with 6 elements of height due to time constraints.

3.3.1 Inlet Flow Pattern

This section explores the parameters that can affect the flow pattern in the inlet: the flow rate (in the form of pressure inlet boundary condition) and the height of the washer.

3.3.1.1 Influence of Pressure Boundary Condition

Simulations were projected with a pressure inlet boundary condition and the objective of converging to a set flow rate. Common methods to achieve this imply setting an initial pressure inlet guess and then iterating until the desired flow rate is achieved. For the simulations performed on work this proved to be a time consuming process

The flow profile is imposed by the resistances encountered along the flow path – essentially these resistances are imposed by the geometry. Based on this, a change in the flow rate would have an effect on the flow magnitude but not on the flow profile.

On this premise, a simulation with pressure inlet boundary condition was converged to meet all the required criteria. From this simulation the inlet mass flow profile was extracted. This profile was used in further simulations in conjunction with an average mass flux boundary condition. This yields the same flow profile but with the desired flow rate without the need to iterate the simulations.

Figure 3.16 shows the inlet dimensionless pressure and velocity profiles for 2 simulations, one with pressure inlet BC and the other with mass flux BC. Dimensionless values were obtained by dividing each value by the maximum registered. These simulations were performed at different mass flow rates and show identical behaviors on the profiles, thus implying that on this case the pressure and velocity distribution in the inlet are independent from the pressure applied.

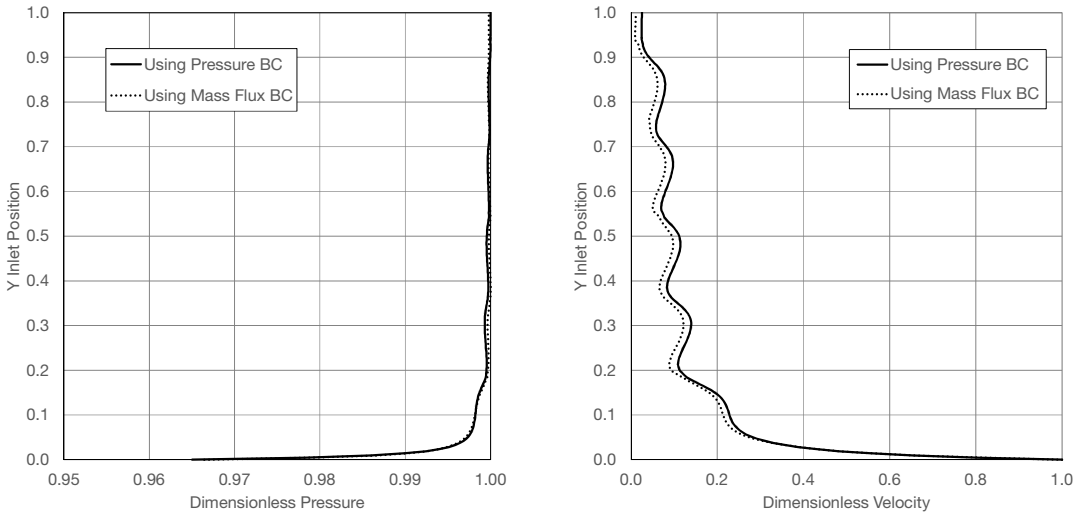

Figure 3.16 Inlet profiles for different boundary conditions: a) pressure profile; b) velocity profile.

3.3.1.2 Influence of Height

After the previous analysis a question that may arise is the independence (or not) of the flow pattern in the inlet from the washer height. To clarify this question two simulations were performed with the same mass flow rates but on different washer heights. Figure 3.17 shows the obtained inlet dimensionless pressure and velocity profiles for these simulations. As expected the change of height does not seem to have an effect on the inlet distribution of pressure and velocity, as the profiles for both height seem to be identical.

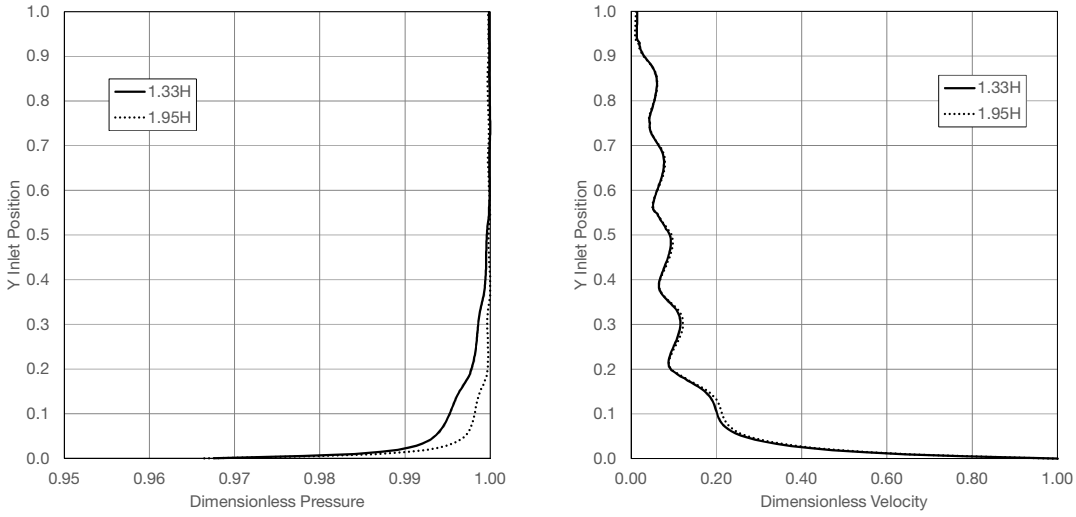

Figure 3.17 Inlet profiles for different washer heights: a) pressure profile; b) velocity profile.

3.3.2 Flow Pattern Overview

This subsection aims to present an overview of the highlights on the flow along the washer and for this purpose the various property fields are presented separately. In order to cover the extent of the observed phenomena the results shown are for the maximum and minimum simulated flow rate.

As property maps are presented an important aspect to clarify is the map scales. For this purpose the scales were chosen with criteria that allow to establish qualitative comparisons between the different flow rates. Scale limits applied to property maps. present a summary of the criteria applied to the map scales.

Table 3.8 Scale limits applied to property maps.

Field	Lowest Value	Highest Values
Velocity Magnitude	0	$3 \times \overline{v}_{\mathrm{G}}$
Static Temperature	Inlet temperature (boundary condition)	Average outlet temperature
Static Pressure	Outlet Pressure (boundary condition)	Average inlet pressure

where $\overline{v}_{\mathrm{G}}$ is the average velocity in the G zone (calculated in a similar way as in Table 3.2).

3.3.2.1 Velocity

Figure 3.18 shows the velocity magnitude contour maps for maximum and minimum flow rates on the washer. As expected, the flow pattern is similar for both cases leading to the conclusion that the flow pattern is – to a certain degree – independent of the flow rate. The

observable differences reside on an increase of the recirculation on the channels and wake regions on the spacers. The complete set of velocity magnitude maps can be found in section D.1.

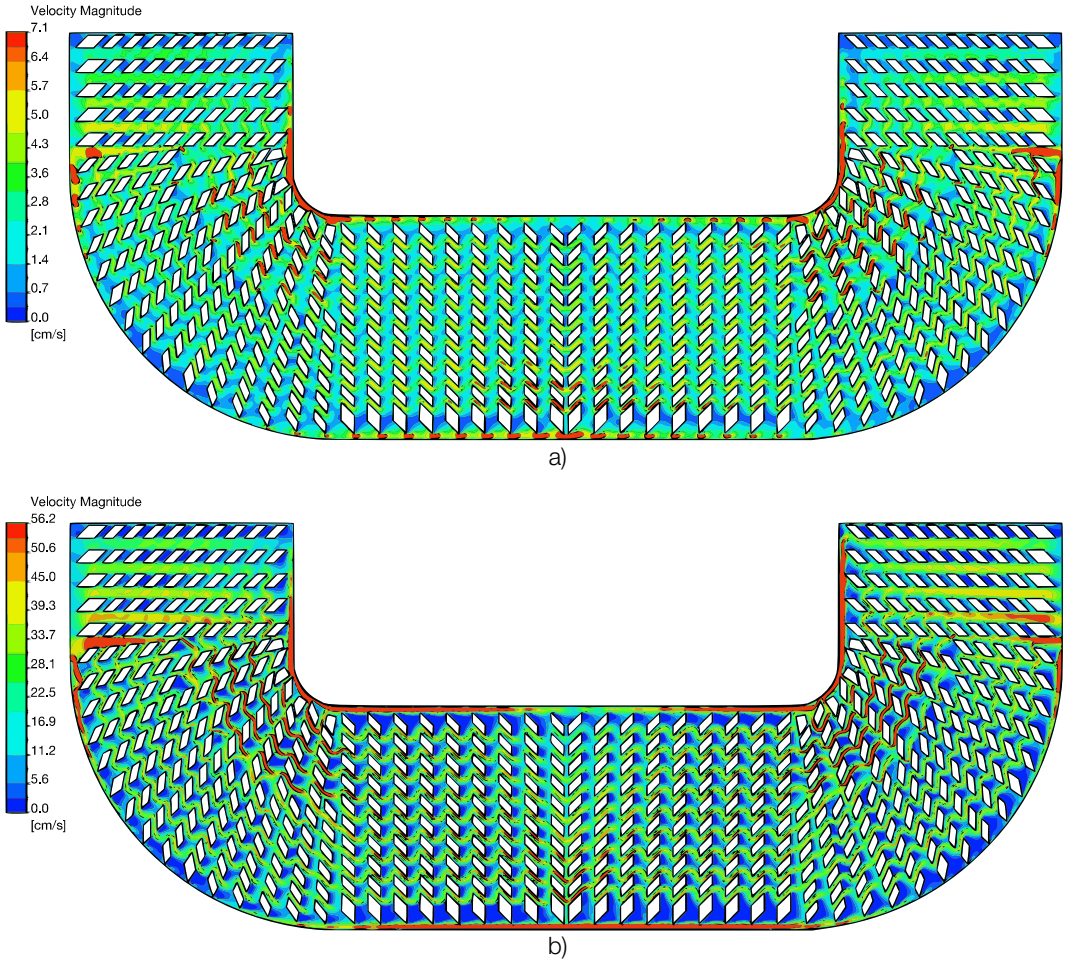

Figure 3.18 Velocity magnitude maps for different flow rates: a) 0.25Q; b) 2Q.

Figure 3.19 shows a close up of the vector field on a representative region (region of channels 24-4, see section A.2) of the washer for both flow rates. It is observable the effect of the flow rate on the increase of the recirculation on the channels. On a side note, it can also be observed that even for the minimum flow rate the inlet and outlet of the channels present a curved velocity profile – foreshadowing the hypothesis that the channels may not fully develop the flow along their length.

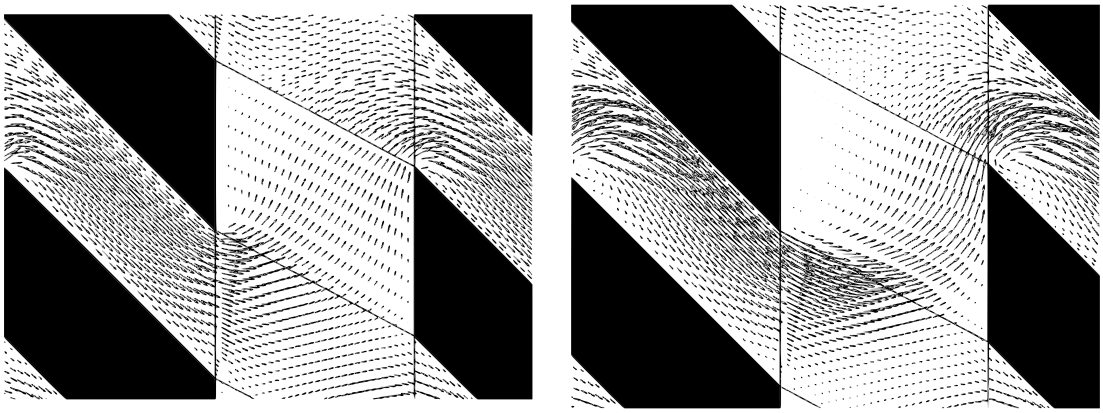

a) b)

Figure 3.19 Velocity magnitude vector field for different flow rates: a) 0.25Q; b) 2Q.

Figure 3.20 shows velocity profiles along a longitudinal centerline on the sampled representative channels. One of the various criteria to evaluate developed flow consists of constant velocity along the length of the channel. It is then observable that the criterion is not verified on the results shown. The complete set of velocity magnitude profiles on the sampled channels can be found in annex E.

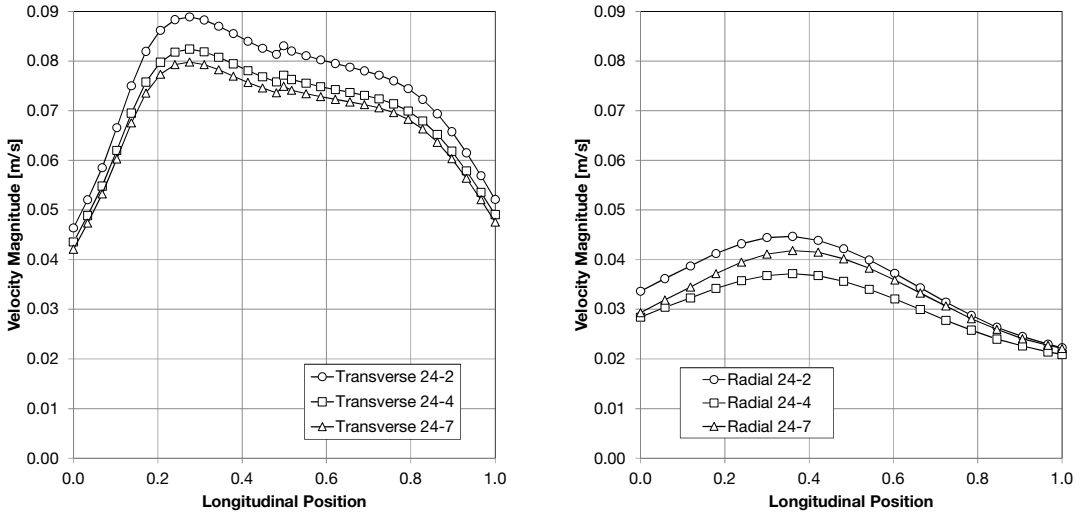

a) b)

Figure 3.20 Velocity magnitude longitudinal profiles: a) transverse channels; b) radial channels.

Figure 3.21 shows the velocity profile along a horizontal line that intersects transverse channels in line 24 (see section A.2). In this analysis the channels near the insulating pieces of the washer were excluded. These plots show a shift in the horizontal velocity magnitude profile as the flow rate increases, going from a balanced distribution at the lowest flow rate to a biased distribution (consequence of flow inertia) at the highest flow rate. The complete set of these plots can be found in section E.4.

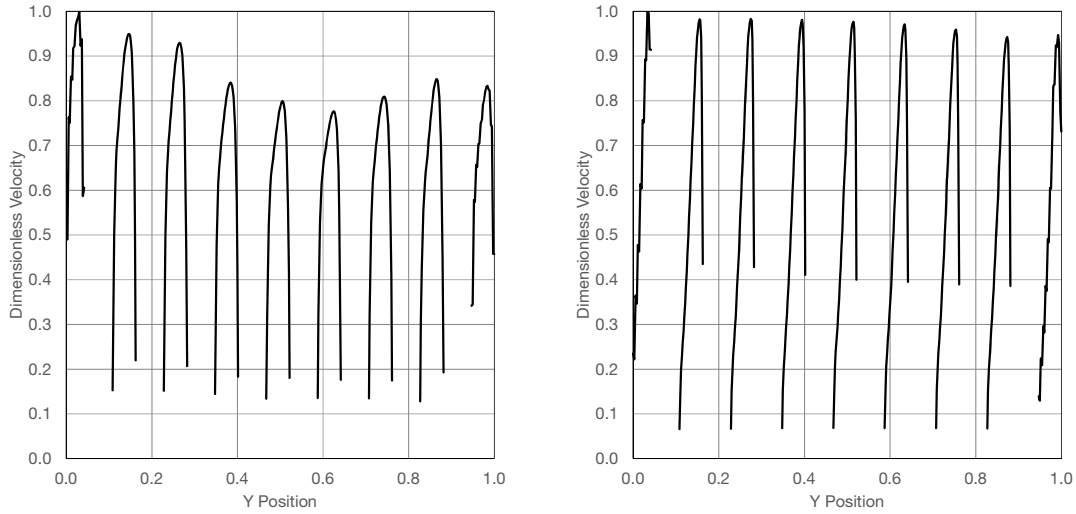

Figure 3.21 Velocity magnitude profiles in G zone for different flow rates: a) 0.25Q; b) 2Q.

3.3.2.2 Temperature

Figure 3.22 shows the static temperature contour maps for the maximum and minimum flow rate. It is observable that although higher flow rates contribute to lower average temperatures, they also reveal a more heterogeneous distribution promoting the appearance of hot pockets of fluid formed on the – larger, for higher flow rates - recirculation zones.

It is also observed the influence of the non-uniform flow distribution. Higher flow rates present larger temperature *red zones* and these zones appear sooner on the washer (in terms of longitude).

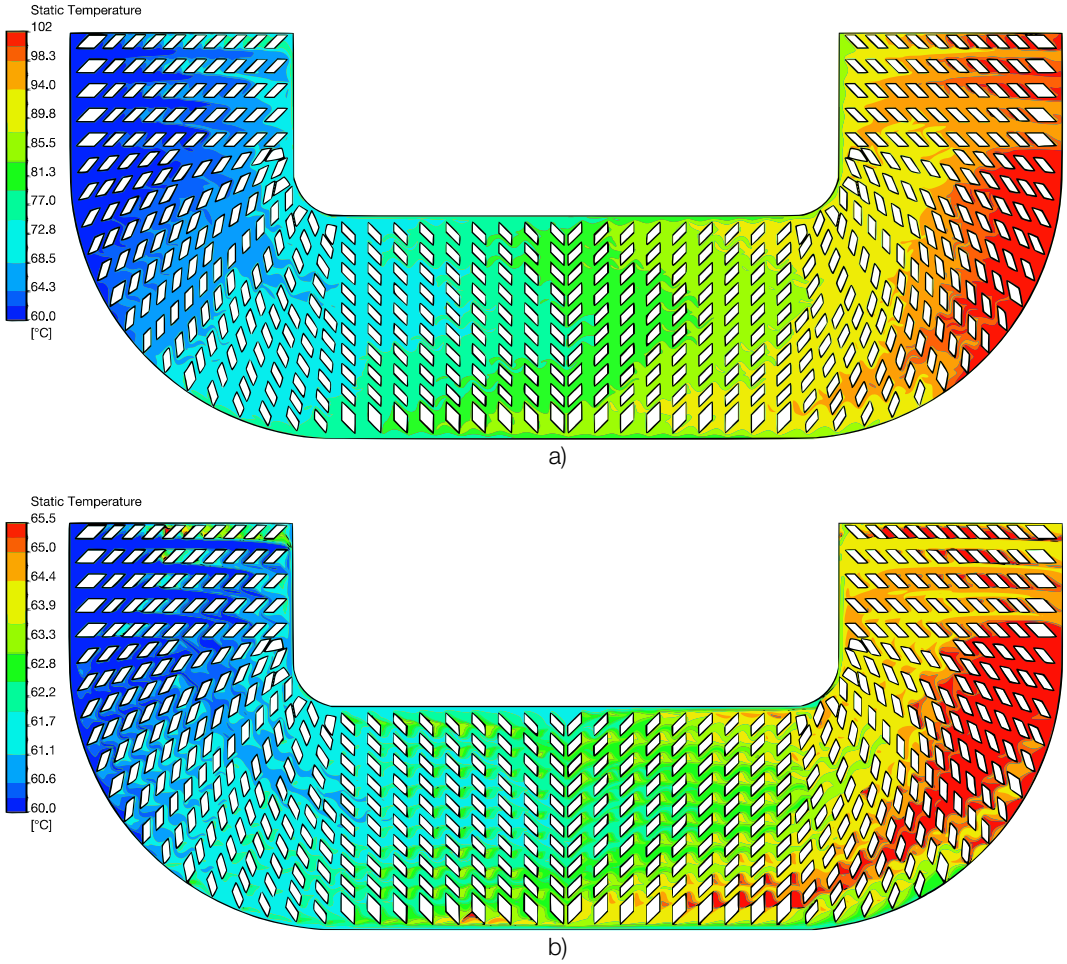

Figure 3.22 Temperature maps for different flow rates: a) 0.25Q; b) 2Q.

Figure 3.23 shows the isothermal lines in the close up region (see section A.2). It is observable hot pockets of fluid developed on the higher wake regions of high flow rates – a consequence of fluid not being renewed on those areas - thus promoting a more heterogeneous temperature distribution.

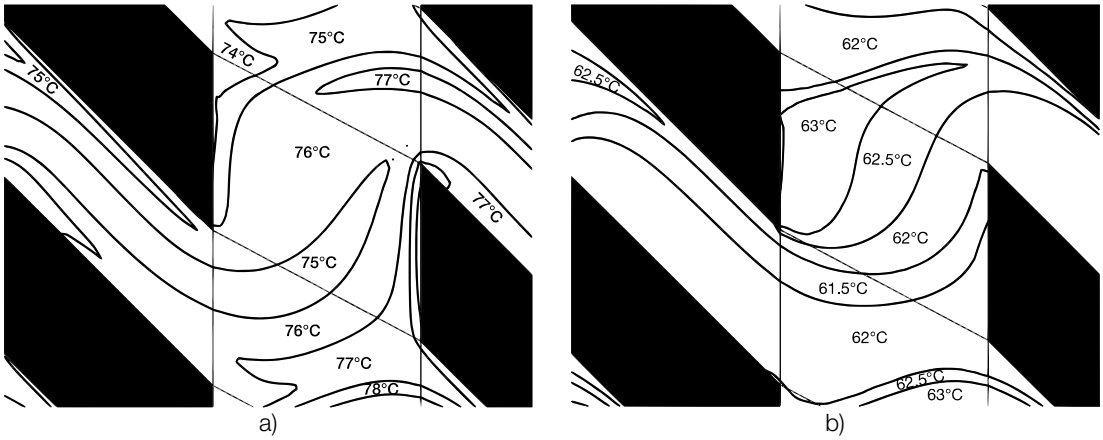

Figure 3.23 Isothermal lines for different flow rates: a) 0.25Q; b) 2Q.

Figure 3.24 shows the average and maximum temperatures for the oil and wall. One important aspect that can be observed it that there is a change of behavior around Q flow

rate. For flow rates below Q the average and maximum temperatures decrease with an increase in the flow rate. For flow rates above Q, the increase in flow rate decreases the average temperatures but increases the maximum temperatures. This is an expected consequence of the increase in recirculation for higher flow rates, as shown before.

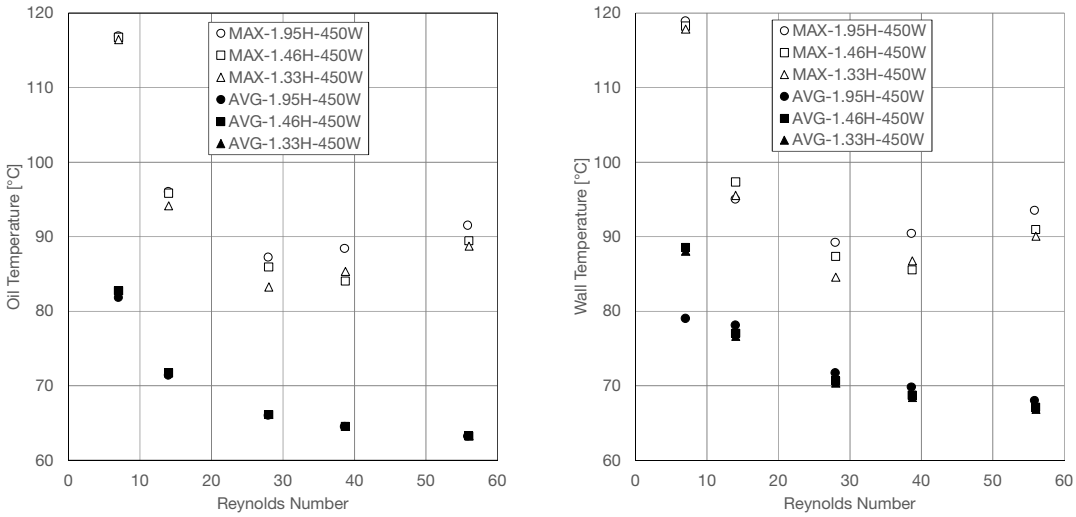

a) b)

Figure 3.24 Average and maximum temperature values: a) oil temperature; b) wall temperature.

3.3.2.3 Pressure

Figure 3.25 shows the static pressure maps for the maximum and minimum flow rate simulations. From this analysis it can be observed that the pressure map is not distributed in a homogeneous way. This pressure distribution contributes to a – already observed – heterogeneous flow distribution.

Pressure drop data is important to design power transformers. Figure 3.26 shows the pressure drop value for the simulations used to develop the correlations. It is observable the effect of washer height for the same mass flow, as well as the behavior of pressure drop as the flow rate increases.

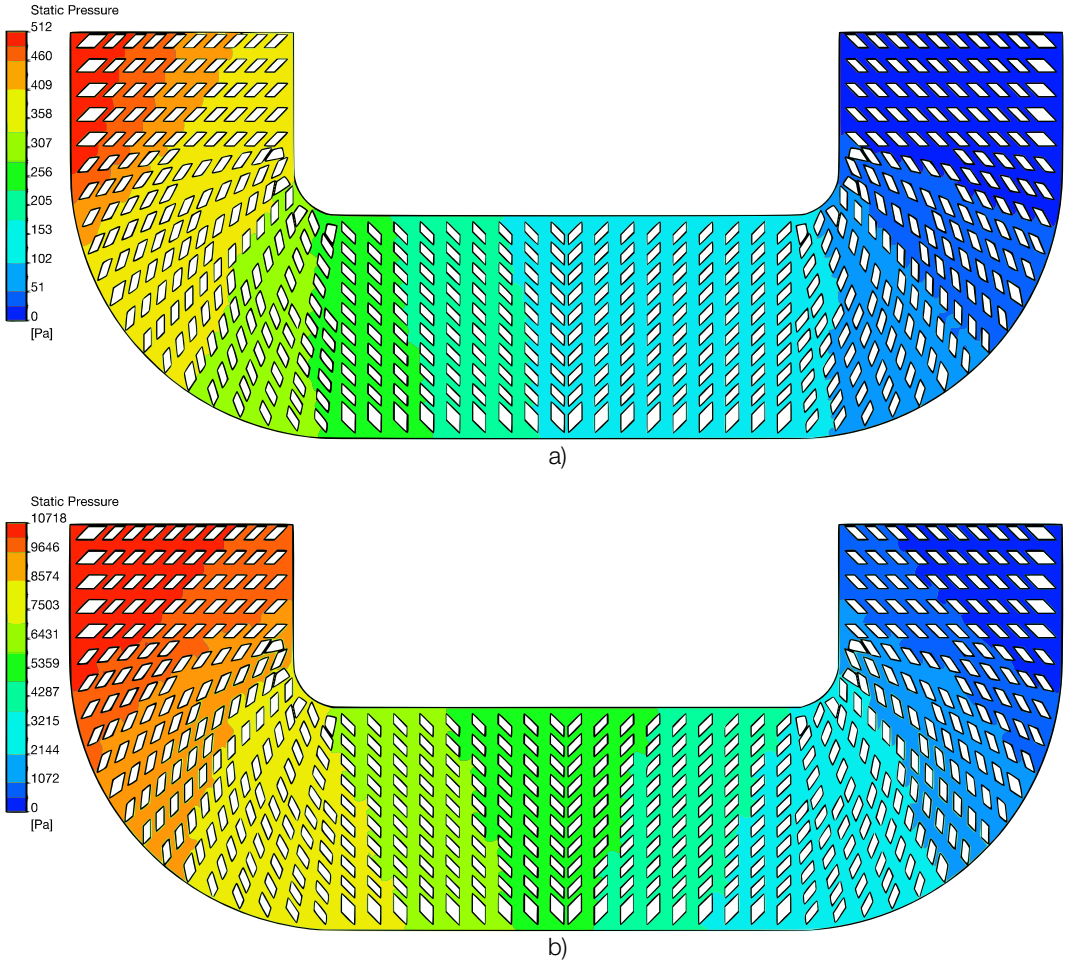

Figure 3.25 Pressure map for different flow rates: a) 0.25Q; b) 2Q.

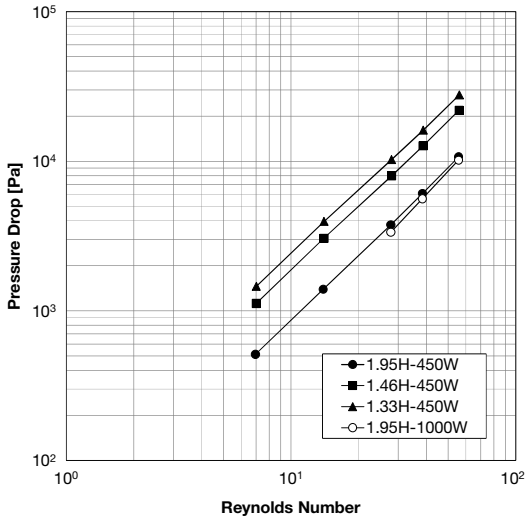

Figure 3.26 Pressure drop for the simulated cases.

3.3.3 Flow Hydrodynamic Conclusions

The inlet flow pattern showed no changes to the variation of flow rate and washer height.

The velocity field results showed that:

- flow shows a non-uniform distribution throughout the washer;
- the flow pattern is essentially the same with the flow rate variation;
- higher flow rate increases the flow curvature in the channels;
- higher flow rate increases the recirculation zones;
- the flow in the channels does not reach a fully developed condition.

The temperature field results showed that:

- the temperature distribution is non-uniform as a consequence of the flow pattern non-uniformity.
- higher recirculation zones lead to *hot pockets* of fluid as a consequence of fluid not being renewed on those locations;
- there is a flow rate point after which, an increase in the flow rate does not imply a decrease in the maximum temperatures registered.

The pressure field results showed that:

- the pressure distribution on the washer is non-uniform which contributes to the flow non-uniformity.
- it is possible to establish simple relationships to predict the global pressure drop on the washer for different flow rates and washer heights.

3.4 Correlations Development

3.4.1 Friction Factor Correlations

The pressure drop in a channel can be obtained by means of a force balance applied on the channel, where the force for the fluid to flow is equal to the friction force on the walls

$$A_f \Delta P = \sum_w \tau_w A_w \tag{3.11}$$

where A_w is the area of the wall in which friction is exerted, A_f is the flow area in the channel, ΔP is the pressure drop in the channel, τ_w is the shear stress on the walls and index w refers to all the channel walls. A schematic representation of the channel can be found in section A.2.

The friction factor can be determined using

$$\Delta P = \frac{1}{2} f \rho \frac{L}{d_h} v^2 \tag{3.12}$$

where f is the friction factor, L is the channel length, d_h is the channel hydraulic diameter and v is the average velocity in the channel. The friction factor can then be determined by

$$f = \frac{2 d_h}{v^2 L} \frac{\sum_w \tau_w A_w}{A_f} \tag{3.13}$$

In laminar flow, the friction factor for developed velocity profiles is inversely proportional to Reynolds number, that is

$$f = \frac{\mathrm{C}}{\mathrm{Re}} \tag{3.14}$$

where C is a constant that depends on the geometry of the flow channel. For the case of flow between parallel plates of infinite width $\mathrm{C} = 96$ (Incropera 2011).

The analytical solution for rectangular ducts with varying aspect ratios has been published by (Kays 1980; Shah 1971) and will be used as a reference to compare the results obtained in this work.

Figure 3.27 shows the C values for the correlations, adjusted to the different sets of data, separated by type of channel. It is also shown the theoretical results of this parameter as published by (Shah 1971).

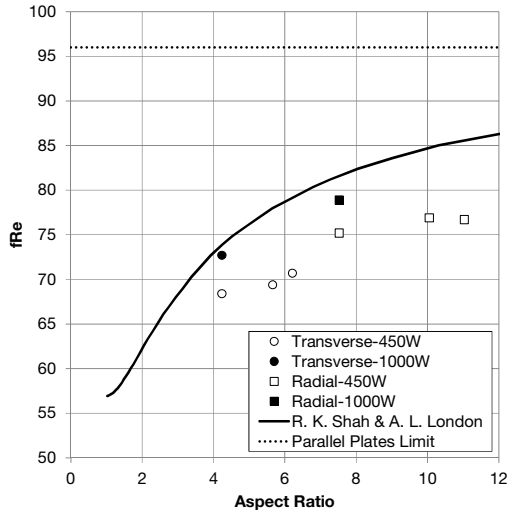

Figure 3.27 Friction factor results.

Friction factor results show similar distributions across the different heights and across the different coil powers. The C values show a deviation from theoretical results – as an expected consequence of not having the same flow conditions of those in the theoretical results. Moreover, the results show that height – and to an extension, aspect ratio for the different types of channel - affects the friction factor within the presented range of C values.

3.4.2 Nusselt Number Correlations

The dissipated heat by the coil is transferred through the washer walls to the oil, and can be determined by

$$W = hA_{hx}\Delta T \tag{3.15}$$

where W is the dissipated heat, h is the heat transfer coefficient, A_{hx} the area available for heat exchange and ΔT the temperature difference in the channel. ΔT is defined as the difference between the average hot wall temperature and the fluid average channel inlet temperature.

$$\Delta T = T_h - T_{in} \tag{3.16}$$

where T_h is the average hot wall temperature on the channel, and T_{in} is the fluid average channel inlet temperature. A schematic representation of the channel can be found in section A.2.

By energy balance the exchanged heat through the walls is equal to the enthalpy output between the inlet and the outlet

$$W = Q\rho C_p \left(T_{out} - T_{in}\right) \tag{3.17}$$

where T_{in} is the fluid average channel inlet temperature, T_{out} is the fluid average channel outlet temperature, Q is the volumetric flow rate in the channel, ρ is the fluid density and C_p is the fluid specific heat capacity in the channel. By means of the enthalpy balance, the exchanged heat can be calculated with CFD simulations.

Once the exchanged heat is known and the temperature differences are calculated, the average heat transfer coefficient can be determined for the channel

$$h = \frac{W}{A_{hx}\Delta T} \tag{3.18}$$

where h is the average heat transfer coefficient. This parameter is usually expressed in terms of the dimensionless Nusselt number

$$\mathrm{Nu} = \frac{h d_h}{\kappa} \tag{3.19}$$

where κ is the fluid thermal conductivity. For a channel with fully developed temperature profile, the Nusselt number is a constant; for the case of parallel plates with constant heat flux on one of the plates, it takes the value of $\mathrm{Nu} = 5.39$ (Shah 1974). However, if the temperature is still developing along the channel the Nusselt number will not be constant, however it can be approximated with an expression of the form

$$\mathrm{Nu} = A\,\mathrm{Re}^n + \mathrm{Nu}_{\mathrm{lim}} \tag{3.20}$$

where A and n are fitting parameters and $\mathrm{Nu}_{\mathrm{lim}}$ is the Nusselt number for fully developed temperature profile conditions. Analytical solutions for rectangular ducts of varying aspect ratio and heat flux on one wall were published by (Shah 1971) and will be a reference for comparing the results obtained in this work.

Figure 3.28 shows the $\mathrm{Nu}_{\mathrm{lim}}$ values for the correlations, adjusted to the different sets of data, separated by type of channel. The theoretical results of this parameter are also shown.

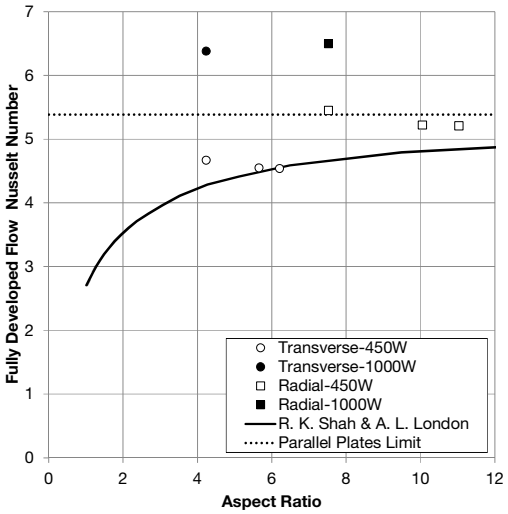

Figure 3.28 Nusselt number results.

Nusselt number results show similar distributions across the different heights and across the different coil powers. The $\mathrm{Nu}_{\mathrm{lim}}$ values show a good degree of agreement with theoretical results, apart from 1000 W simulations for which $\mathrm{Nu}_{\mathrm{lim}}$ appears higher than expected.

3.5 FluSHELL Performance

The developed correlations were implemented in the FluSHELL simulator to analyze the impact on its performance. This analysis was conducted with the nominal conditions of 1.33H and 450 W in order to compare with previous FluSHELL results.

For this comparison several locations were sampled along the G zone, as the more representative part of the geometry. A representation of the sampling locations can be found in section A.3.

3.5.1 FluSHELL Overview

While this work is focused on the development of mathematical expression for the FluSHELL simulator, it is important to remember that FluSHELL is a network model developed to predict the flow and temperature fields on shell transformers coils and washers.

For a qualitative analysis, with the results obtained from CFD simulations, FluSHELL was set with the parameters Q, 450W and 1.33H. Figure 3.29 shows the flow field map predicted by FluSHELL, where it is observable that FluSHELL predicts a flow pattern with all the important features observable in CFD maps. Figure 3.30 shows the temperature field map on the washer, where it can be observed that FluSHELL captures the temperature pattern and the location of the hottest zones. Additionally FluSHELL can also predict the temperature field for the coil, but unfortunately in this work there is no CFD map with which to establish a comparison.

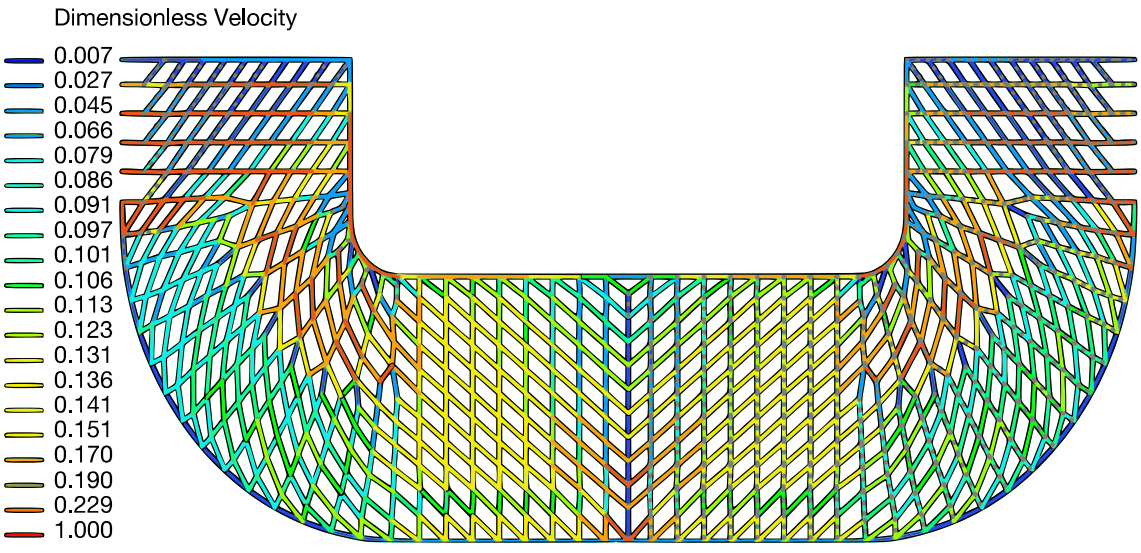

Figure 3.29 FluSHELL velocity map for Q, 450W and 1.33H.

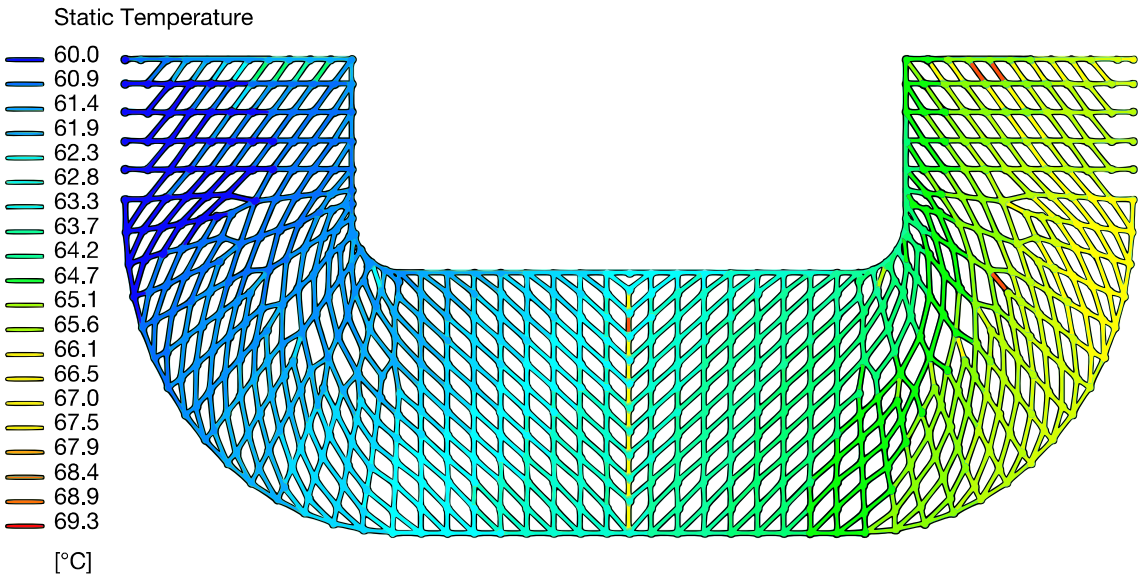

Figure 3.30 FluSHELL temperature map for Q, 450W and 1.33H.

3.5.2 Results

This analysis compares the difference between FluSHELL and CFD predictions for a simulation with equal mass flow rate on both simulators. The comparisons focus on the temperature field of both washer and coil.

Figure 3.31 shows the difference between FluSHELL and CFD predictions for the original FluSHELL correlations (FluSHELL-Base) and the correlations developed in this work (FluSHELL-i1). Each point in the chart represents the respective average difference between FluSHELL and CFD on the sampled line. Each line is composed of several channels and coil bundles, and the point represents the average temperature deviation for these channels/bundles. The detailed plots of the sampled lines can be found in annex F.

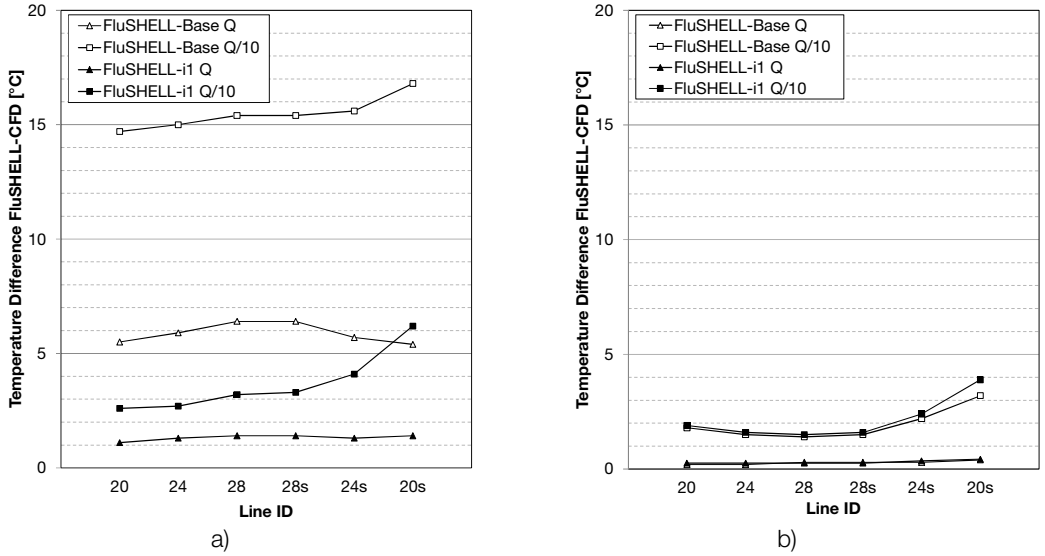

Figure 3.31 FluSHELL performance results.

3.5.3 FluSHELL Performance Conclusions

The correlations developed in this work show a significant increase in the accuracy – relative to CFD prediction – of the temperature in the coil. While at the same time keeping the already achieved degree of accuracy in the fluid temperature.

4 Conclusions

4.1 Objectives Accomplished

The project main objectives were:

- study and description of the flow in the cooling channels of a shell-type transformer;
- development of mathematical expressions to integrate the FluSHELL simulator;
- compare the performance of the FluSHELL simulator with the developed mathematical expressions.

Objective 1: This objective was completed successfully. The flow in the cooling channels was described in relation to most important property fields. The analysis performed explored the important aspects of each property field allowing for conclusions both at a global and local scale. Also this study allowed for new questions to arise and contributed to broaden the field when it comes to shell transformers.

Objective 2: This objective was completed successfully. The mathematical expressions developed are consistent with the available literature, and accurately model conditions that beyond the literature expressions.

Objective 3: This objective was completed successfully. The mathematical expressions developed resulted in a considerable improve in FluSHELL accuracy, while at the same time keeping the accuracy on the aspects not improved.

4.2 Limitations and Future Work

The greatest limitation on this work was time. As CFD simulations are time intensive, the time limitation forced strategic decisions on where to concentrate resources in order to obtain a balance of quality and quantity of simulations. More time available would imply more extensive analysis and a greater set of simulation conditions.

For future work the most interesting suggestions would be:

- replicate these analysis segregating the channel modeling by other criteria besides the geometric one. More specifically, it would be interesting to explore criteria based on dynamics;
- research of possible physical phenomena not accounted for is of great interest, i.e., researching the influence that natural convection has in this system;
- improving the topological details not accounted for in this work, as the inclusion of detailed insulating pieces on the washer.

4.3 Final Appreciation

The developed work was very interesting and provided a great challenge. The context of the problem was unusual for a chemical engineering student, but was an opportunity to learn more about electricity and electrical concepts. It provided familiar topics to explore in a deeper level of detail (fluid dynamics and heat transfer). The main motivation was being able to work in an area of my interest (CFD). It is motivating to see from the future work suggestions that this work can be of help to other studies that will delve deeper in the modelling of similar problems.

References

- Assembleia, André, 2008. Simulação do Escoamento e Transferência de Calor em Transformadores de Potência (Simulation of Flow and Heat Transfer in Power Transformers). M.Sc. Dissertation, Faculdade de Engenharia da Universidade do Porto, Porto, Portugal.
- Campelo, H. et al., 2012. Network Modelling Applied to CORE Power Transformers and Validation with CFD Simulations. International Colloquium Transformer Research and Asset Management, Dubrovnik, Croatia.
- Campelo, H. et al., 2009. Detailed CFD Analysis of ODAF Power Transformer. International Colloquium Transformer Research and Asset Management, Cavtat, Croatia.
- Gomes, P.J. et al., 2007a. Studies in a Large Transformer – Heat Transfer and Flow Optimization using CFD. ARWtr 2007 – Advanced Research Workshop on Transformers, Baiona, Spain.
- Gomes, P.J. et al., 2007b. Large Power Transformer Cooling – Flow Simulation and PIV Analysis in an Experimental Prototype. ARWtr 2007 – Advanced Research Workshop on Transformers, Baiona, Spain.
- Grigsby, L., 2001. The electric power engineering handbook. CRC Press, Boca Raton.
- Hochart, Bernard., 1987. Power Transformer Handbook. Butterworth & Co, Saint Ouen.
- Incropera, Frank P., 2011. Fundamentals of Heat and Mass Transfer. Wiley, Hoboken.
- Kays, W.M., Crawford, M., 1980. Convective Heat and Mass Transfer. McGraw-Hill, New York.
- López-Fernández, X.M., 2013. Transformers: Analysis, Design, and Measurement. CRC Press, Boca Raton.
- Shah, R.K., London, A.L., 1974. Thermal Boundary Conditions and Some Solutions for Laminar Duct Flow Forced Convection. Journal of Heat Transfer 96, 159-165.
- Shah, R.K., London, A.L., 1971. Laminar Flow Forced Convection Heat Transfer and Flow Friction in Straight and Curved Ducts – A Summary of Analytical Solutions. Stanford University.

A General Schematics

A.1 Washer Schematics

In order to uniquely identify a location in the washer a reference system was adopted. The system takes the shape of two-dimensional matrix (Figure A.1) where each position on the matrix corresponds to node (confluence of channels). The channels are identified by the reference of the node on the inlet of the channel.

Figure A.1 shows the samples zones for the correlations with the dotted line. In this zones there are indications to identification of the reference matrix rows and columns. Each matrix position (and consequentially each channel) is referenced in the way of *row-column*, e.g., transverse channel 24-4. An important aspect to take into account is after row 28, the row numbering is symmetric adding only an *s* to denote the row is positioned in the symmetry zone.

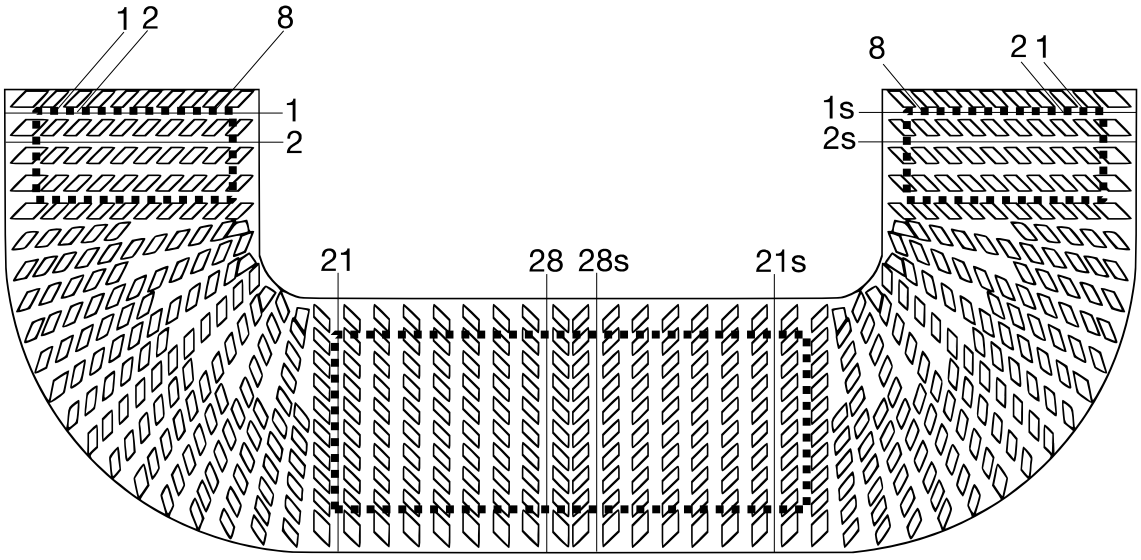

Figure A.1 Matrix of reference nodes on the washer.

Figure A.2 shows an applied example of the channel reference system. In this figure are shown the samples locations used in the mesh studies, taking into account that each location has a transverse and radial channel associated.

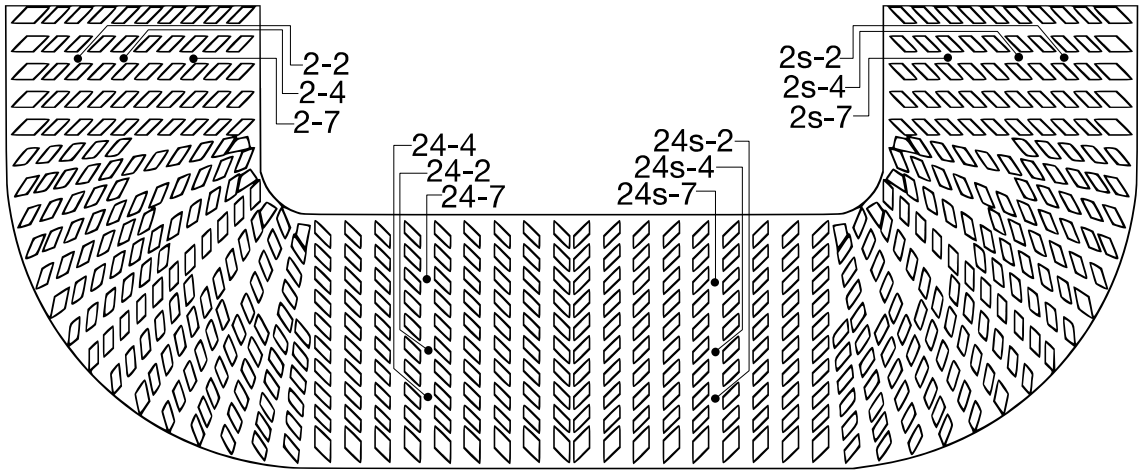

Figure A.2 Sampling locations used in the mesh studies.

A.2 Channel Schematics

This section consists of schematics to help comprehend the geometry around a channel, and the nomenclature used when describing the channel.

Figure A.3 shows an isometric representation of a generic channel. Apart from the labeled surfaces it is important to understand that alongside the channel vertical walls exist two spacers (as the channel is formed by the gap between spacers).

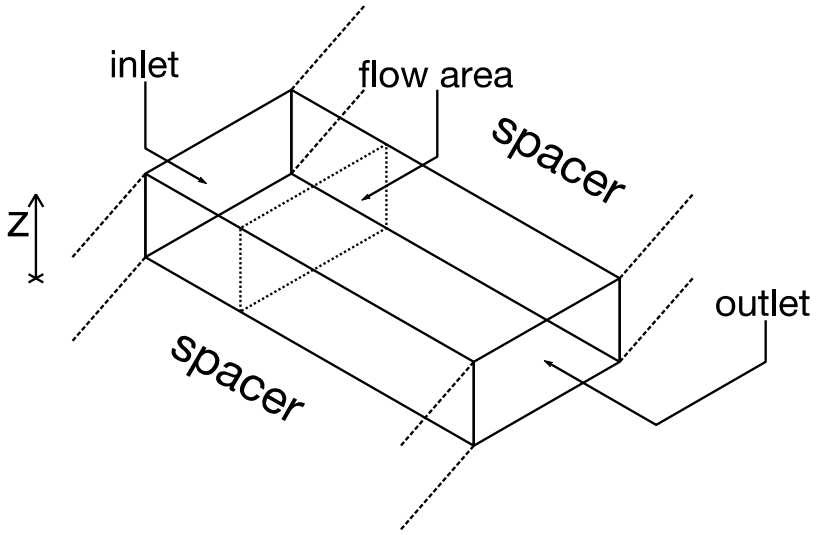

Figure A.3 Basic channel representation.

Figure A.4 shows a representation of a mesh section on the channel. This has the purpose of better illustrating the mesh discretization direction used in the number of elements mesh study.

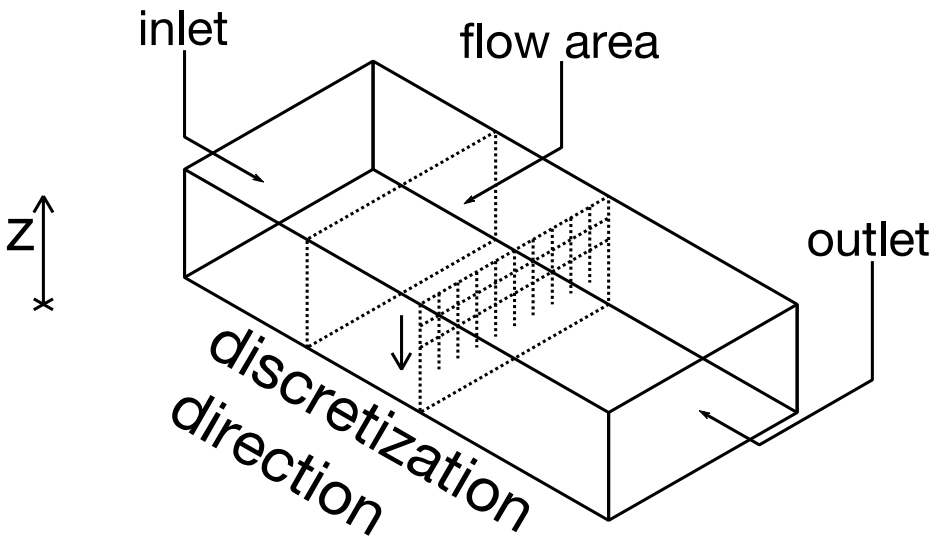

Figure A.4 Representation of channel mesh discretization.

Figure A.5 shows the location within the channel where the profiles for velocity, temperature and pressure were taken.

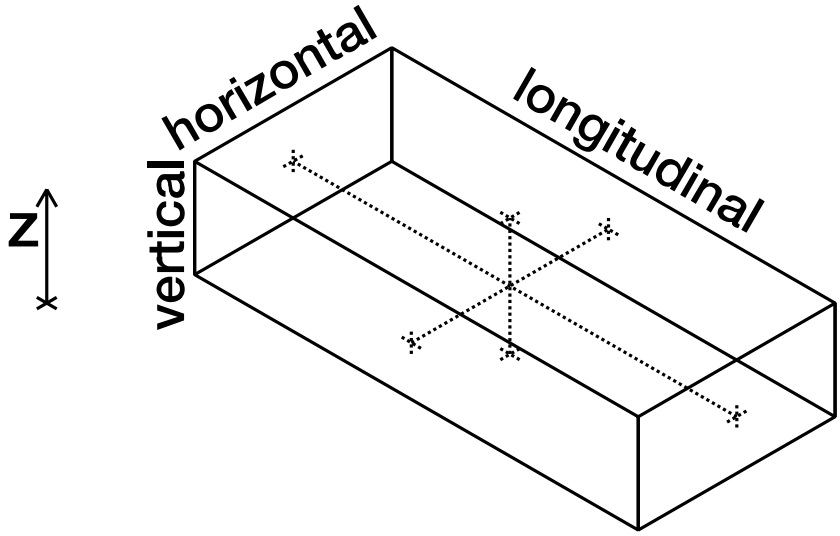

Figure A.5 Representation of channel profile locations.

Figure A.6 shows a representation of the heat dissipation of coil bundles above a washer channel.

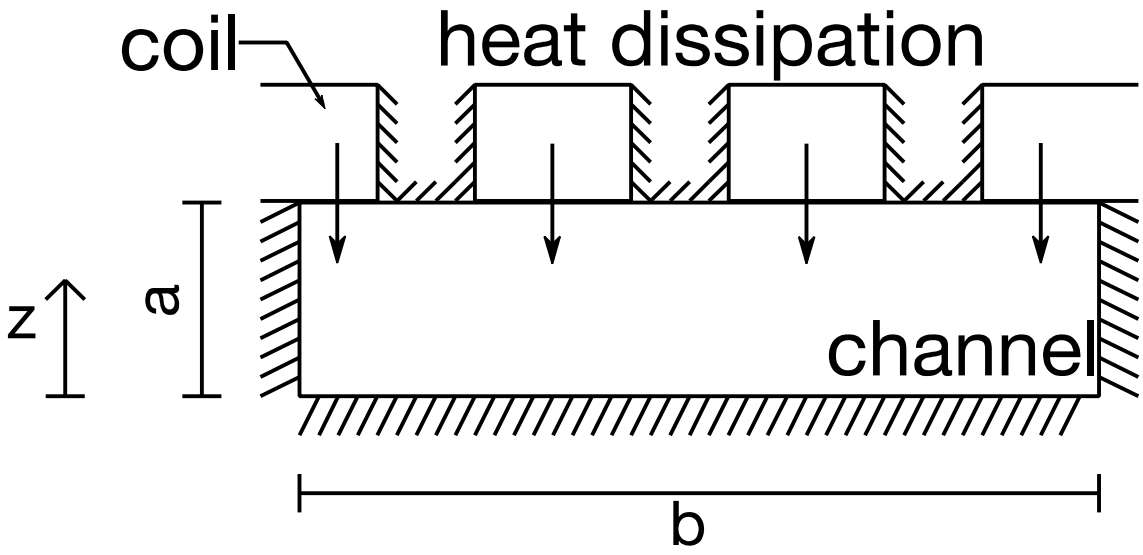

Figure A.6 Heat dissipation model representation.

Figure A.7 shows a representation of the *hot plate* model implemented, where the coil bundles are replaced by a constant heat flux in the channel wall that contacted with the coil bundles.

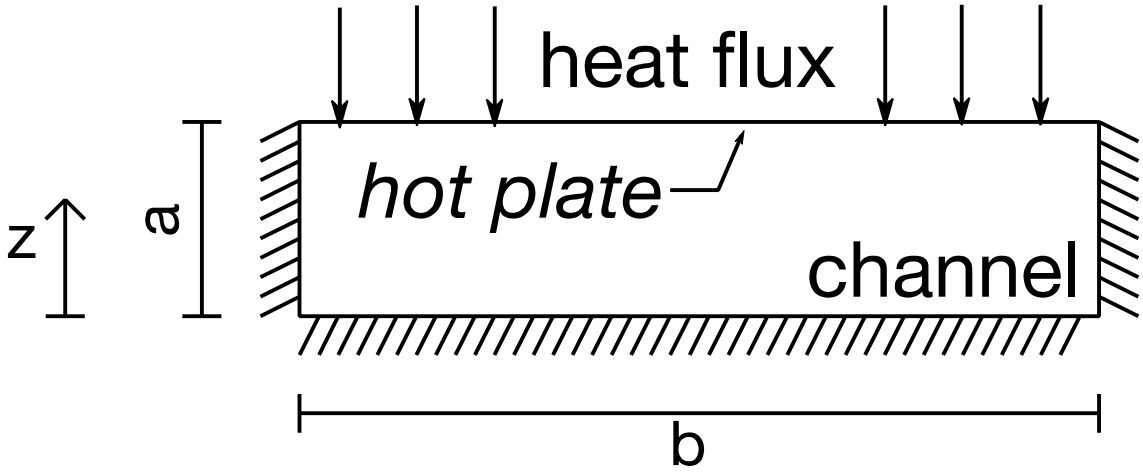

Figure A.7 Heat flux model representation.

A.3 FluSHELL Performance Schematics

Figure A.8 shows the location of lines sampled on the FluSHELL performance analysis and their respective reference.

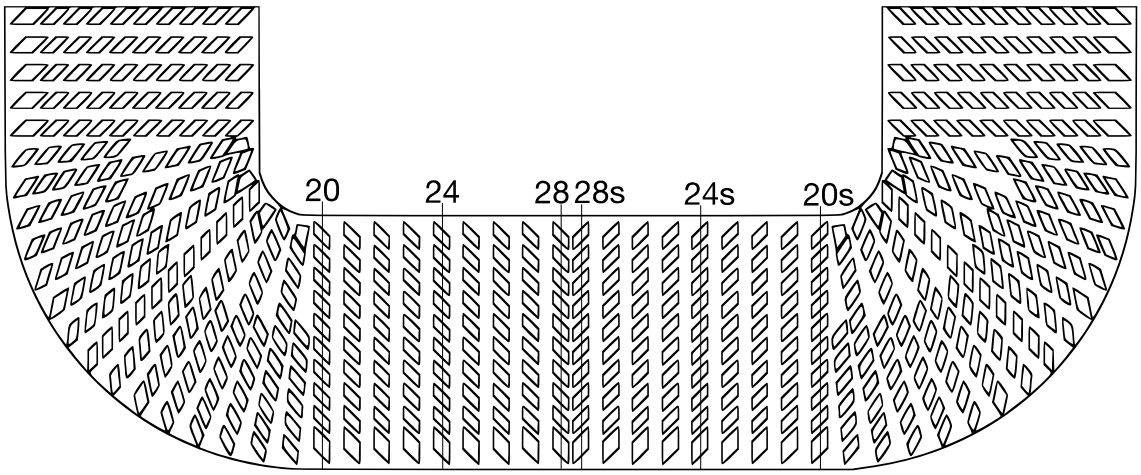

Figure A.8 Lines sampled in FluSHELL performance analysis.

B Fluid Properties

Figure B.1 shows the fluid property dependences with temperature sampled for common operating temperatures.

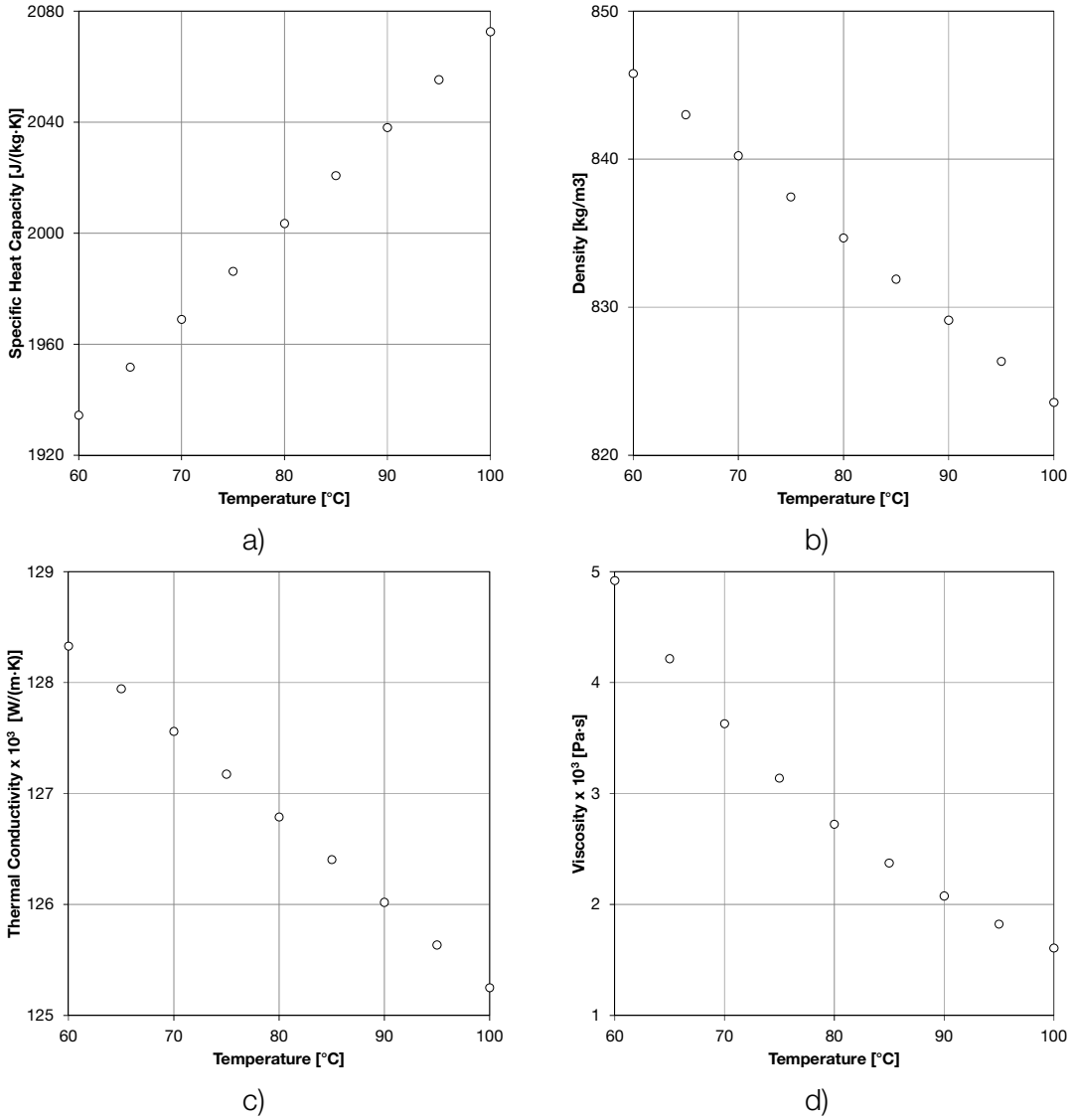

Figure B.1 Fluid property dependences with temperature: a) specific heat capacity; b) density; c) thermal conductivity; d) viscosity.

C Global Results

C.1 Mesh Studies Global Results

C.1.1 Number of Elements Results

Error! Reference source not found. shows the global results for the simulations performed for the number of elements mesh study.

Table C.1 Global results for number of elements mesh study simulations.

	Mesh6	Mesh9	Mesh12
Total Oil Flow Rate [kg/h]	24.9	24.6	24.3
Outlet Oil Temperature [°C]	92	93	93
Average Oil Temperature [°C]	76	77	77
Maximum Oil Temperature [°C]	105	108	108
Average Wall Temperature [°C]	84	84	84
Maximum Wall Temperature [°C]	107	109	109

C.1.2 Solver Discretization Scheme Results

Error! Reference source not found. shows the global results for the simulations performed for the solver discretization scheme mesh study.

Table C.2 Global results for solver discretization scheme mesh study simulations.

	Mesh6	Mesh9	Mesh12
Total Oil Flow Rate [kg/h]	24.4	24.1	23.8
Outlet Oil Temperature [°C]	105	108	109
Average Oil Temperature [°C]	77	76	78
Maximum Oil Temperature [°C]	105	108	109
Average Wall Temperature [°C]	83	84	84
Maximum Wall Temperature [°C]	107	109	110

C.2 Flow Analysis Global Results

Error! Reference source not found. shows the global results for the simulations performed for flow analysis and correlations development.

Table C.3 Global results for simulations.

Simulation	Outlet Oil Temp [˚C]	Avg Oil Temp [˚C]	Max Oil Temp [˚C]	Avg Wall Temp [˚C]	Max Wall Temp [˚C]
1.95H-450W-0.25Q	102.5	81.9	117.0	79.1	119.0
1.95H-450W-0.5Q	81.7	71.5	96.1	78.2	95.1
1.95H-450W-Q	71.0	66.1	87.3	71.8	89.3
1.95H-450W-1.38Q	68.0	64.6	88.5	69.9	90.5
1.95H-450W-2Q	65.5	63.3	91.6	68.1	93.6
1.46H-450W-0.25Q	64.1	82.8	116.8	88.6	118.3
1.95H-450W-0.5Q	82.4	71.8	95.9	77.1	97.4
1.95H-450W-Q	71.4	66.2	86.0	70.7	87.4
1.95H-450W-1.38Q	68.2	64.6	84.1	68.8	85.6
1.95H-450W-2Q	65.7	63.3	89.5	67.2	91.0
1.33H-450W-0.25Q	104.1	82.8	116.5	88.1	117.9
1.33H-450W-0.5Q	82.4	71.8	94.2	76.7	95.6
1.33H-450W-Q	71.3	66.2	83.3	70.4	84.6
1.33H-450W-1.38Q	68.2	64.6	85.4	68.5	86.8
1.33H-450W-2Q	65.7	63.3	88.8	66.9	90.1
1.95H-1000W-Q	84.4	73.2	115.6	85.7	120.0
1.95H-1000W-1.38Q	77.8	70.0	112.3	81.5	116.8
1.95H-1000W-2Q	72.3	67.2	114.9	77.4	119.4

D CFD Maps

CFD property maps are shown in the following sections grouped by property. The maps were obtained for 1.95H-450W simulations.

D.1 Velocity Magnitude

Figure D.1 to Figure D.5 show the velocity magnitude maps for flow rates from 0.25Q to 2Q respectively.

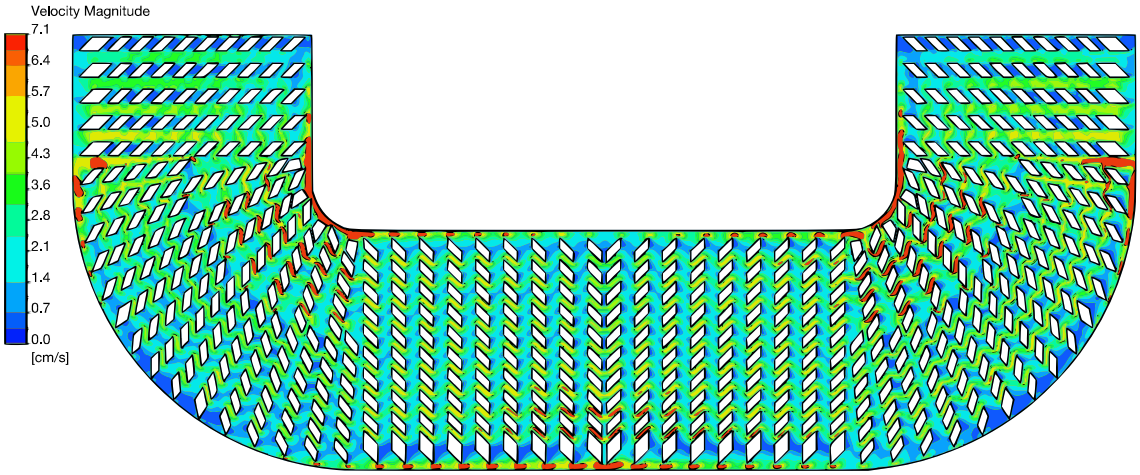

Figure D.1 Velocity magnitude map for 0.25Q flow rate.

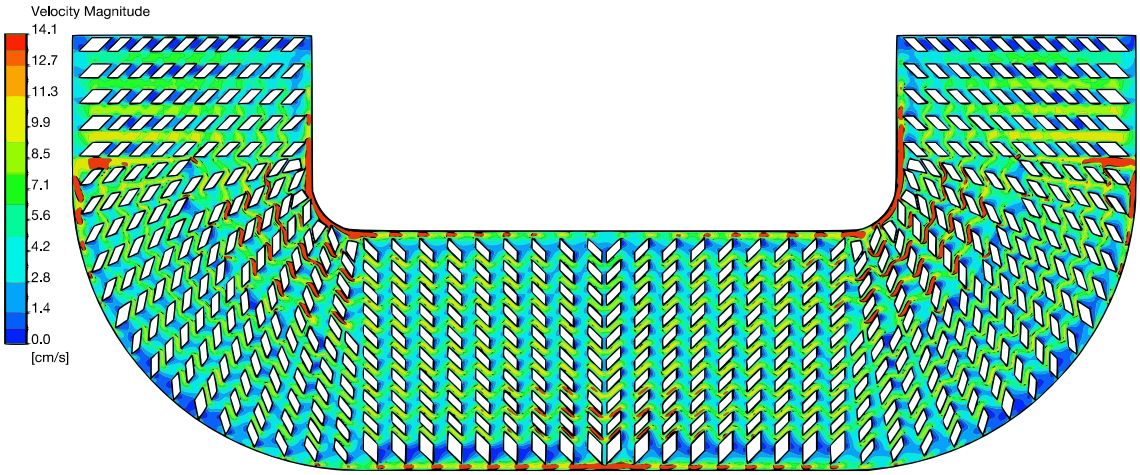

Figure D.2 Velocity magnitude map for 0.5Q flow rate.

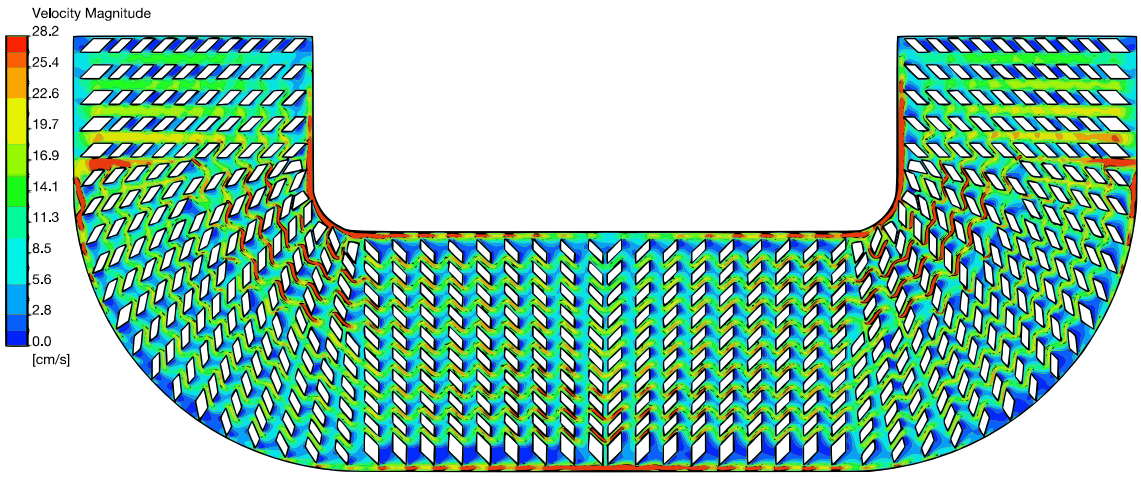

Figure D.3 Velocity magnitude map for Q flow rate.

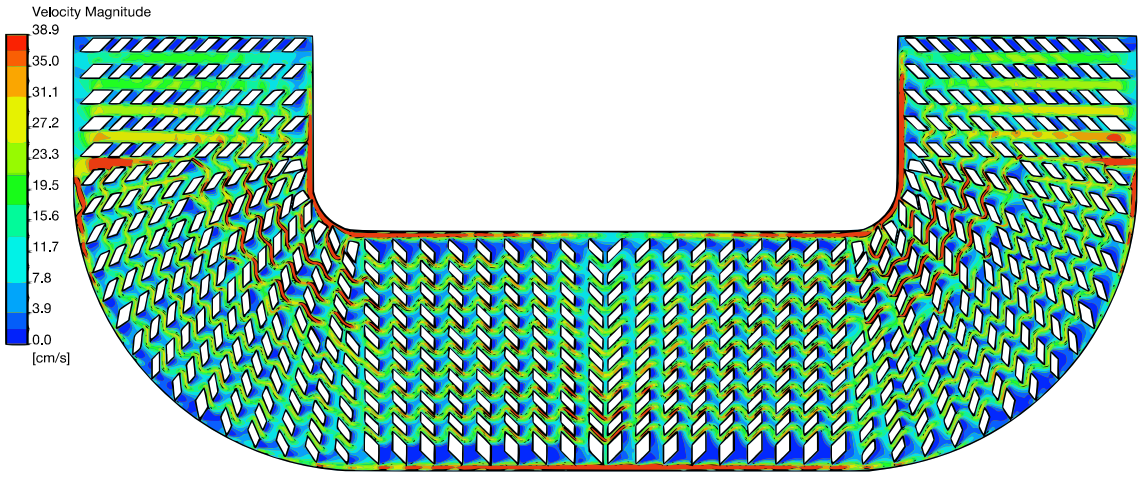

Figure D.4 Velocity magnitude map for 1.38Q flow rate.

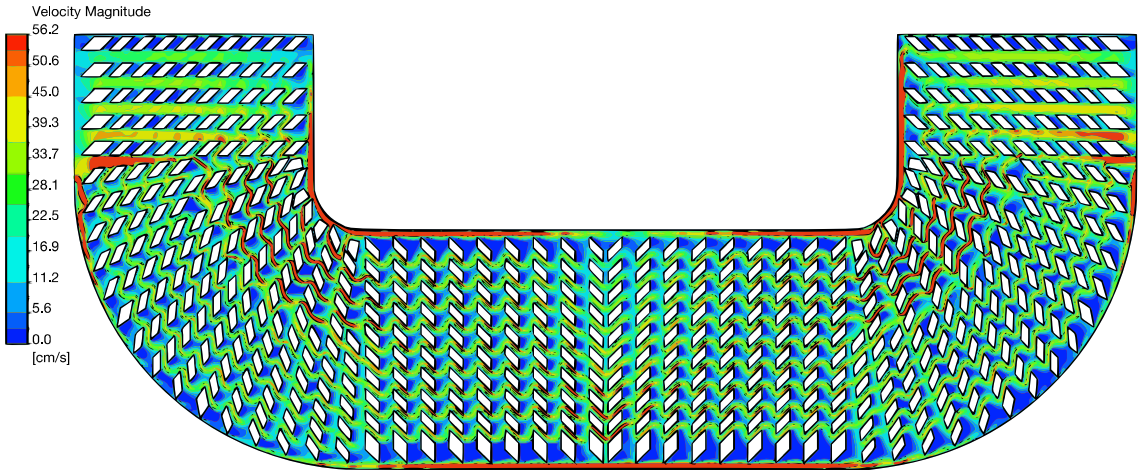

Figure D.5 Velocity magnitude map for 2Q flow rate.

D.2 Static Temperature

Figure D.6 to Figure D.10 show the static temperature maps for flow rates from 0.25Q to 2Q respectively.

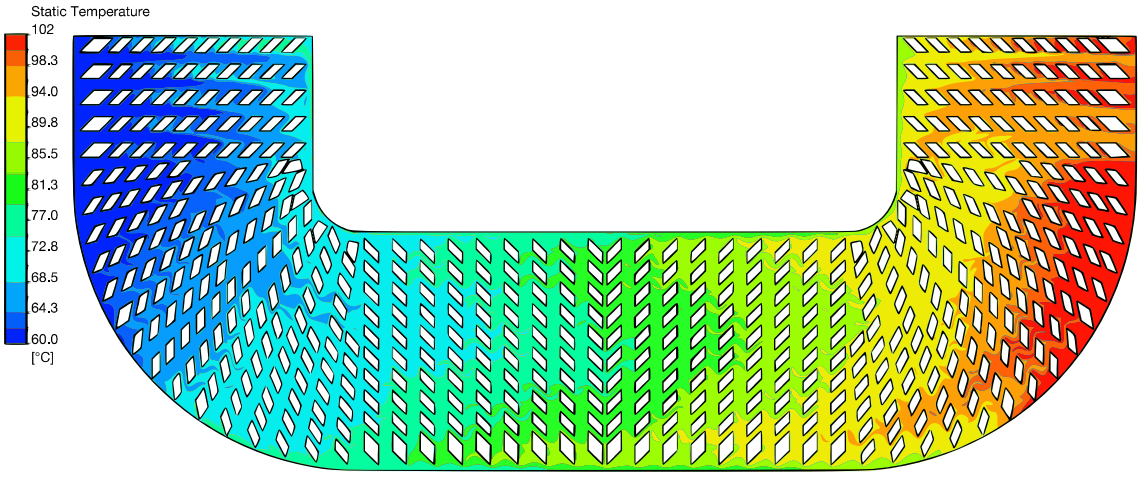

Figure D.6 Static temperature map for 0.25Q flow rate.

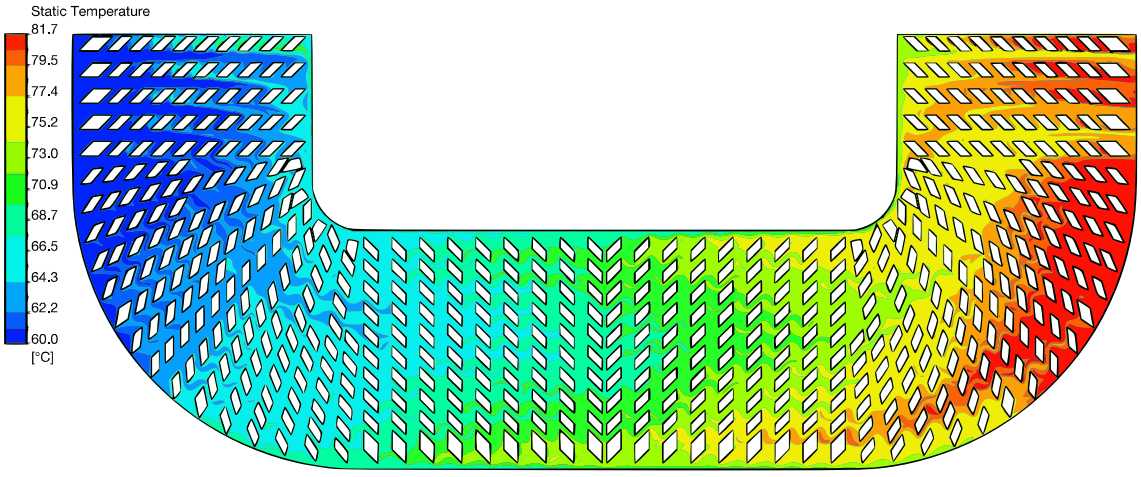

Figure D.7 Static temperature map for 0.5Q flow rate.

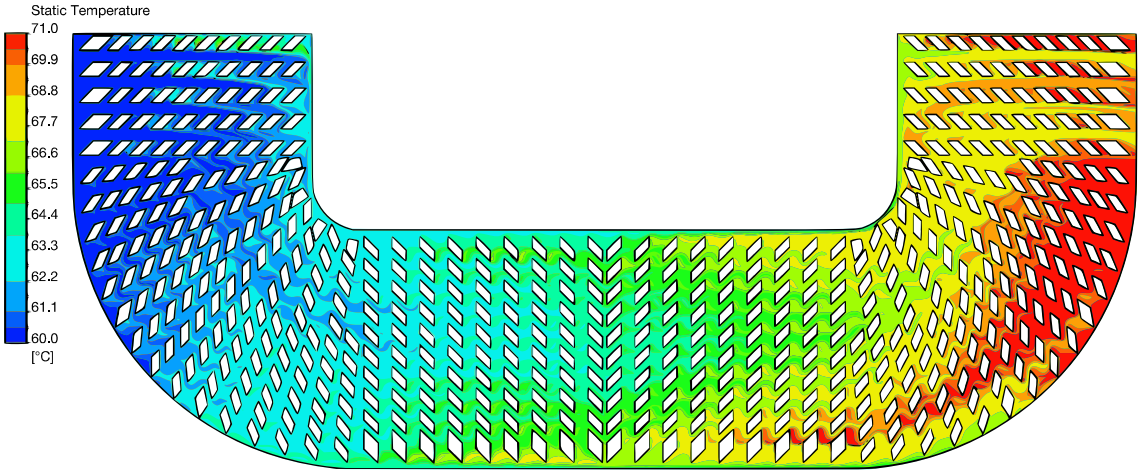

Figure D.8 Static temperature map for Q flow rate.

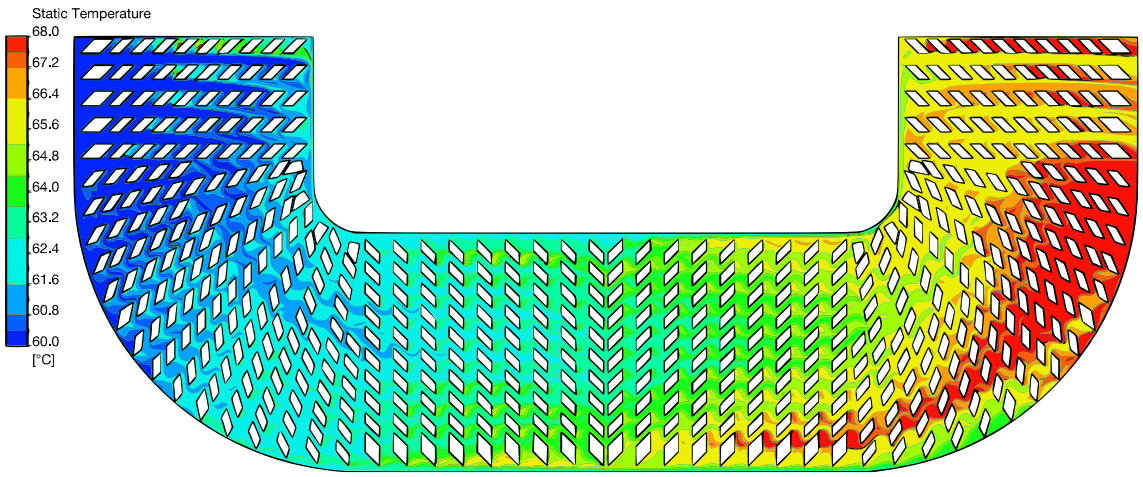

Figure D.9 Static temperature map for 1.38Q flow rate.

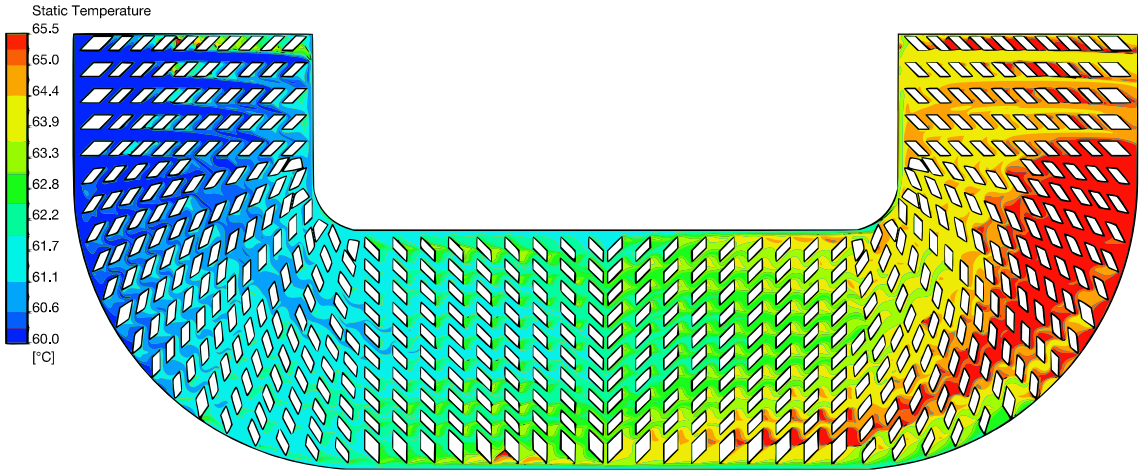

Figure D.10 Static temperature map for 2Q flow rate.

D.3 Static Pressure

Figure D.11 to Figure D.15 show the static pressure maps for flow rates from 0.25Q to 2Q respectively.

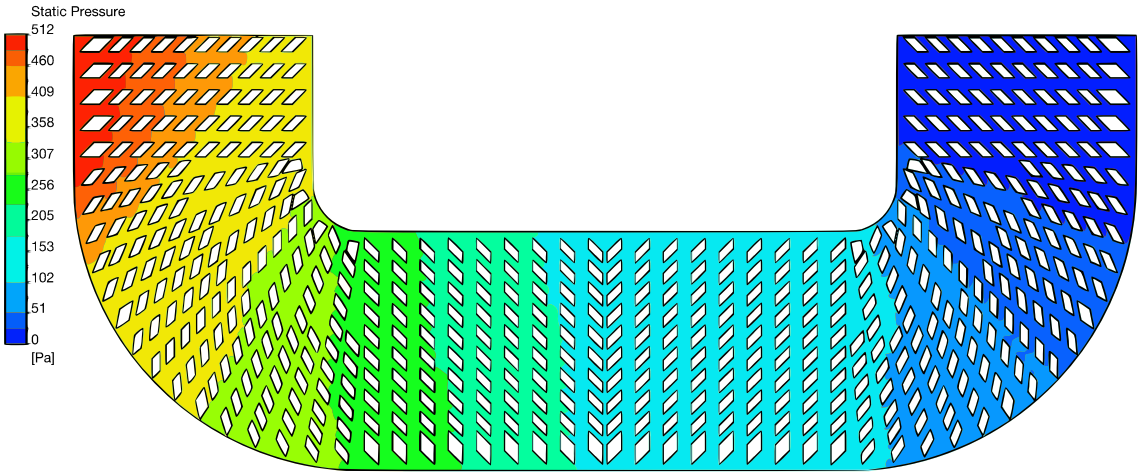

Figure D.11 Static pressure map for 0.25Q flow rate.

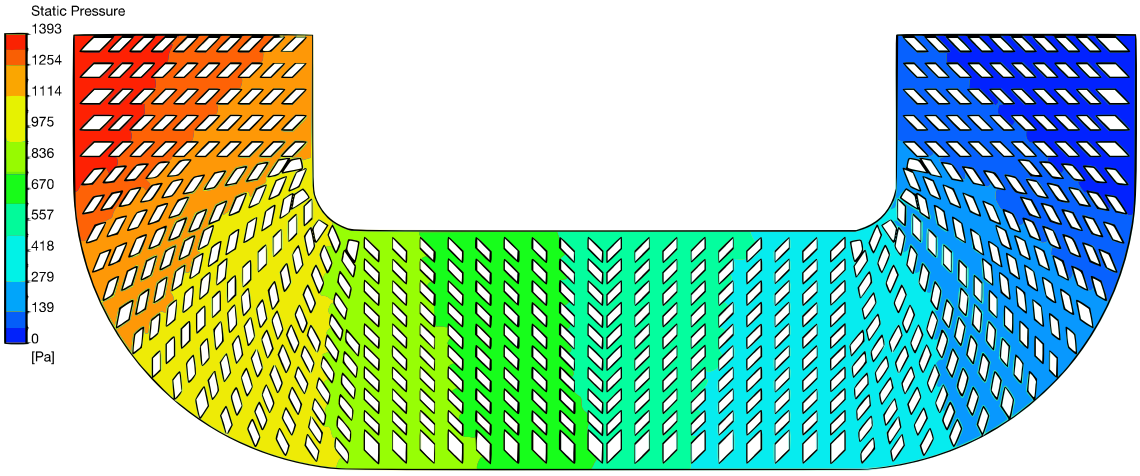

Figure D.12 Static pressure map for 0.5Q flow rate.

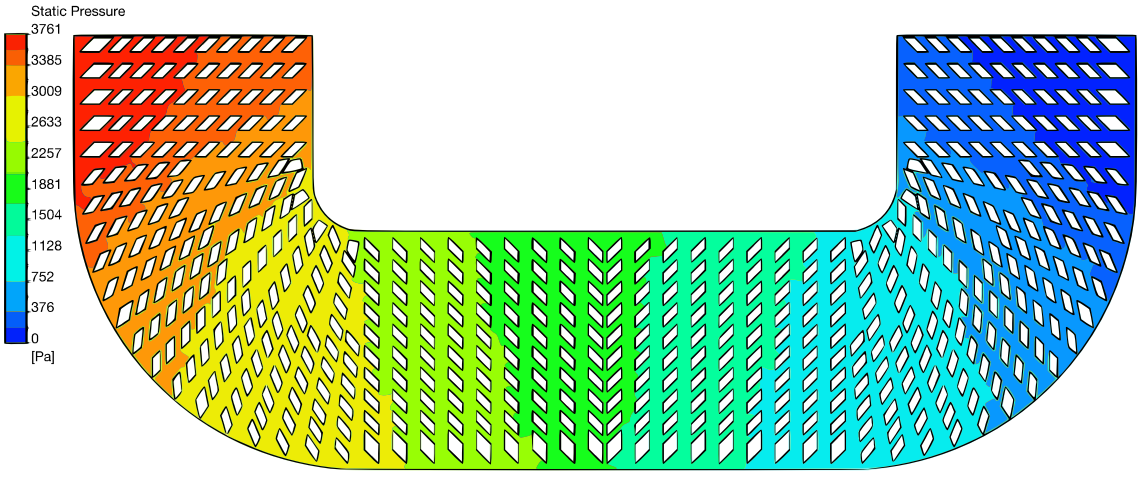

Figure D.13 Static pressure map for Q flow rate.

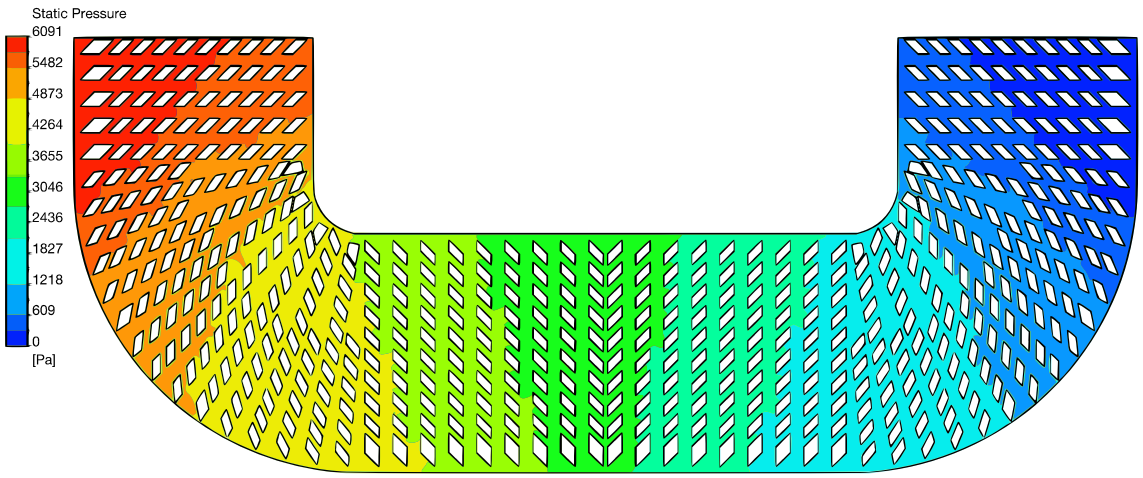

Figure D.14 Static pressure map for 1.38Q flow rate.

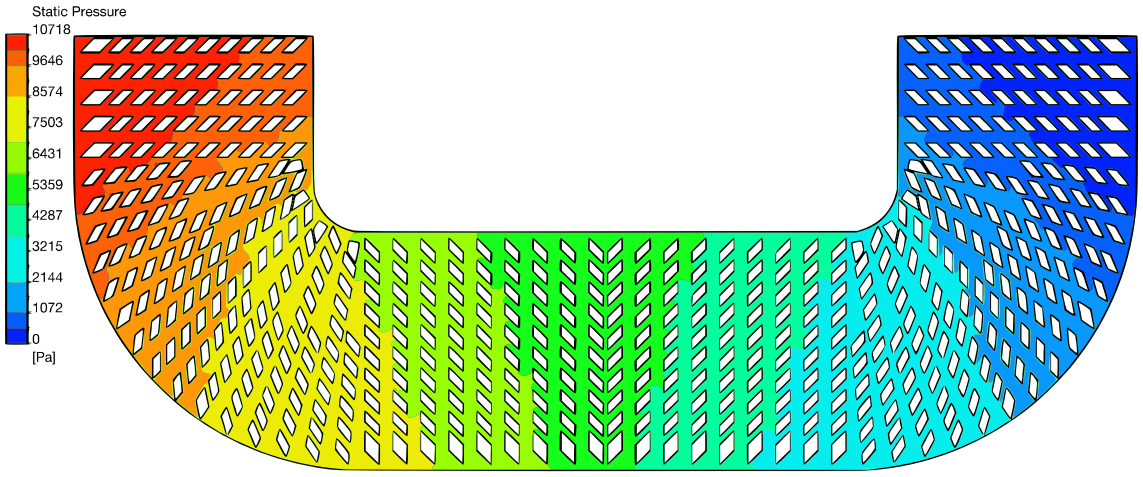

Figure D.15 Static pressure map for 2Q flow rate.

E Channel Profiles

The channel profiles were taken in the sampled channels for the mesh studies. Since on these conditions a simulation with Mesh12 was available these were the results used on the profiles, as the higher discretization of the mesh lead to the best possible accuracy.

Also shown the velocity profiles on the G zone for the simulated flow rates. These profiles were taken in line 24 of the reference matrix, on a line along the Y coordinate intersecting spacers and transverse channels.

E.1 Vertical Profiles

E.1.1 Velocity Magnitude

Figure E.1 to Figure E.4 show the vertical profiles for velocity magnitude on the sampled channels.

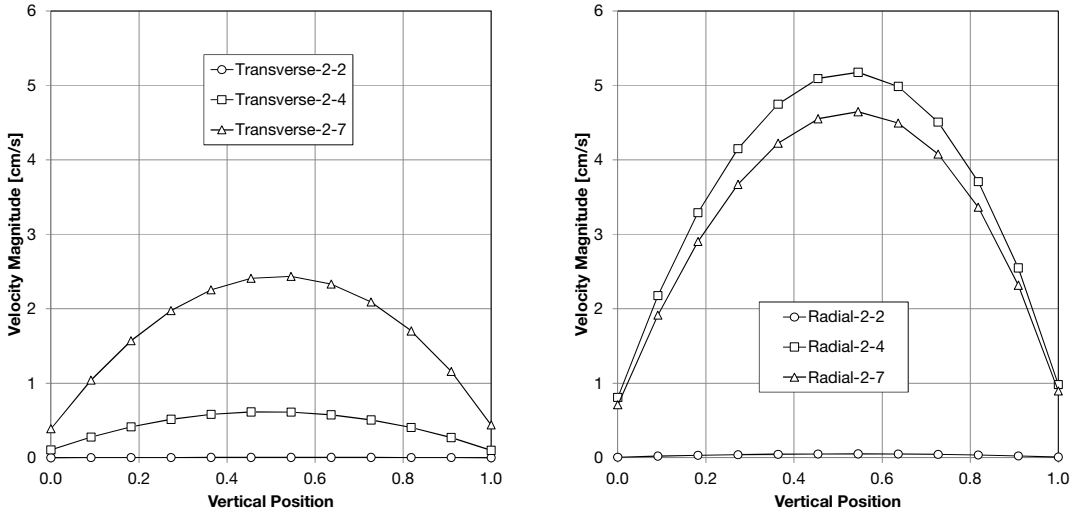

a) b)

Figure E.1 Vertical velocity magnitude profiles for line 2: a) transverse channels; b) radial channels.

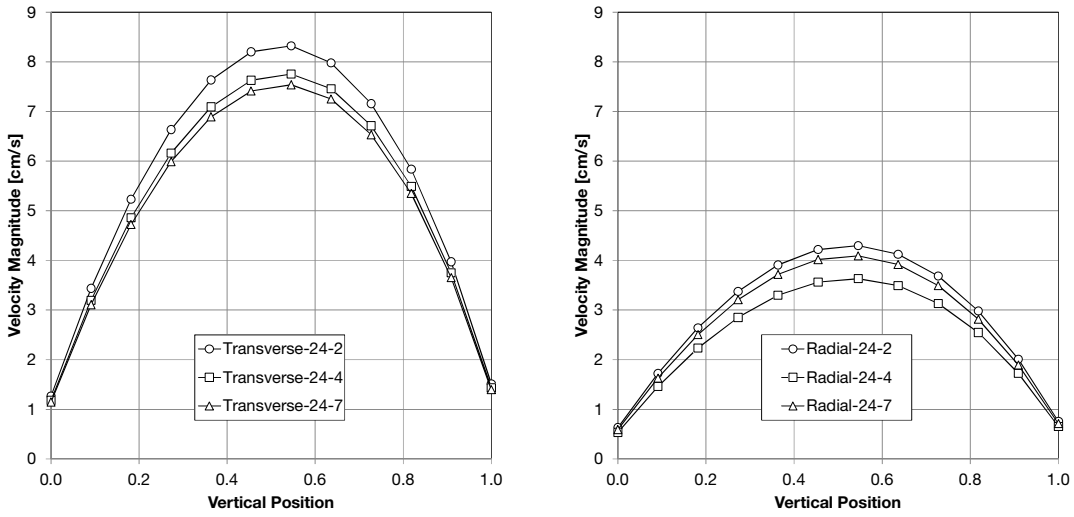

a) b)

Figure E.2 Vertical velocity magnitude profiles for line 24: a) transverse channels; b) radial channels.

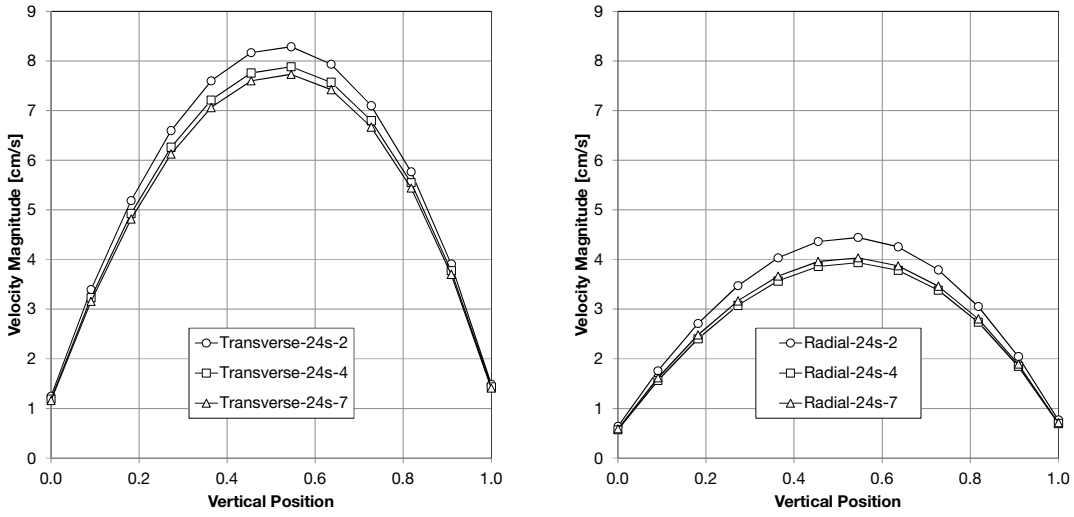

a) b)

Figure E.3 Vertical velocity magnitude profiles for line 24s: a) transverse channels; b) radial channels.

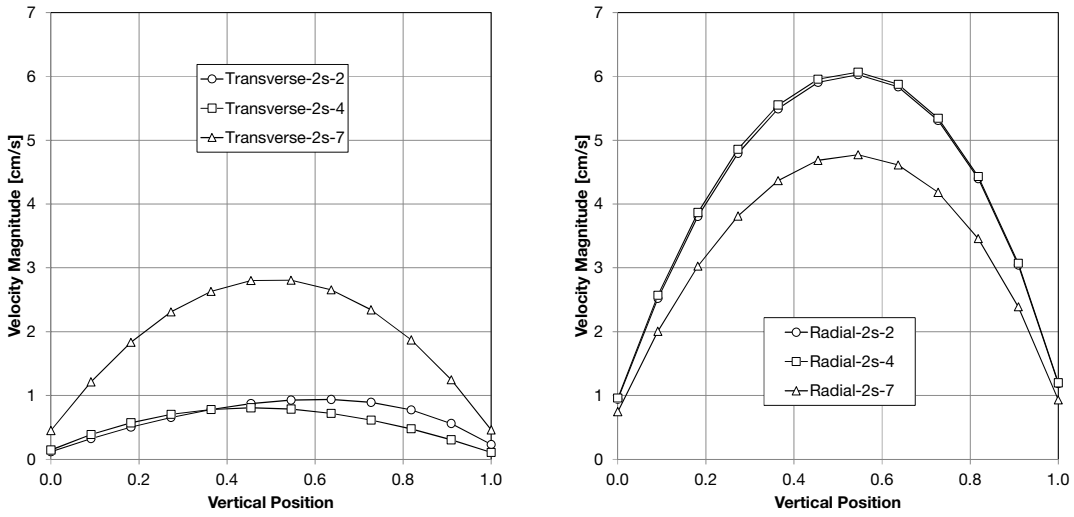

a) b)

Figure E.4 Vertical velocity magnitude profiles for line 2s: a) transverse channels; b) radial channels.

E.1.2 Static Temperature

Figure E.5 to Figure E.8 show the vertical profiles for static temperature on the sampled channels.

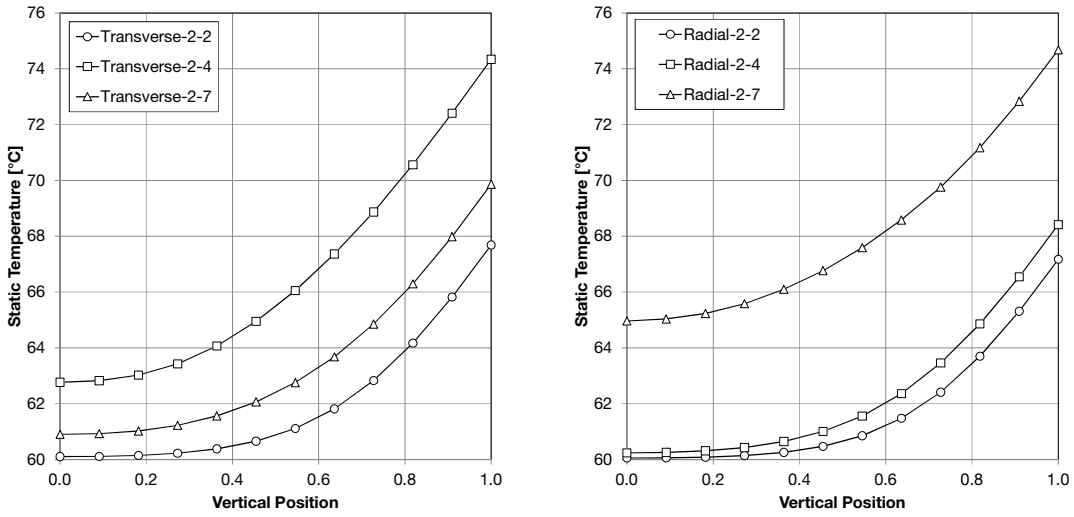

a) b)

Figure E.5 Vertical static temperature profiles for line 2: a) transverse channels; b) radial channels.

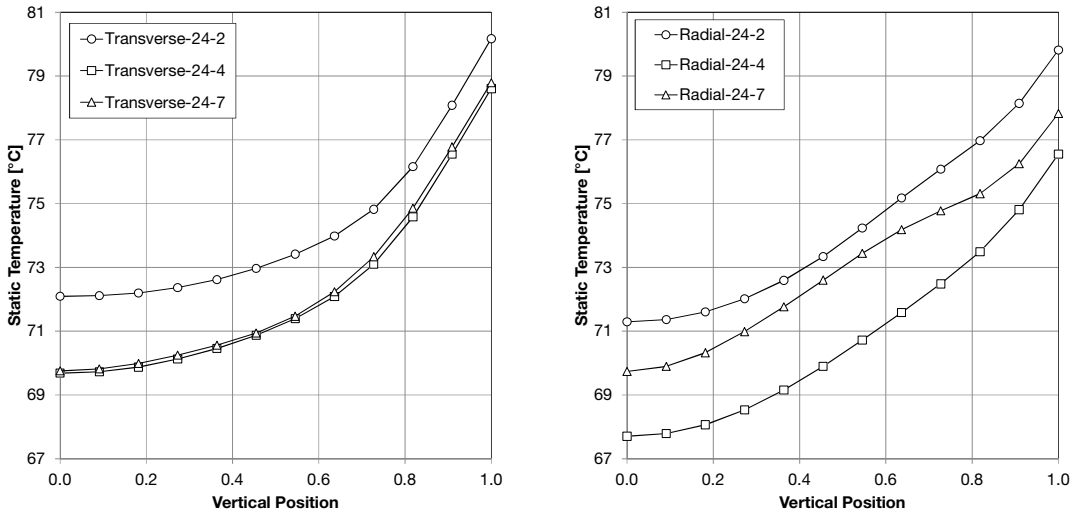

a) b)

Figure E.6 Vertical static temperature profiles for line 24: a) transverse channels; b) radial channels.

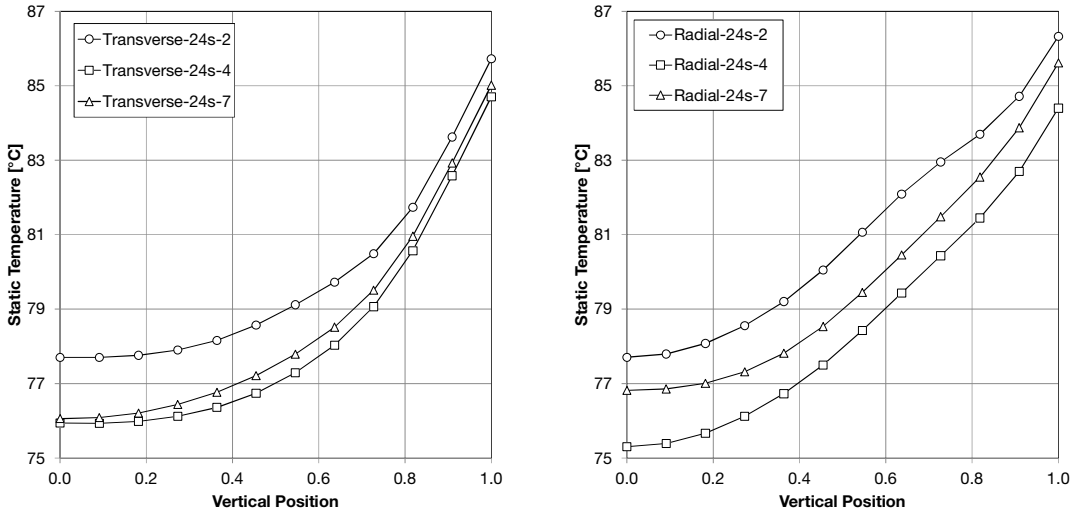

a) b)

Figure E.7 Vertical static temperature profiles for line 24s: a) transverse channels; b) radial channels.

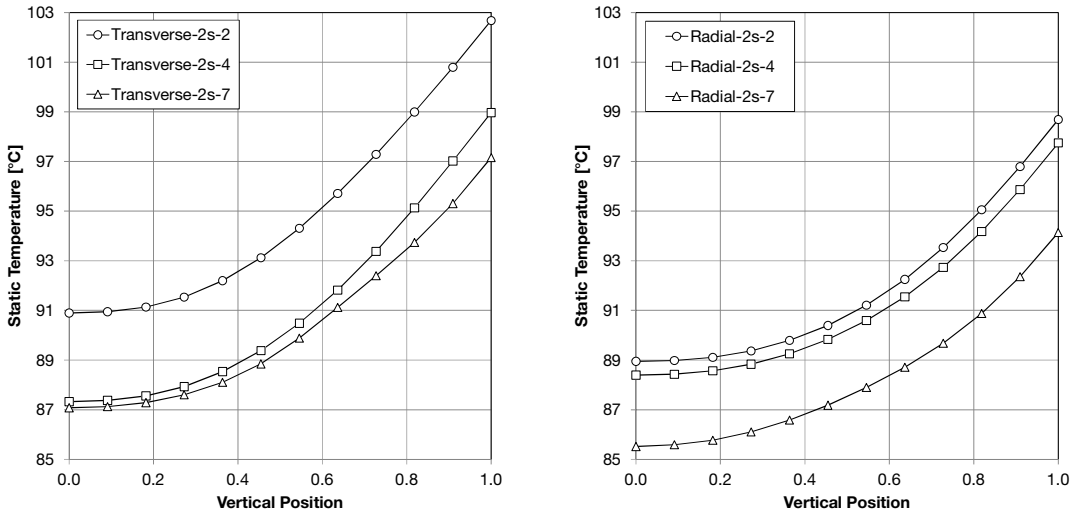

a) b)

Figure E.8 Vertical static temperature profiles for line 2s: a) transverse channels; b) radial channels.

E.2 Horizontal Profiles

E.2.1 Velocity Magnitude

Figure E.9 to Figure E.12 show the horizontal profiles for static temperature on the sampled channels.

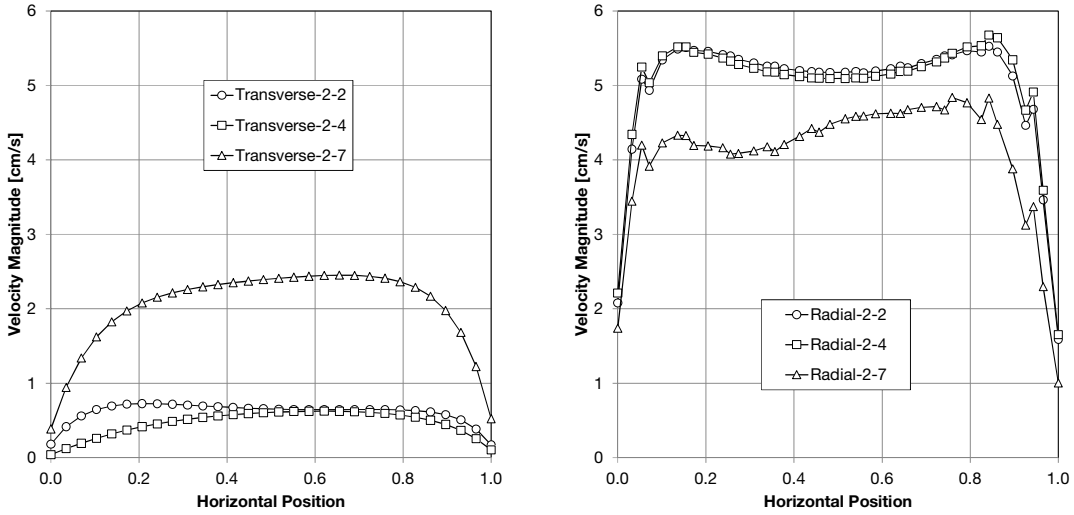

a) b)

Figure E.9 Horizontal velocity magnitude profiles for line 2: a) transverse channels; b) radial channels.

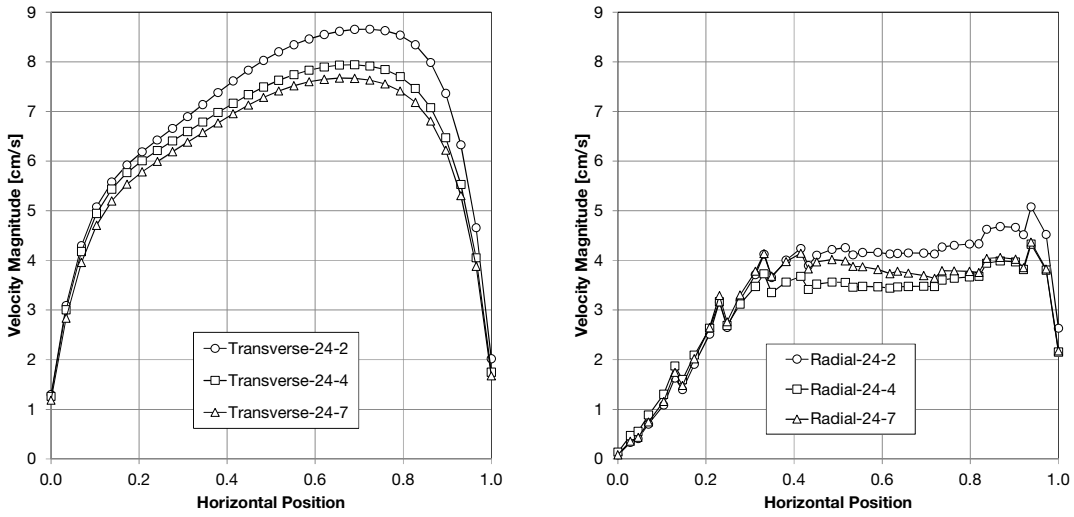

a) b)

Figure E.10 Horizontal velocity magnitude profiles for line 24: a) transverse channels; b) radial channels.

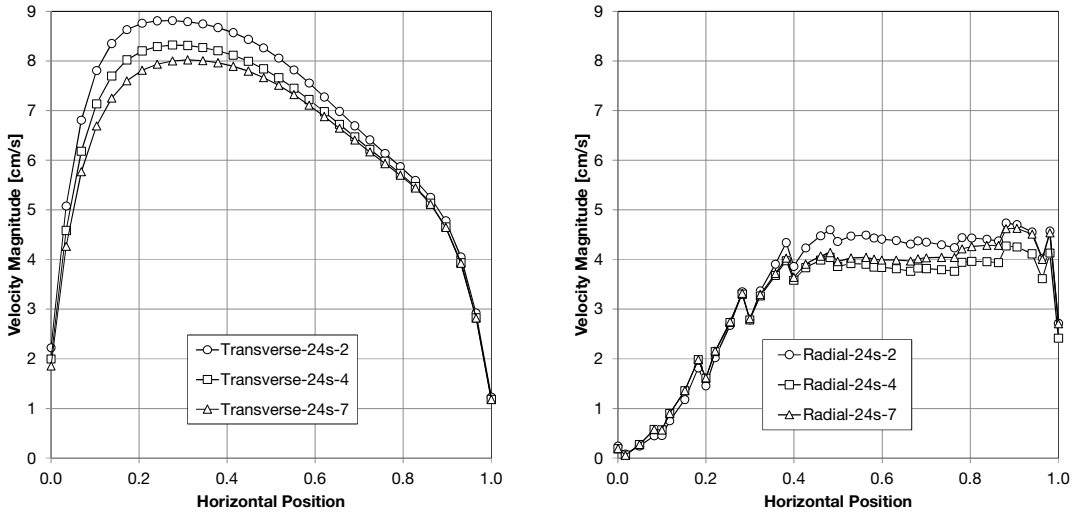

a) b)

Figure E.11 Horizontal velocity magnitude profiles for line 24s: a) transverse channels; b) radial channels.

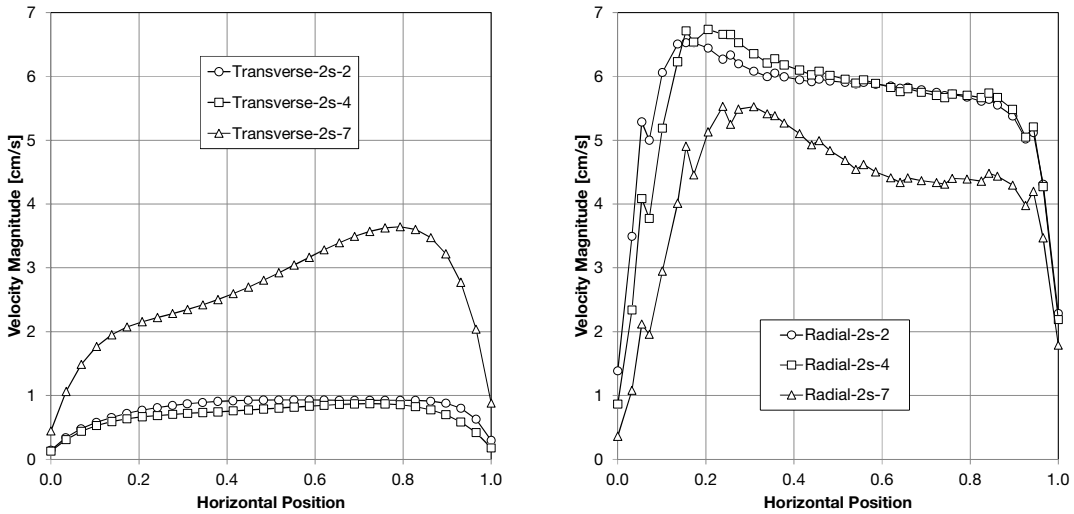

a) b)

Figure E.12 Horizontal velocity magnitude profiles for line 2s: a) transverse channels; b) radial channels.

E.2.2 Static Temperature

Figure E.13 to Figure E.16 show the horizontal profiles for static temperature on the sampled channels.

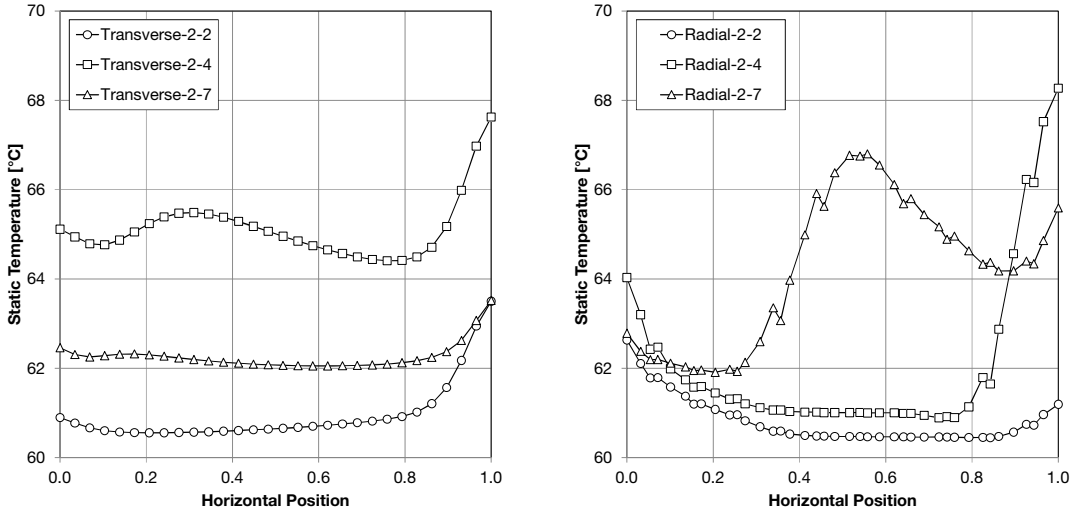

a) b)

Figure E.13 Horizontal static temperature profiles for line 2: a) transverse channels; b) radial channels.

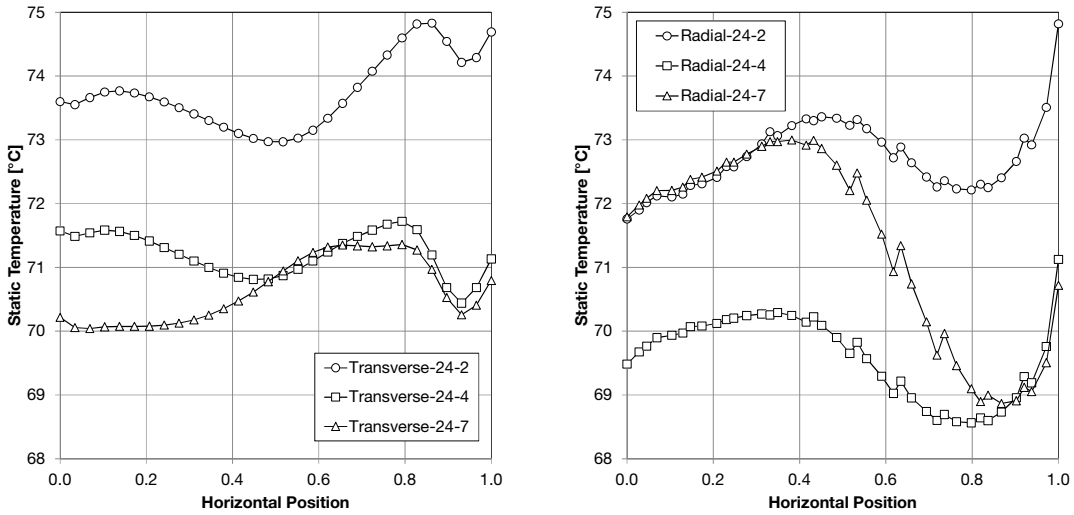

a) b)

Figure E.14 Horizontal static temperature profiles for line 24: a) transverse channels; b) radial channels.

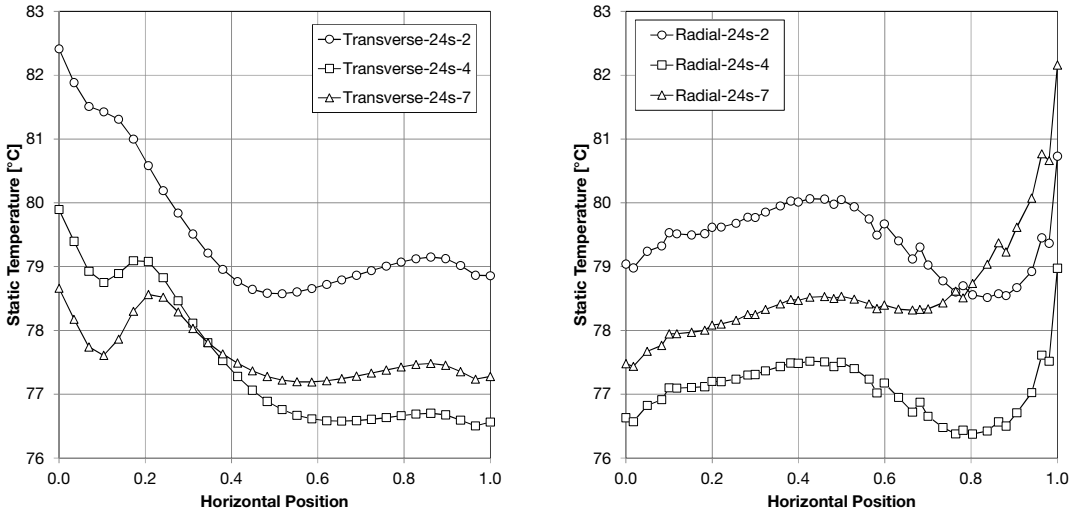

a) b)

Figure E.15 Horizontal static temperature profiles for line 24s: a) transverse channels; b) radial channels.

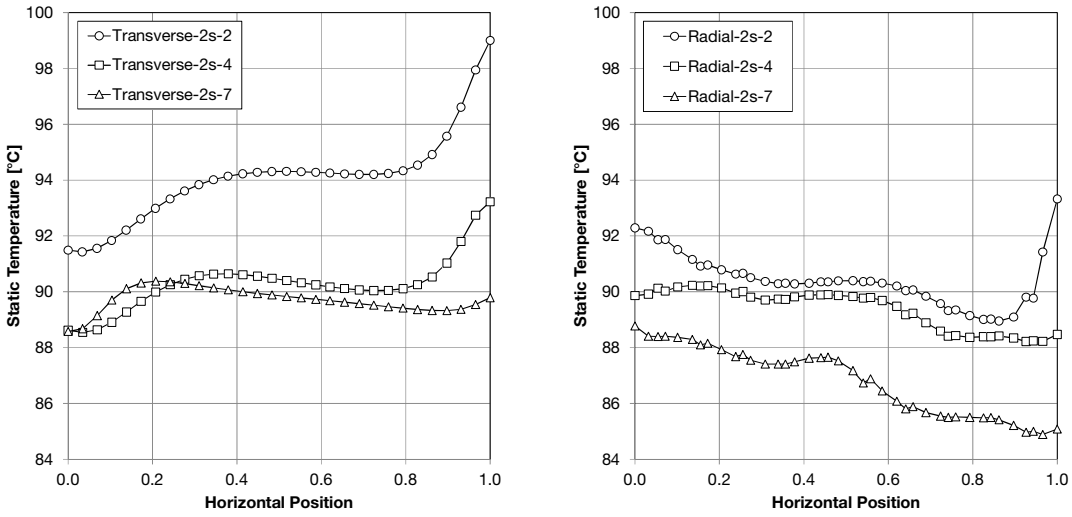

a) b)

Figure E.16 Horizontal static temperature profiles for line 2s: a) transverse channels; b) radial channels.

E.3 Longitudinal Profiles

E.3.1 Velocity Magnitude

Figure E.17 to Figure E.20 show the longitudinal profiles for velocity magnitude on the sampled channels.

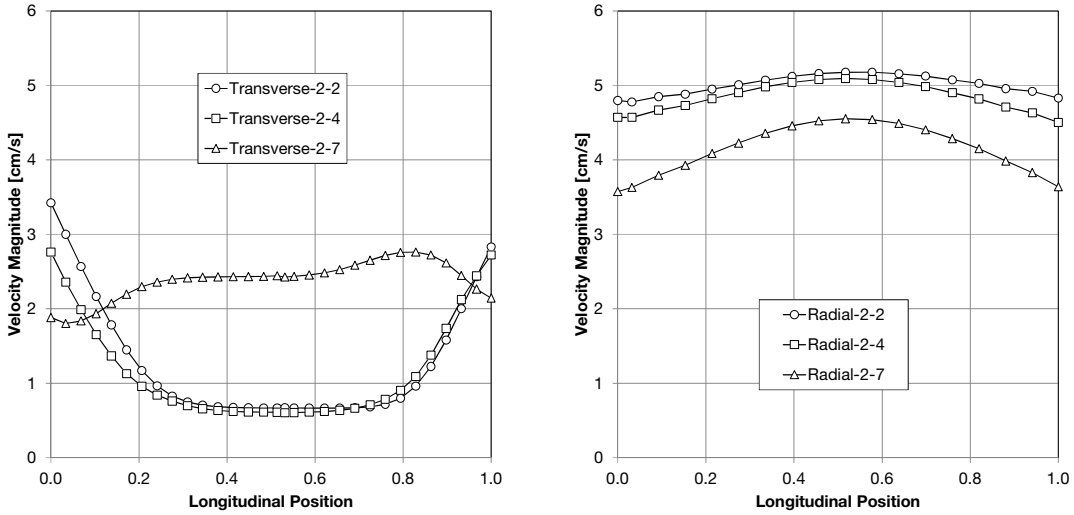

a) b)

Figure E.17 Longitudinal velocity magnitude profiles for line 2: a) transverse channels; b) radial channels.

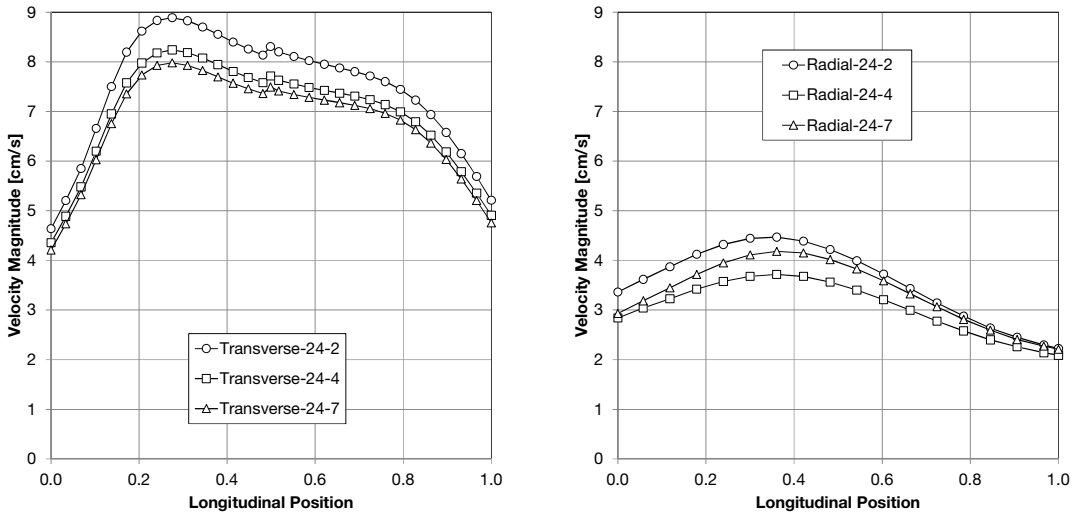

a) b)

Figure E.18 Longitudinal velocity magnitude profiles for line 24: a) transverse channels; b) radial channels.

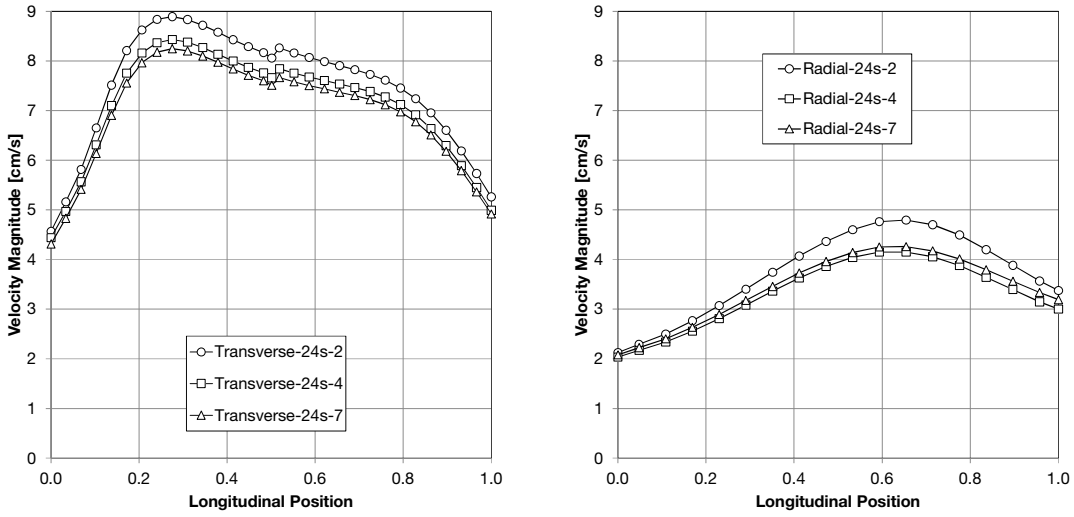

a) b)

Figure E.19 Longitudinal velocity magnitude profiles for line 24s: a) transverse channels; b) radial channels.

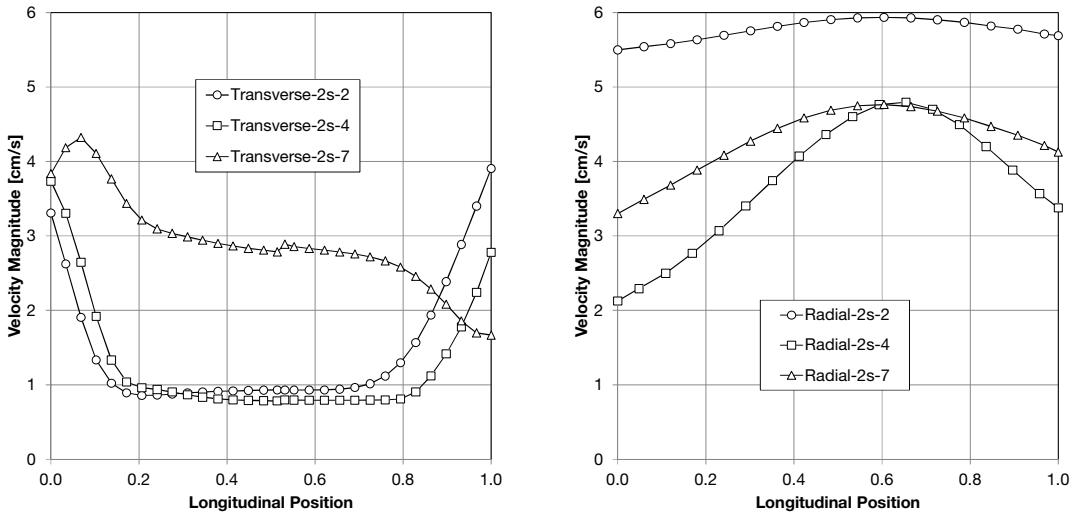

a) b)

Figure E.20 Longitudinal velocity magnitude profiles for line 2s: a) transverse channels; b) radial channels.

E.3.2 Static Temperature

Figure E.21 to Figure E.24 show the longitudinal profiles for static temperature on the sampled channels.

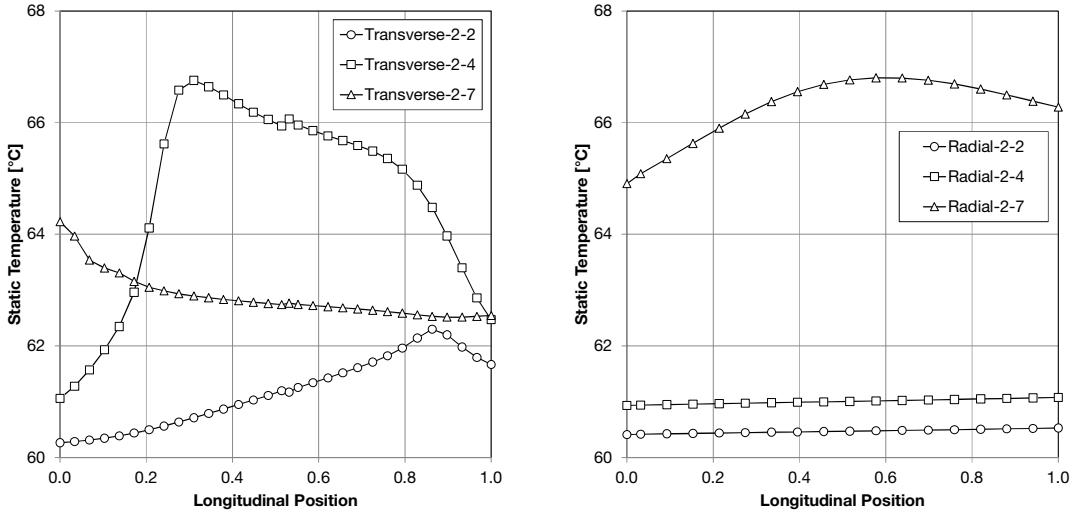

a) b)

Figure E.21 Longitudinal static temperature profiles for line 2: a) transverse channels; b) radial channels.

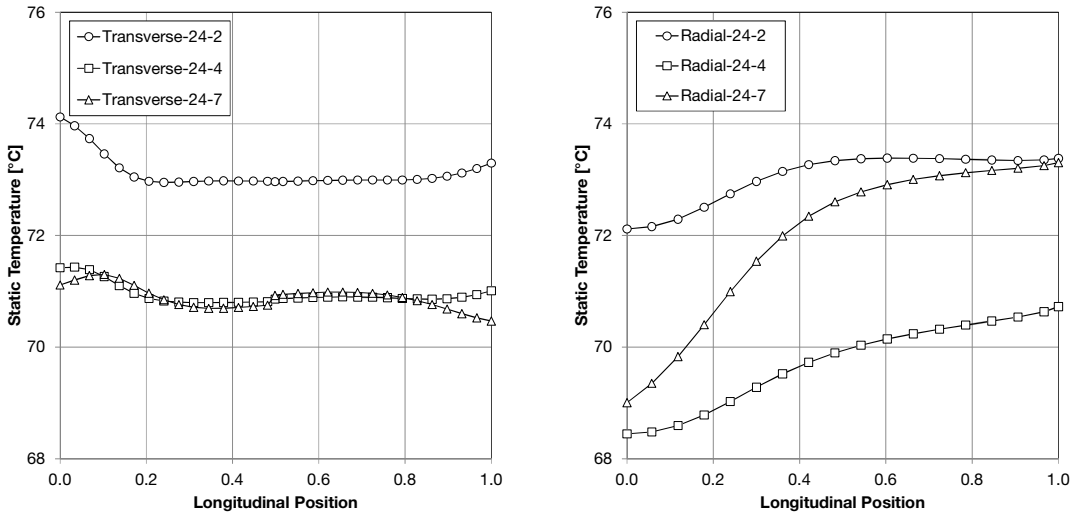

a) b)

Figure E.22 Longitudinal static temperature profiles for line 24: a) transverse channels; b) radial channels.

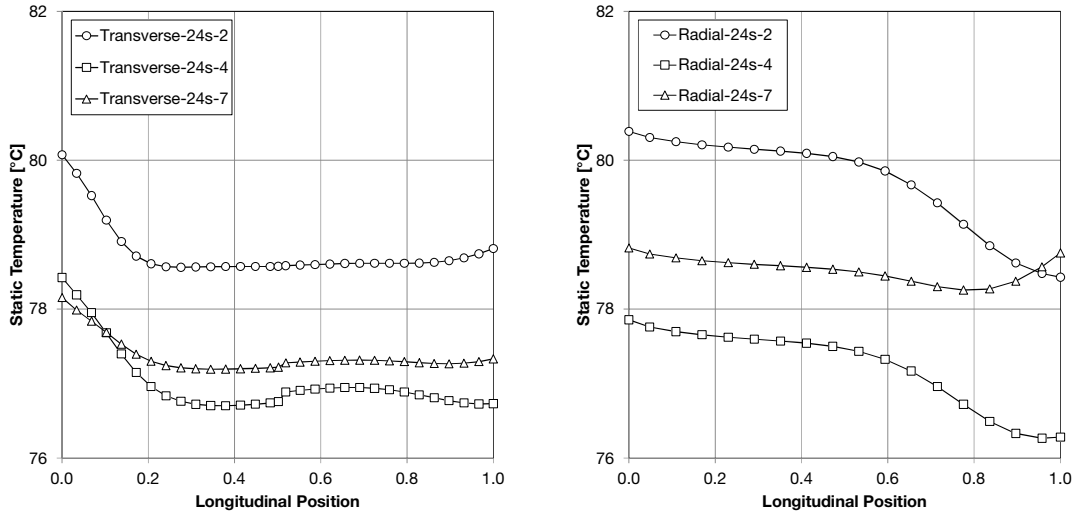

a) b)

Figure E.23 Longitudinal static temperature profiles for line 24s: a) transverse channels; b) radial channels.

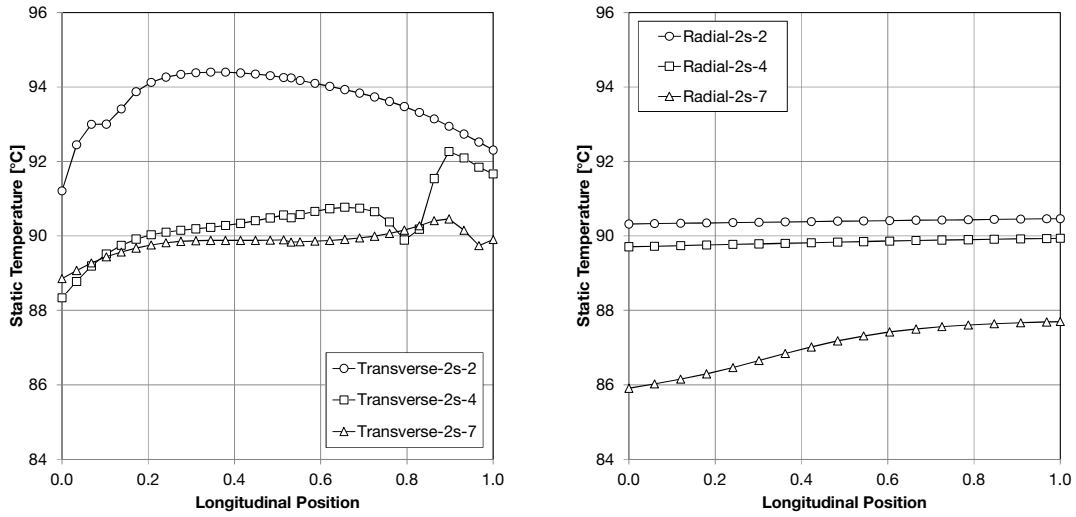

a) b)

Figure E.24 Longitudinal static temperature profiles for line 2s: a) transverse channels; b) radial channels.

E.3.3 Static Pressure

Figure E.25 to Figure E.28 show the longitudinal profiles for static pressure on the sampled channels.

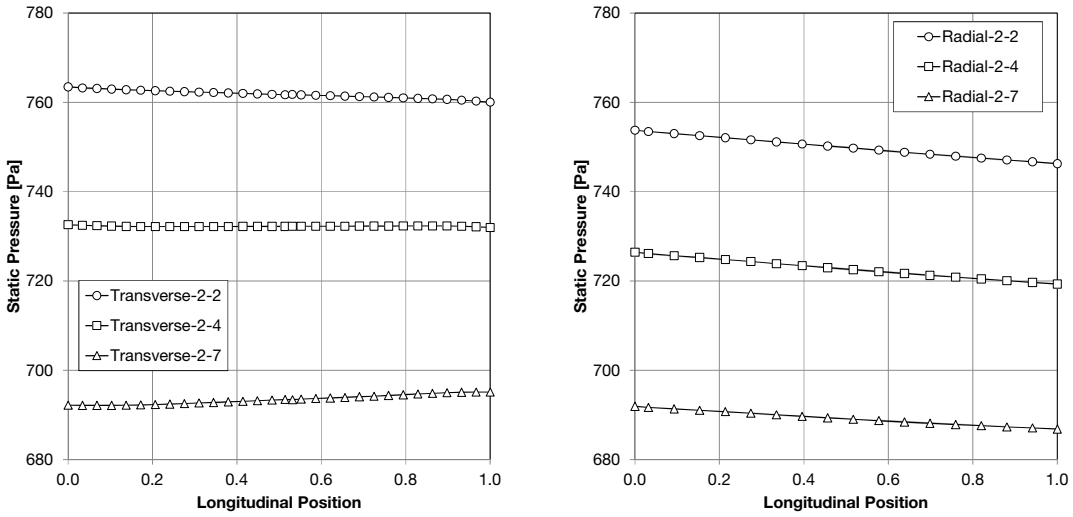

a) b)

Figure E.25 Longitudinal static pressure profiles for line 2: a) transverse channels; b) radial channels.

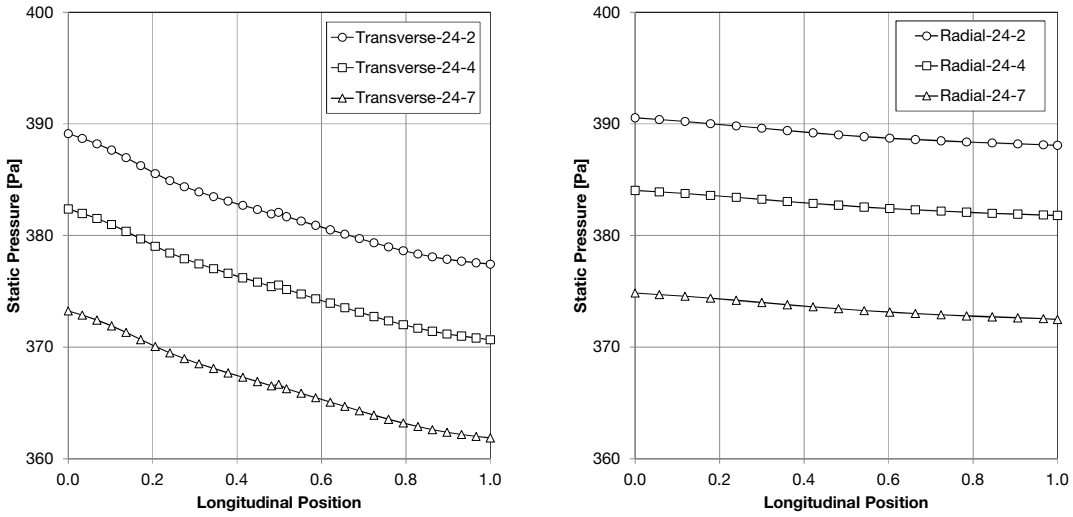

a) b)

Figure E.26 Longitudinal static pressure profiles for line 24: a) transverse channels; b) radial channels.

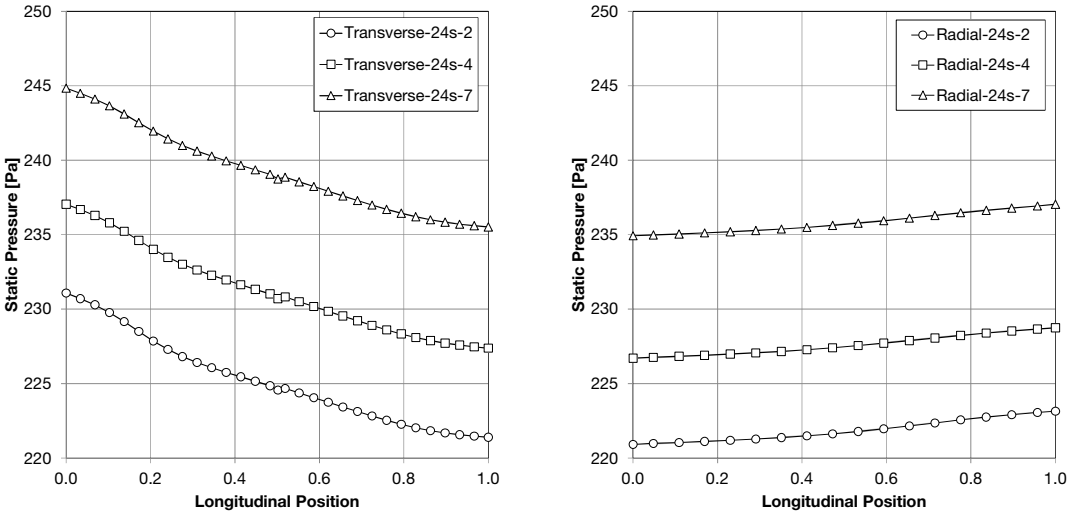

a) b)

Figure E.27 Longitudinal static pressure profiles for line 24s: a) transverse channels; b) radial channels.

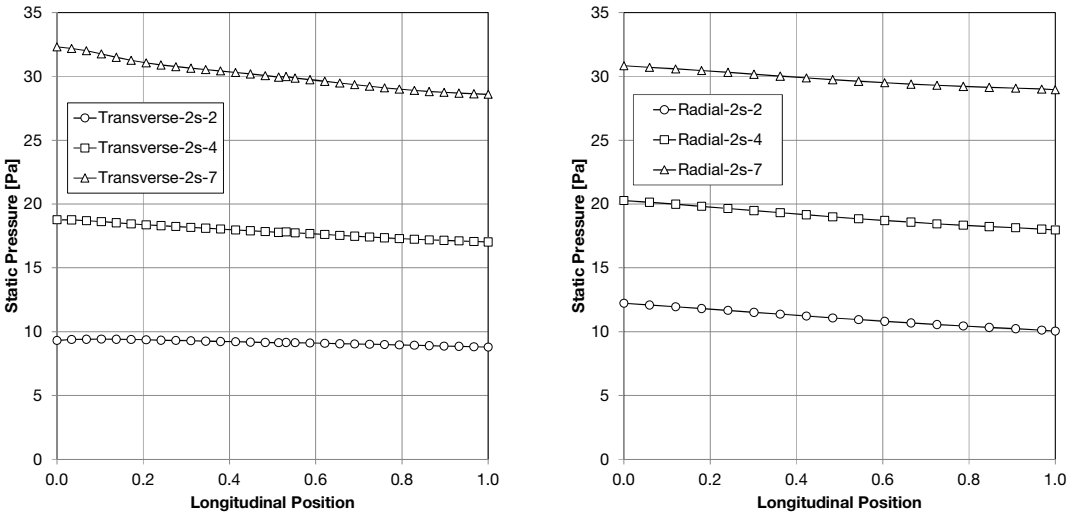

a) b)

Figure E.28 Longitudinal static pressure profiles for line 2s: a) transverse channels; b) radial channels.

E.4 G Zone Profiles

Figure E.29 to Figure E.33 show the velocity magnitude profiles on line 24 intersecting spacers and transverse channels.

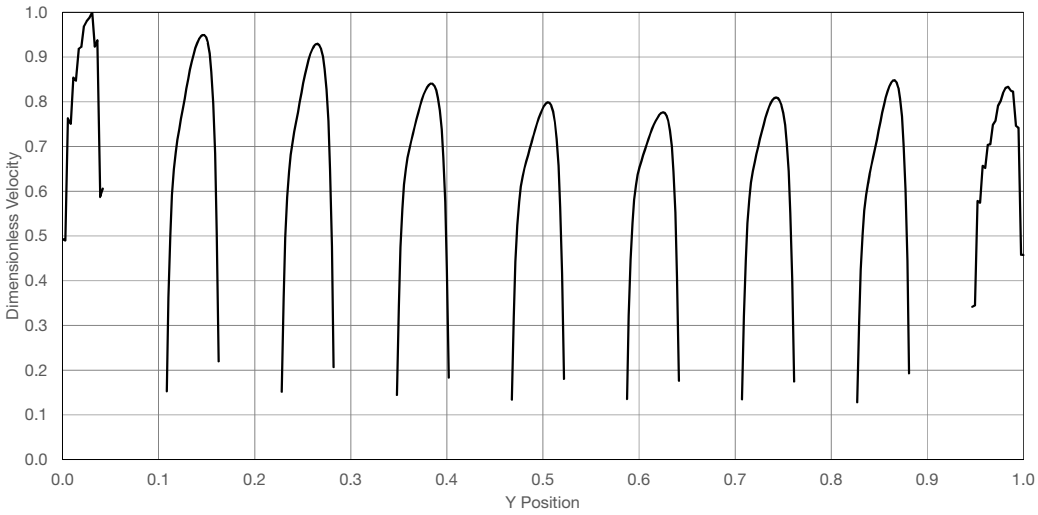

Figure E.29 Velocity magnitude profile on G zone for 0.25Q flow rate.

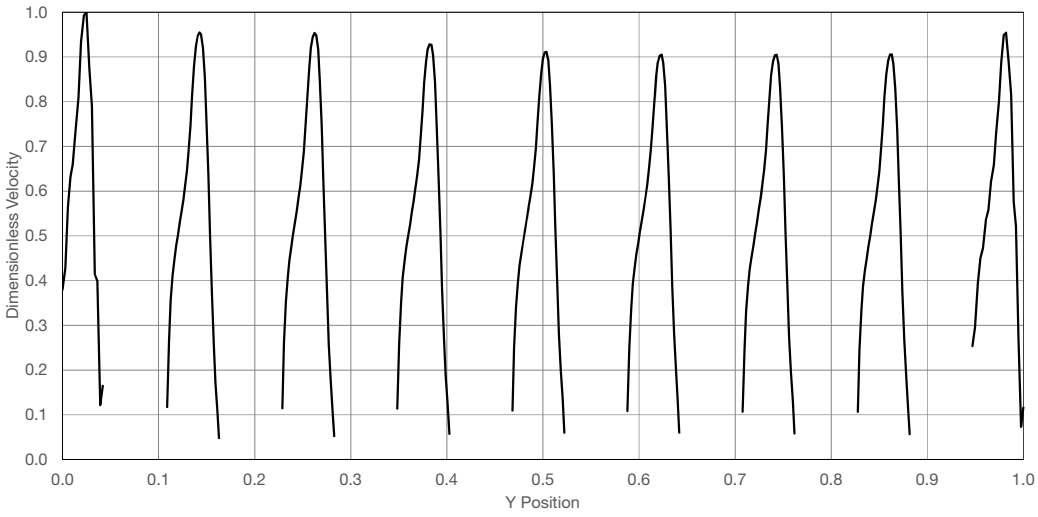

Figure E.30 Velocity magnitude profile on G zone for 0.5Q flow rate.

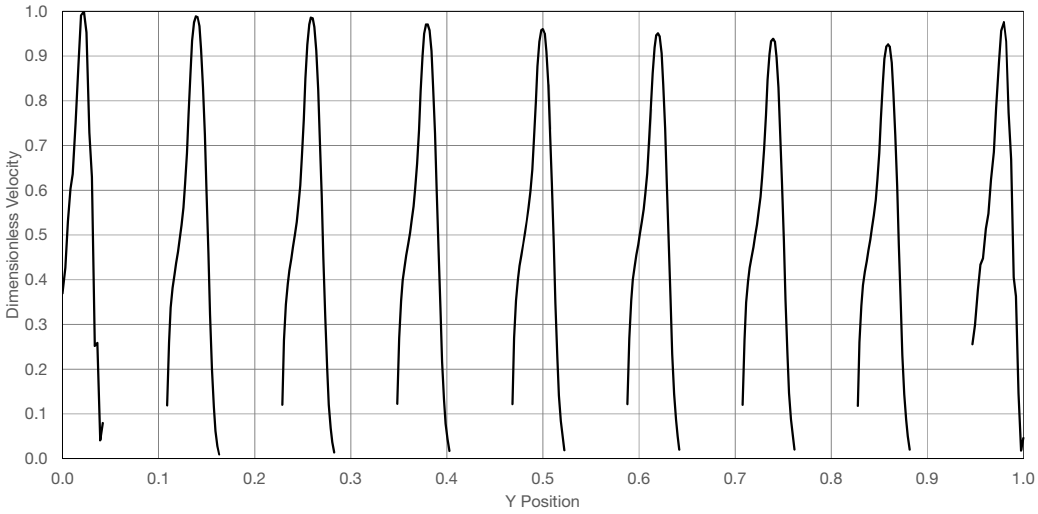

Figure E.31 Velocity magnitude profile on G zone for Q flow rate.

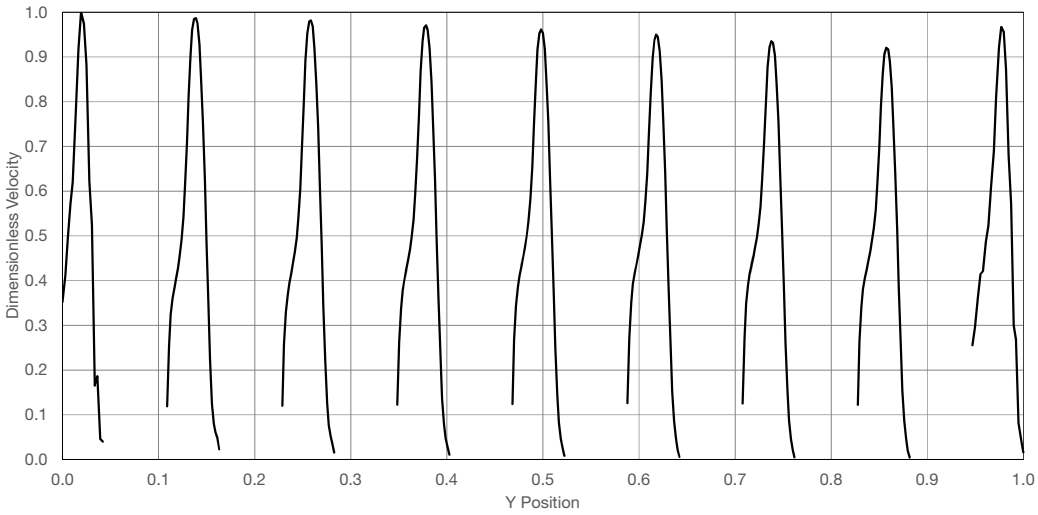

Figure E.32 Velocity magnitude profile on G zone for 1.38Q flow rate.

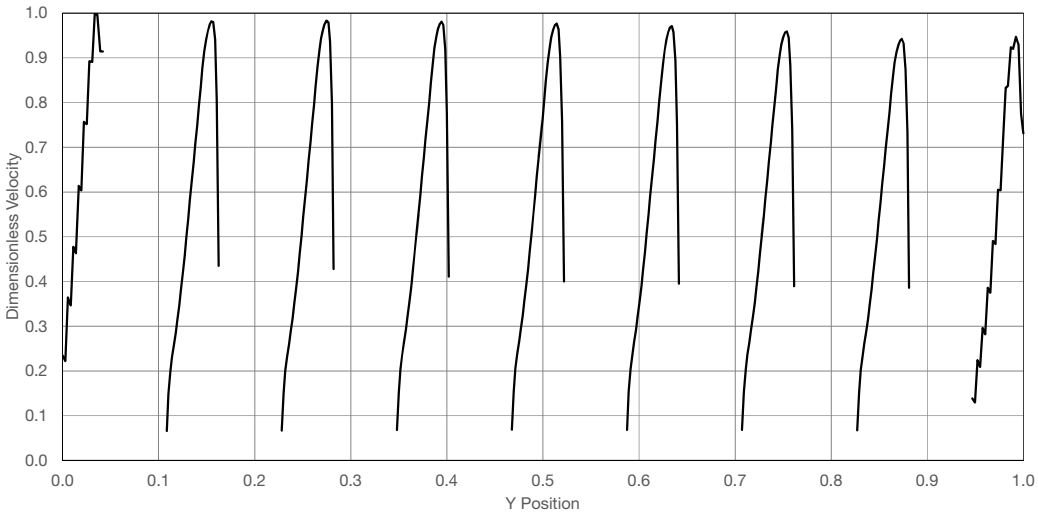

Figure E.33 Velocity magnitude profile on G zone for 2Q flow rate.

F FluSHELL Performance Plots

This section shows the detailed plots of FluSHELL performance on the analyzed lines. For each plot the values of oil and coil bundle temperatures are shown for: CFD results, FluSHELL-Base results and FluSHELL-i1 results.

F.1 Q Flow Rate

Figure F.1 to Figure F.6 show the detailed FluSHELL performance plots for Q flow rate.

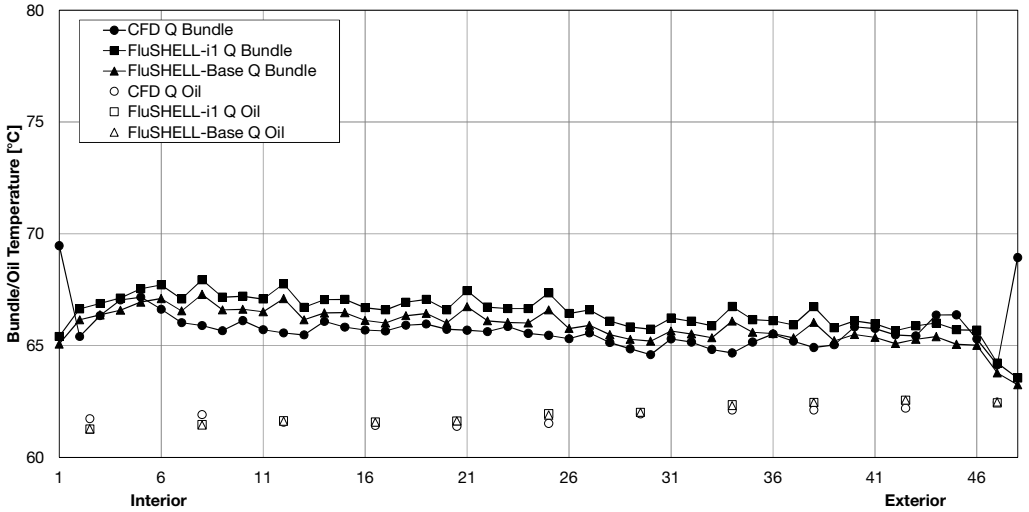

Figure F.1 FluSHELL performance for Q flow rate on line 20.

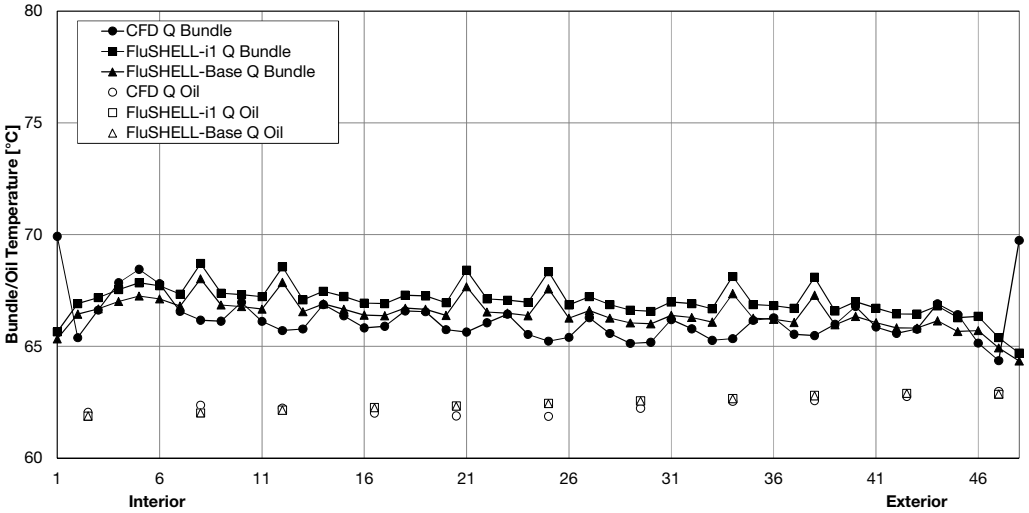

Figure F.2 FluSHELL performance for Q flow rate on line 24.

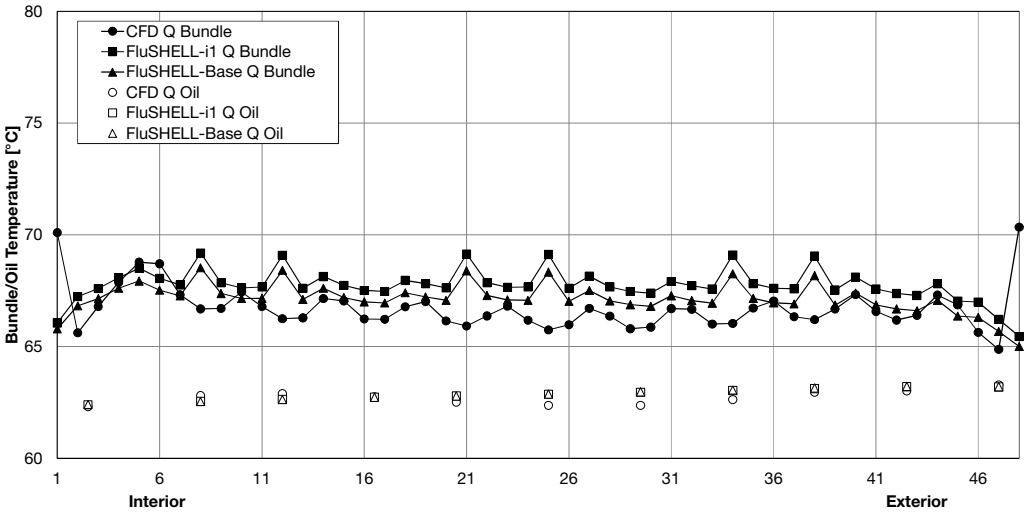

Figure F.3 FluSHELL performance for Q flow rate on line 28.

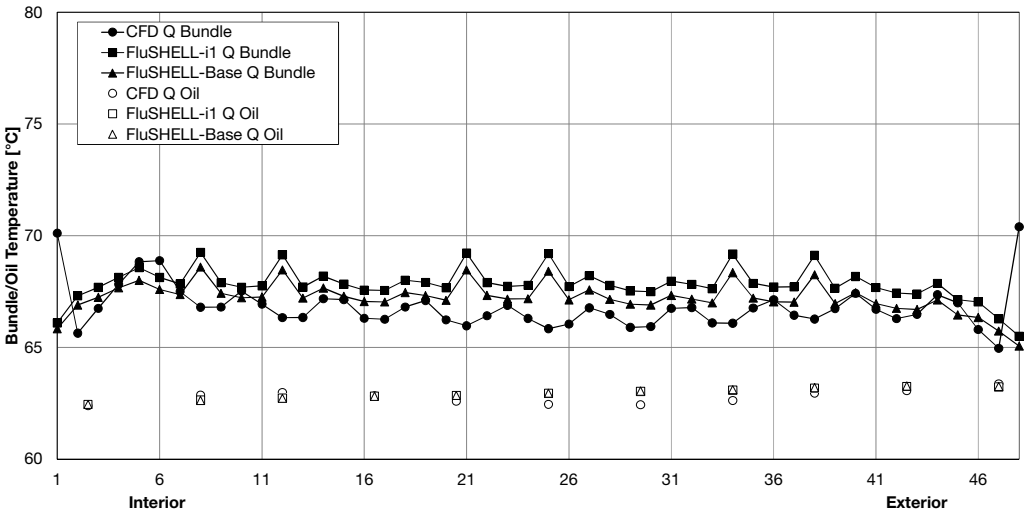

Figure F.4 FluSHELL performance for Q flow rate on line 28s.

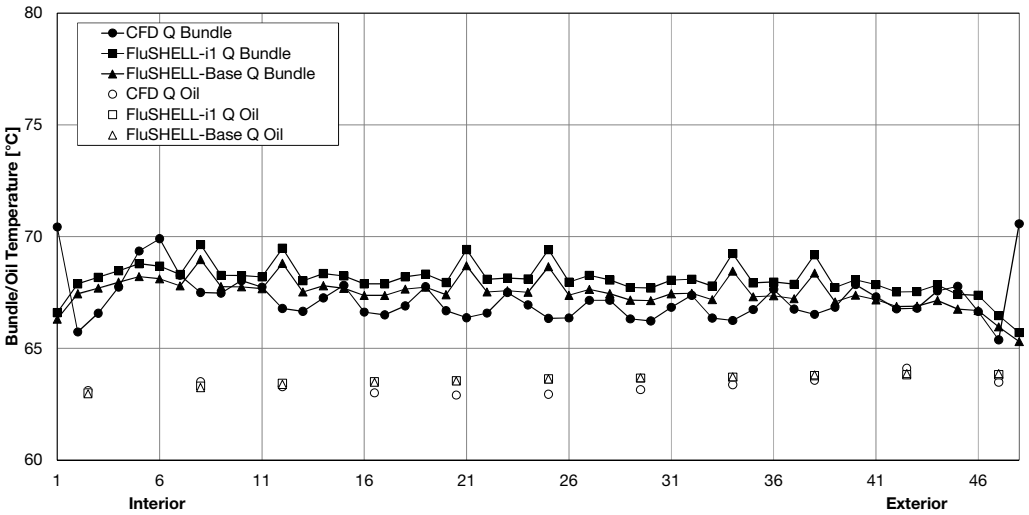

Figure F.5 FluSHELL performance for Q flow rate on line 24s.

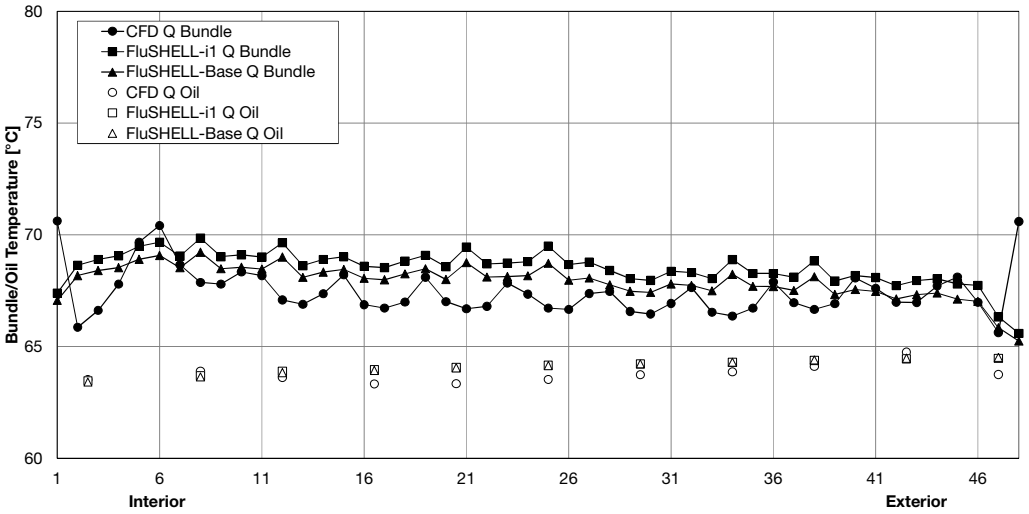

Figure F.6 FluSHELL performance for Q flow rate on line 20s.

F.2 Q/10 Flow Rate

Figure F.7 to Figure F.12 show the detailed FluSHELL performance plots for Q flow rate.

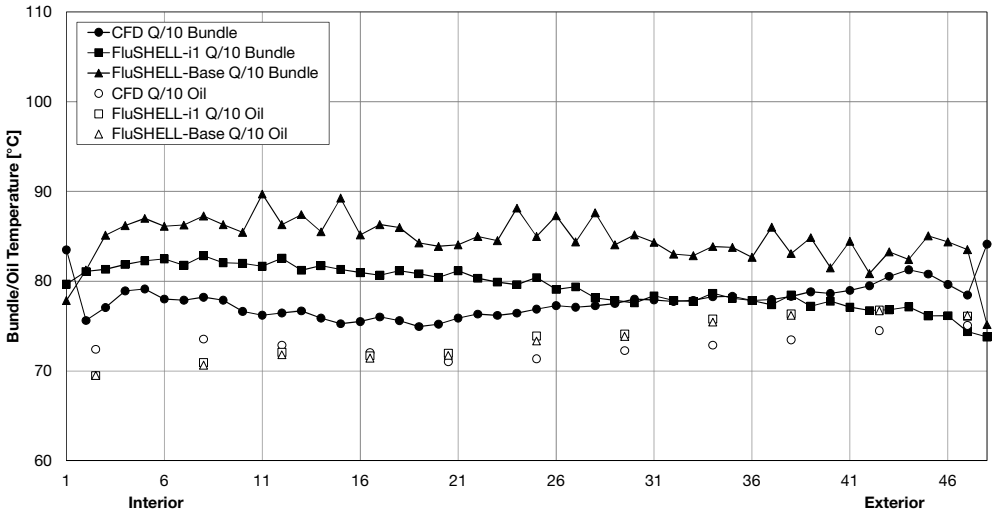

Figure F.7 FluSHELL performance for Q/10 flow rate on line 20.

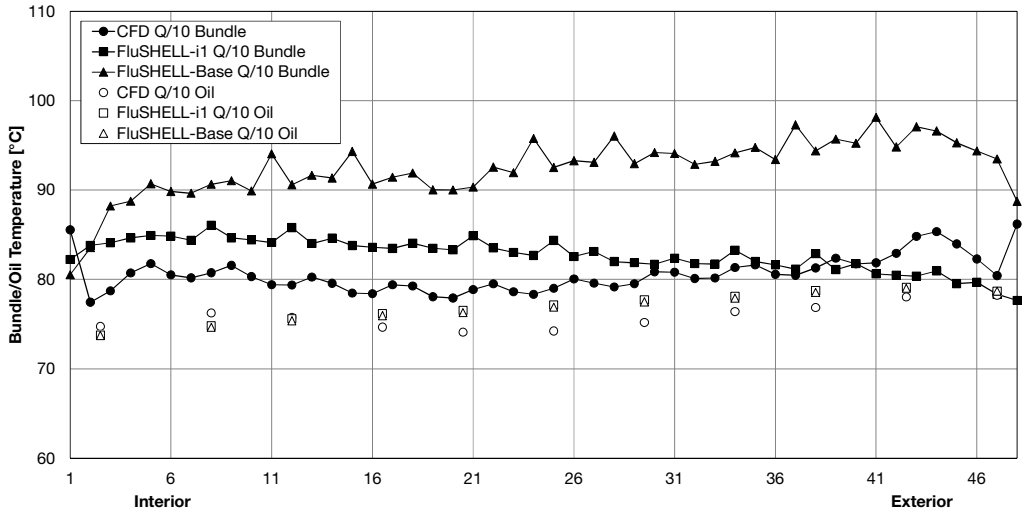

Figure F.8 FluSHELL performance for Q/10 flow rate on line 24.

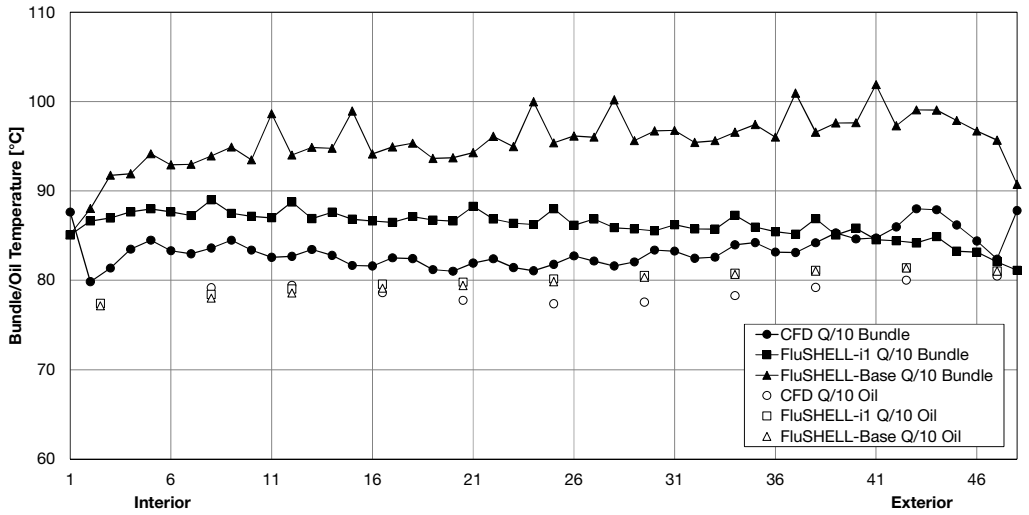

Figure F.9 FluSHELL performance for Q/10 flow rate on line 28.

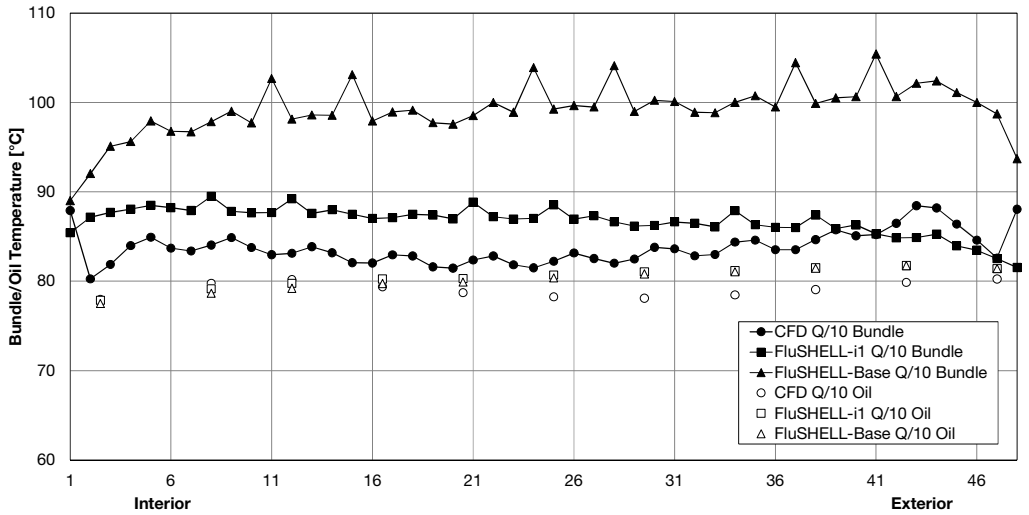

Figure F.10 FluSHELL performance for Q/10 flow rate on line 28s.

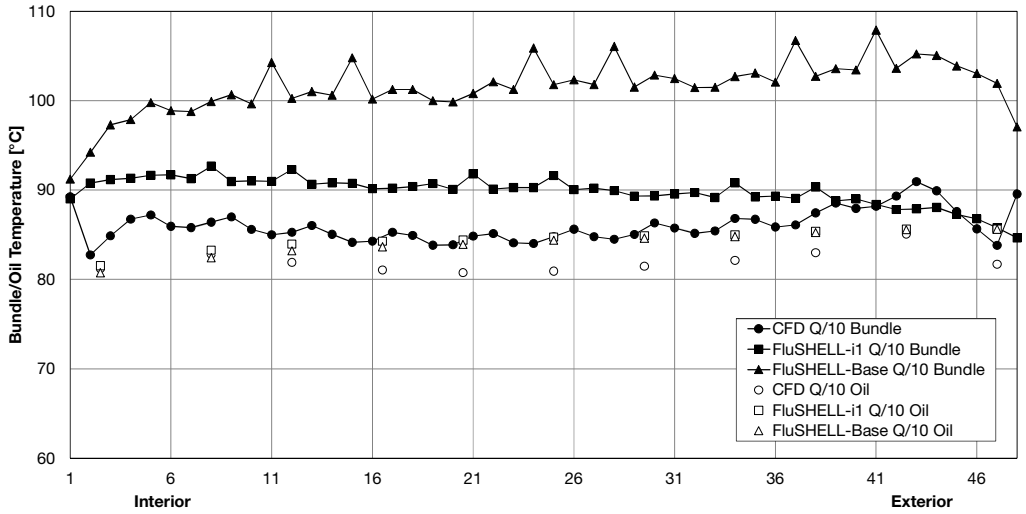

Figure F.11 FluSHELL performance for Q/10 flow rate on line 24s.

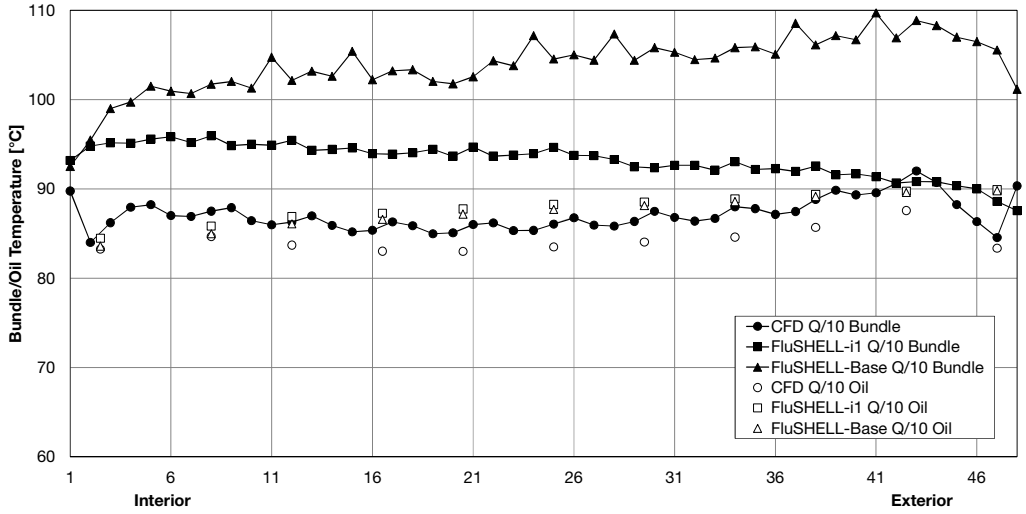

Figure F.12 FluSHELL performance for Q/10 flow rate on line 20s